1989

Photochemical Vapor Deposition of Gallium-Arsenide Utilizing Ultraviolet Radiation.

David Paul Norton
Louisiana State University and Agricultural & Mechanical College

Order Number 9002164

Photochemical vapor deposition of gallium arsenide utilizing ultraviolet radiation

Norton, David Paul, Ph.D.

The Louisiana State University and Agricultural and Mechanical Col., 1989

U·M·I
300 N. Zeeb Rd.
Ann Arbor, MI 48106

PHOTOCHEMICAL VAPOR DEPOSITION OF GALLIUM ARSENIDE UTILIZING ULTRAVIOLET RADIATION

A Dissertation

Submitted to the Graduate Faculty of the
Louisiana State University and
Agricultural and Mechanical College
in partial fulfillment of the
requirements for the degree of
Doctor of Philosophy

in

The Department of
Electrical and Computer Engineering

by
David Paul Norton
B.S., Louisiana State University, 1984
May 1989

ACKNOWLEDGEMENTS

I wish to express my gratitude to Dr. Pratul K. Ajmera for his continued guidance, assistance and friendship during my graduate program. I would like to express my thanks to Dr. R.E. Ferrell and Dr. H.C. Eaton for their assistance in the use of the X-ray diffractometer, the scanning electron microscope and the Auger electron spectrometer. Appreciation is also expressed to Mr. Golden Hwuang for both his assistance and friendship in the laboratory. I would also like to thank Mr. James Breedlove for his assistance as well.

Special recognition must be given to my wife, Tammie, whose support, understanding and love has made my life so wonderful. No matter what the circumstances, I always know that she will be by my side and I by hers.

I would like to thank my parents, Paul and Marie, for their love and support throughout my educational endeavors.

Finally, I wish to express my thanks to my Lord and Savior, Jesus Christ, in whom I place my life, faith and trust.

This research was supported by the Alumni Federation, the Troy H. Middleton Scholarship program, the Department of Defense (Army Research Office), the Center for Energy Studies at Louisiana State University and the Louisiana Education Quality Support Fund. Their support is greatly appreciated.

TABLE OF CONTENTS

TABLE OF CONTENTS (cont'd)

TABLE OF CONTENTS (cont'd)

LIST OF TABLES

LIST OF FIGURES

LIST OF FIGURES (cont'd)

LIST OF FIGURES (cont'd)

LIST OF FIGURES (cont'd)

LIST OF FIGURES (cont'd)

LIST OF FIGURES (cont'd)

LIST OF FIGURES (cont'd)

LIST OF FIGURES (cont'd)

LIST OF FIGURES (cont'd)

ABSTRACT

Photochemical means have been utilized to deposit arsenic, gallium and gallium arsenide thin films in an attempt to achieve deposition of gallium arsenide at substrate temperatures lower than those utilized in conventional organometallic chemical vapor deposition. Photolysis, Hg-photosensitization and light-driven pyrolysis have been utilized to obtain thin films on quartz, fused silica, gallium arsenide and silicon substrates. Triethylgallium and arsine served as the reactants with a low pressure Hg lamp, a high pressure Hg-Xe arc lamp and an ArF excimer laser serving as the ultraviolet radiation sources.

Deposition of arsenic and gallium arsenide thin films on quartz was investigated utilizing Hg-photosensitization. Arsenic thin films were deposited on quartz by means of Hg-sensitized decomposition of arsine at substrate temperatures ranging from 50 to 240°C. Films deposited below 200°C were found to be amorphous while those deposited above 200°C consisted of rhombohedral arsenic. Gallium arsenide deposition at temperatures less than 250°C utilizing Hg- photosensitization occurred only in the presence of an additional broadband ultraviolet light source. Polycrystalline gallium arsenide thin films were obtained on quartz substrates using both a low pressure Hg lamp and a Hg-Xe arc lamp.

Direct photochemical vapor deposition of gallium arsenide was also achieved on fused silica, gallium arsenide and silicon substrates. The film stoichiometry was highly dependent on the substrate temperature with arsenic-rich films obtained for substrate temperatures below approximately 250°C. Single crystal gallium arsenide thin

films were obtained on gallium arsenide substrates at a substrate temperature of approximately 315°C with room temperature Hall mobility values as high as 4000 $cm^2/V-sec$. It was found that, for perpendicular beam geometry, both photolytic and pyrolytic mechanisms contributed to the thin film growth.

A mass spectroscopic study of the photolytic decomposition of the two reactants was also performed. In addition, a simple first-order model is presented for light-driven chemical vapor deposition of gallium arsenide at low substrate temperatures for which both gas-phase and surface-adsorbed species photodissociate. Results of this work indicate that the photodissociation of surface-adsorbed species is the more useful process for achieving stoichiometric GaAs deposition at low temperatures using photochemical means.

CHAPTER 1

INTRODUCTION

Gallium arsenide is utilized in several areas of technology including high-speed electronics, microwaves, optoelectronics and photovoltaics. In efforts to fabricate various device structures with this semiconductor material, it is often desirable to increase the flexibility of the fabrication process. Some attention has recently been given to reduce the processing temperatures necessary for device fabrication including the deposition of the material at reduced temperatures. In this work, photochemical mechanisms are utilized as a potential means for depositing gallium arsenide at substantially reduced substrate temperatures.

It is of use to consider the advantages of low temperature processing of semiconductor devices as this is a major principle impetus for this study. At present, epitaxial growth of single crystal gallium arsenide thin films is achieved at substrate temperatures in excess of 500°C. With lower processing temperatures, sharper dopant profiles can be realized as diffusion of these impurities is reduced. When the deposition chamber and the susceptor can be maintained at lower temperatures, diffusion of impurities out of the reactor components is reduced thus improving process purity. For heteroepitaxy in which the substrate and the film consist of different materials, a decrease in the temperature required for deposition results in a decrease in the interfacial stress due to the difference in the thermal expansion coefficients for the substrate and the film. At reduced processing temperatures, unique device structures become possible as additional processing steps can be performed without significantly affecting

the structure resulting from the prior steps.

1.1 Objectives

This research investigates the use of ultraviolet radiation in the deposition of arsenic, gallium and gallium arsenide thin films at reduced substrate temperatures. Photolysis, light-driven pyrolysis and Hg-photosensitization are considered as means by which the reactants are decomposed and deposition achieved. The objective of this work is two-fold. The first objective is to deposit GaAs thin films utilizing photochemical means at very low substrate temperatures. This includes determination of the pertinent growth parameters for obtaining stoichiometric GaAs films and subsequent characterization of the films obtained. The second objective is to understand the mechanisms involved in the growth process with emphasis on how the ultraviolet radiation interacts with the chemical system. Particular attention is given to understanding the limiting factors in achieving epitaxial growth at low substrate temperatures.

CHAPTER 2

LITERATURE REVIEW

2.1 Review of Thermally-Driven Organometallic Chemical Vapor Deposition of Gallium Arsenide

In this section, conventional Organometallic Chemical Vapor Deposition (OMCVD) of GaAs is reviewed and discussed. This will provide a backdrop for understanding how photonic energy can be substituted for thermal energy in the deposition of GaAs. The treatment here will be restricted to GaAs deposition even though OMCVD has been successfully used to grow epitaxial layers of a number of other III-V compound semiconductors based on other elements such as In, Al, Sb and P. In addition, only systems employing arsine (AsH_3) and trimethylgallium (TMG) or triethylgallium (TEG) will be discussed in detail. Although all of the original work reported in later Chapters involves the use of TEG instead of TMG, the pyrolytic growth of GaAs utilizing TMG and arsine will be extensively discussed as the majority of detailed studies on the growth of GaAs by OMCVD involve TMG and AsH_3.

Organometallic chemical vapor deposition of GaAs was first reported by Manasevit in 1968.[1] The main advantage of OMCVD is its ability to deposit Ga, As, In, Al, P and Sb based III-V semiconductor compounds in a thin film form. Over the years, some of the highest quality III-V compound semiconductor epitaxial films have been produced using this technique. Organometallic chemical vapor deposition is generally carried out in a stainless steel or a quartz reactor with the latter being more generally accepted. As with any semiconductor growth scheme, reactant purity must be

maintained throughout. Both vertical and horizontal reactor tubes have been used with only the susceptor heated. Total pressure is generally maintained anywhere from 760 to 10 Torr although some work has also been reported where ultra high vacuum is utilized. Since many of the reactants are either toxic, flammable or pyrophoric, special care must be taken to properly dispose of the reactor exhaust. Figure 2.1 shows a schematic of a typical low pressure OMCVD system. As mentioned earlier, the remaining discussion will focus on the use of OMCVD in the deposition of GaAs unless specified otherwise.

The OMCVD process can be divided into five major sub-processes which, although certainly coupled, can be treated as separate steps for clarity in understanding. These processes are:

1) Initial reactant input and mixing
2) Entry effects
3) Chemical reactions in the gas phase
4) Mass transport (diffusion)
5) Surface kinetics

Reactant input and mixing generally involves controlling the gas flow rates in order to provide the correct reactant ratios and, in some cases, maintaining the reactants separate in the reactor as much as possible. Organometallic reactants, used mostly for the group III species, are delivered to the reactor by bubbling a carrier gas (generally hydrogen) through the organometallic utilizing the reactant vapor pressure for transport. Hydrides, such as arsine, are gases delivered either as a single component or as a mixture in hydrogen. Reactant interaction in the initially cold input

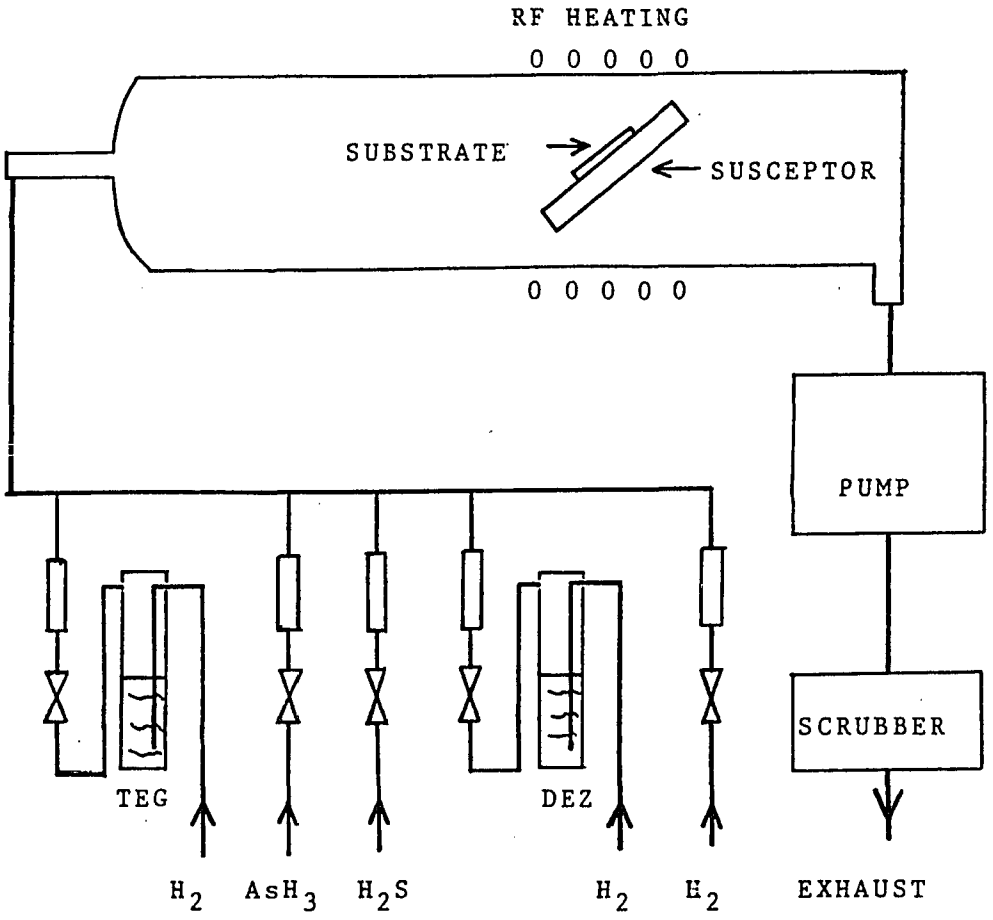

Figure 2.1 Schematic of a Typical Low Pressure OMCVD System.

stage is especially important in many In-based systems where premature involatile adduct formation between the In alkyl and the group V hydride may lead to reactant depletion.[2]

Entry effects involve the flow dynamics as the incoming reactant gases encounter the hot susceptor. Entry effects can introduce turbulence in the gas flow and are more important in high flow rate systems.[3,4] In general, the gas flow is characterized by Reynolds number Re

$$Re = \frac{ud_h}{\nu} \tag{2.1}$$

where u is the mean gas velocity, d_h is the hydraulic diameter of the tube (four times the area divided by the perimeter) and ν is the kinematic viscosity of the carrier gas. If Re is greater than 2000, flow will be turbulent. For most CVD reactors, Re is less than 100 with the gas flow being laminar. In addition, heat transfer in the gas is characterized by the Peclet number Pe

$$Pe = \frac{ud_h}{K} \tag{2.2}$$

where K is the thermal diffusivity of the carrier gas. For most atmospheric pressure CVD systems, the distance over which the concentration gradients (due in part to flow dynamics) are maintained is approximately equal to the distance over which the thermal gradient is maintained. This allows for the use of a single "boundary layer" above the substrate which can be used to treat all of the gradients in the gas phase. As such, this "boundary layer" exists between the substrate surface and the main stream of input reactants with significant gas temperature and velocity gradients present in the boundary layer. It is clear that diffusion of the reactants through the boundary layer is

necessary for growth to occur. The thermal and concentration gradients have been measured by Ban who distinguished two regions above the hot susceptor surface.[4,5] Immediately above the susceptor surface, steep thermal and concentration gradients exists. This has also been confirmed using Raman spectroscopy by Monteil[6] and Koppitz.[7] The gas temperature was found to be very high with flow nearly laminar. At greater distances above the susceptor, the flow becomes more turbulent due to entry effects and buoyancy forces from the heated susceptor. From this work, it was concluded that most OMCVD reactors do not operate with fully developed flow profiles in the deposition zone. However, in the region just above the susceptor surface, the boundary layer is formed in most cases. This situation was modeled with the upper zone treated as a "cold finger" of the reactant gases which serves to supply the reactants to the growing surface. The lower zone is the "boundary layer" through which the reactants must diffuse. Due to reactant depletion, the growth rate in a horizontal reactor decreases exponentially as a function of distance along the horizontal susceptor although this dependence can be eliminated by tilting the substrate with respect to the input gases. When considering deposition at reduced pressure, the increased gas velocity must be taken into account. Although reduced pressure can eliminate the need for substrate tilting, the increased gas velocity reduces the reactant usage efficiency.

Mass transport of the reactants to the growing semiconductor surface occurs by means of diffusion through the boundary layer. By considering the flux, J, of reactants to the surface, one can write[8]

$$J_{III} = \frac{D_{III} (P^{o}_{III} - P_{III})}{RTd_o} \tag{2.3}$$

for the gallium-bearing alkyl where D_{III} is the diffusion coefficient, P^{o}_{III} is the alkyl partial pressure outside of the boundary layer, P_{III} is the partial pressure at the semiconductor-gas interface, R is the gas constant, T is the temperature and d_o is the boundary layer thickness. An analogous expression holds for the arsenic species.

Although the previous steps described in the OMCVD process are fairly well understood, the subjects of gas phase reactions and surface kinetics carry with them a great deal of uncertainty. Before considering the case where AsH_3 and TMG or TEG are simultaneously involved, let us first consider the decomposition of each individual component. The thermal decomposition of arsine in the presence of and in the absence of an arsenic surface was first studied by Tamaru.[9] It was found that the decomposition of arsine proceeded by a surface- catalytic reaction in the presence of an arsenic surface with an activation energy of 23.2 kcal/mole (1.01 eV/molecule). The reaction appears to be a first order one with the rate-limiting step being

$$AsH_3(a) \rightarrow AsH_2(a) + H(a) \qquad (2.4)$$

where (a) signifies a surface-adsorbed species. Below 620°C, only As and H_2 are produced by thermal decomposition while above 620°C, both As_2 and As_4 appear in the gas phase .[10]

The thermal decomposition of TMG and TEG has been studied by several workers. It has been found that the decomposition of TMG proceeds by sequential elimination of the methyl groups with the 1st, 2nd and 3rd $Ga–CH_3$ bond energies determined to be 59.5, 35.4 and 77.5 kcal/mole (2.58, 1.54 and 3.36 eV/molecule).[11] From a mass spectroscopic study, it was found that the decomposition of TMG in H_2 proceeds by hydrogenolysis which forms methane while the decomposition of TMG in

N_2 is real pyrolysis with the methyl radical formed by homolytic fission .[12] The dominant product in either N_2 or H_2 ambient is methane with small amounts of ethane produced. The hydrogenolysis takes place at a lower temperature than the homolytic pyrolysis with complete decomposition in H_2 occurring at 460°C while complete decomposition in N_2 occurs at 570°C. TMG decomposition in H_2 follows first order kinetics.

The mechanism for decomposition of TEG differs from that for TMG with the decomposition proceeding by β-elimination forming ethylene with small amounts of butane but virtually no ethane. The reported activation energy for this decomposition is 21.8 kcal/mole (0.95 eV/molecule).[13] Decomposition of TEG in H_2 is complete at 330°C with complete decomposition in N_2 occurring at 380°C.

In considering the case where both the Ga alkyl and arsine are present, it is useful to first discuss the observed behavior of the deposition process. Reep and Ghandi studied the deposition of GaAs using TMG and AsH_3 at atmospheric pressure over a wide range of substrate temperatures.[10] In this work, three distinct growth regimes were observed. These are distinguished as the mid-temperature or mass transport limited regime, the high temperature regime and the low temperature or kinetically-controlled regime. The kinetically-controlled regime will be discussed last as this will lead into a discussion of the possible gas phase reactions and surface kinetics occurring in the OMCVD process.

The mid-temperature regime (600-850°C) is characterized by almost no dependence of the growth rate on the substrate temperature. In this regime, mass transport appears to be the limiting process in the growth with an apparent activation energy of

1.5 to 2.4 kcal/mol indicative of a diffusion- controlled process. The growth rate is independent of substrate orientation and the AsH_3 flow rate over this temperature range (provided that an overpressure of arsine exists). The growth rate is, however, linearly dependent on the concentration of TMG indicating that growth is limited by the transport of the gallium-bearing species to the semiconductor surface. As the diffusion process is rate-limiting, the absolute growth rate in this temperature regime gives very little information about the reaction mechanisms. In this growth regime, near-equilibrium conditions do not exist throughout the system. It is the difference in the electrochemical potential which drives the process leading to deposition.[8] In the mass transport limited regime, near- equilibrium conditions may exist near the semiconductor-gas interface but not in the gas phase. This growth regime is by far the most important in producing high quality epitaxial films.

Although, in this mass transport limited growth regime, the growth rate does not depend on the arsine flow rate, the GaAs film properties do depend on the AsH_3/TMG ratio.[14] It has been observed that the carrier type for unintentionally doped films changes from n- type to p-type with decreasing AsH_3/TMG ratio. As the chamber pressure is lowered, the n- to p-type conversion occurs at higher AsH_3/TMG ratios.

Growth behavior using TEG instead of TMG is similar to what has been described above with the only major difference being that the temperature range over which the deposition rate remains constant is narrower for TEG than for TMG. In addition, the transition to the kinetically-limited regime occurs at a lower temperature for TEG than for TMG.[15]

For substrate temperatures greater than 850°C, the rate- limiting step changes with the growth rate falling with increasing temperature and becoming highly orientation dependent. The growth rate depends linearly on the TMG flow rate and is independent of the arsine flow rate for this temperature regime. There is some uncertainty as to the mechanism which leads to this observed behavior. One explanation is that increased desorption of the reactant species is involved. As the growth varies linearly with TMG partial pressure and is independent of arsine partial pressure, it appears that the desorption of the gallium species is the dominant mechanism.[10] Another explanation which has been suggested involves the premature decomposition of the reactants in the gas phase leading to homogeneous nucleation and parasitic deposition in the reactor.[3] This would lead to a depletion of the reactants with a subsequent decrease in the growth rate. Similar behavior in this temperature regime has been observed using TEG as well.

For substrate temperatures below 600°C, the growth of GaAs using arsine and TMG is kinetically-controlled with the deposition rate decreasing with decreasing temperature.[10] The growth is found to depend sublinearly on arsine and TMG partial pressure for this temperature range with growth on the (111)Ga face higher than that for the (111)As face. The overall activation energy was determined to be 16 kcal/mole for (111)As and 22 kcal/mole for (111)Ga. Results for growth with TEG are quite analogous. Based on these results, Reep and Ghandi have suggested that non-competitive adsorption based on a Langmuir-Hinshelwood mechanism best explains the surface kinetics in which adsorption sites do not overlap.[10] This model predicts that

$$R_g = K_2\theta_{AsH_3}\theta_{TMG} \tag{2.5}$$

where R_g is the deposition rate, K_2 is the rate constant and θ_{AsH_3} and θ_{TMG} are the surface coverages for AsH_3 and TMG, respectively. By the Langmuir adsorption isotherm,

$$\theta_{AsH_3} = \frac{\beta_{AsH_3} P_{AsH_3}}{1 + \beta_{AsH_3} P_{AsH_3}} \tag{2.6}$$

where β_{AsH_3} is the ratio of the rate constant of adsorption to the rate constant of desorption and P_{AsH_3} is the partial pressure of AsH_3. From this, one obtains

$$R = \frac{K_2 \beta_{AsH_3} \beta_{TMG} P_{AsH_3} P_{TMG}}{(1 + \beta_{AsH_3} P_{AsH_3})(1 + \beta_{TMG} P_{TMG})} \tag{2.7}$$

Central to this model is the assumption that the gallium- and arsenic-bearing species (be they undecomposed molecules, radicals or complexes) arrive independently to the growing semiconductor surface and that their adsorption sites do not overlap on the substrate. Reep and Ghandi also propose that the arsenic adsorption process dominates as the growth rate on the (111)Ga face is higher than on the (111)As face. The fact that the measured activation energy (22 kcal/mole) is approximately the same as the activation energy for heterogeneous decomposition of arsine over an arsenic surface further suggests that the adsorption and decomposition of arsine is the rate-limiting step in the low temperature regime although work reported by Tsang[16] and Bhat[17] suggests that the cracking of the alkyl is rate limiting.

The question of whether the decomposition of the TMG and AsH_3 occurs before or after adsorption onto the GaAs surface remains debatable at this time. A study by Schlyer and Ring suggests that the reaction of AsH_3 and TMG is surface-catalytic in nature.[18] In this study, the reaction of TMG and AsH_3 was studied at 203

and 259°C. It was found that, at 203°C, the solid product $(CH_3)_{1.9}GaAsH_{1.9}$ is formed with the product of the reaction at 259°C being $(CH_3)_{0.8}GaAsH_{0.8}$. Upon heating this solid to 420°C, hydrogen was liberated presumably from the AsH polymer formed. It is suggested that TMG and AsH_3 decompose after adsorption onto the surface with the methyl radical from TMG combining with a hydrogen atom from the AsH_3 molecule to form methane. A study of the gas phase using Raman spectroscopy also suggests that TMG is transported to the surface undecomposed.[7]

There is evidence, however, that TMG decomposes in the gas phase prior to adsorption onto the substrate surface. Using infrared absorption spectroscopy, the gas phase just above the substrate surface appears to contain CH_4 with no undecomposed TMG detected.[3,19] This suggests that TMG undergoes homogeneous decomposition in the gas phase. This view is further supported by the observation of methyl radicals in the gas phase using high resolution infrared-diode laser spectroscopy.[20] In this study, the Q(6,6) rotational feature of the ν_2 vibrational mode of CH_3 was monitored and detected. Other work has shown that the thermal decomposition of TMG is unaffected by the presence of GaAs wafers providing further doubt about the importance of surface-catalytic effects in the TMG decomposition process.[21] However, most studies have concluded that, aside from the formation of the CH_3 radical, methane is the only major hydrocarbon product present in the gas phase whether or not AsH_3 is present.[3,12,19]

There appears to be little debate that, in the TMG-AsH_3 or TEG-AsH_3 systems, surface-catalysis plays a major role in the thermal decomposition of AsH_3. There is some question, however, as to whether interaction between the gas phase molecules (or

radicals produced by decomposition) occurs. Obviously, those holding to the idea that TMG and AsH_3 diffuse undecomposed to the growing surface assume no gas phase interaction. However, evidence does exists suggesting that interaction does take place at the temperatures utilized during growth. When mixed at high temperatures, Nishizawa and Kurabayashi observed a new feature in the infrared absorption spectrum for the mixture of AsH_3, TMG and H_2 which could not be explained by superposition of the spectra of the individual components.[19] It has also been observed that the decomposition of AsH_3 proceeds much faster in the presence of TMG although it is not possible to distinguish between the effects of the TMG and the effects of GaAs or Ga droplets on the decomposition rate. Using Raman spectroscopy, it has been observed that the TMG Raman spectral features become much weaker when AsH_3 is added at high temperatures.[7] In addition, recent work performed on organometallic molecular beam epitaxy of GaAs using TMG and AsH_3 has revealed that deposition does not occur for ultra high vacuum conditions unless the arsine is pre-cracked prior to impingement onto the substrate suggesting that interaction of the TMG molecules with certain arsenic-bearing species (excluding undecomposed AsH_3) is necessary for deposition to occur.[22]

Organometallic chemical vapor deposition is one of the most successful and versatile technique for obtaining high quality compound semiconductor thin films. In spite of its success, many of the reaction mechanisms involved in OMCVD lack sufficient understanding. Much work remains before a complete understanding of the mechanisms of growth is obtained for OMCVD of GaAs using TMG or TEG with AsH_3.

2.2 Photonic Interaction with Chemical Systems

In the previous section, we reviewed the mechanisms involved in organometallic chemical vapor deposition of gallium arsenide. In order to understand how ultraviolet light interaction can assist in the deposition process, it is useful at this point to review some basic photonic processes which may be involved. Obviously, the subject of light interaction with physical systems is too broad to be effectively covered here. We will, therefore, concentrate this brief review on those basic photonic processes which may be relevant when considering the interaction of optical radiation with the OMCVD process with particular attention given to gas phase reactions and surface kinetics. The photochemical processes which may affect deposition involve the interaction of light with the gas phase or surface- adsorbed atoms or molecules or by the substrate itself. In this section, these basic optical mechanisms will be discussed.

Light possesses both wave-like and particle-like characteristics with the energy of each quantized photon given by

$$E = h\nu \tag{2.8a}$$

where ν is the frequency of the light and h is Planck's constant.[23] When considering the interaction of light with physical systems, absorption is a possibility when the energy difference between an unoccupied and an occupied state of the system is equal to the energy of the incoming photon

$$h\nu = E_{final} - E_{initial} \tag{2.8b}$$

Higher order non-linear processes have been shown to allow absorption of photons with energy less than the energy difference of the initial and final states. However, these processes are important only when the photon density is extremely high. The

dominant optical processes are usually characterized by Eqn. (2.8b).

When considering absorption of monochromatic light by a homogeneous medium, the absorption process is characterized by Beer-Lambert's Law which states that

$$\frac{I_{trans}}{I_o} = \exp(-\alpha c l) \tag{2.9}$$

where I_o is the incident intensity, I_{trans} is the light intensity a distance l into the absorbing medium, c is the concentration of absorbing molecules and α is the optical extinction coefficient at frequency ν.

Molecules, by definition, contain more than one atom. As such, the interaction of light with molecules must involve the energy of the electrons as well as the energy of the atomic nuclei through rotations and vibrations of the bound system. In general, the electronic and nuclear systems are coupled and are properly described by a single Hamiltonian. It is often possible, however, to treat the electronic and nuclear systems separately and obtain results which adequately describe the molecular system. This is known as the Born- Oppenheimer approximation. Put into quantum-mechanical terms, the complete wavefunction of the molecule is separable into a product of an electronic part and a nuclear part as the electronic wavefunction does not vary rapidly with a small change in the nuclear coordinates. The validity of this approximation stems mainly from the fact that the electrons, being much less massive than the nuclei, can rapidly adjust to a small change in the position of the nuclei. This approximation allows the energy of the molecule to be separated into an electronic contribution and a vibrational- rotational contribution. Figure 2.2 shows a one dimensional energy

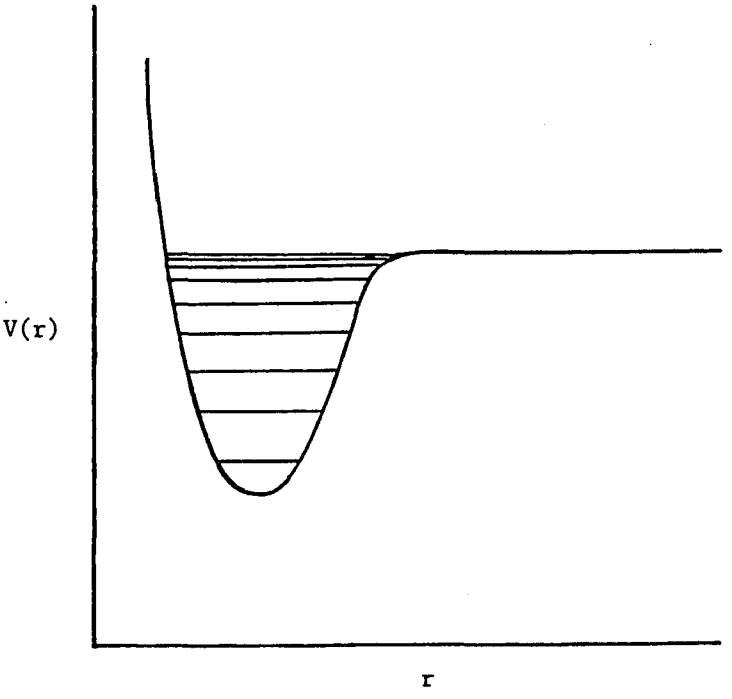

Figure 2.2 Energy Diagram Showing Electronic and Vibrational States of a Molecule.

diagram of an electronic state with the vibrational states superimposed with V(r) being the potential energy and r being the radial distance form the center of the molecule. In many cases, it is also possible to separate the vibrational and rotational energy of the molecule although the energy associated with rotation is relatively unimportant when considering photochemical change.

Electronic transitions are always associated with a change in the electric dipole moment of the molecule when photochemical change is considered. The selection rules which determine whether photon absorption by the molecule will occur are based on having a non-zero transitional dipole moment given by

$$\mu_{i\rightarrow f} = \int_{-\infty}^{\infty} \Psi_f^* \hat{M} \Psi_i d\tau \qquad (2.10)$$

where $\hat{M}$ is the dipole moment operator, Ψ_f is the total wavefunction of the final molecular state and Ψ_i is the total wavefunction of the initial state. Under the Born-Oppenheimer approximation, $\mu_{i\rightarrow f}$ is separable into two separate integrals with one involving the electronic part and the other involving the nuclear part. If, for instance, the electronic wavefunction is separable into spin and spatial parts (negligible spin-orbit coupling), the selection rule gives that $\Delta S = 0$ where S is the total spin. If spin-orbit coupling becomes more significant, as with many polyatomic molecules, this selection rule becomes much less rigorous.

The selection rules for the vibrational states are governed by the Franck-Condon principle which states that there can be little change in the molecular geometry with an electronic transition. The Franck-Condon principle states that the vibrational part of the transitional dipole moment, $(R_{if})_v$, is determined by

$$(R_{if})_v = \int_{-\infty}^{\infty} \Psi^*_{v,f} \Psi_{v,i} d\tau \qquad (2.11)$$

where $\Psi_{v,f}$ and $\Psi_{v,i}$ are final and initial vibrational parts of the molecule wavefunction, respectively. This is also known as the vibrational overlap integral, and it determines the intensity of the transition. The average number of transitions per second, P_{if}, can be related to the transitional dipole moment, R_{if}, by the relation

$$P_{if} = n_i \, g_f \, \rho(\nu_{if}) \, B_{if} \qquad (2.12)$$

where n_i is the number of molecules which can absorb the light of frequency ν_{if}, g_f is the degeneracy of the final state and $\rho(\nu_{if})$ is the radiation energy density per unit frequency and B_{if} is the Einstein coefficient of induced absorption defined by

$$B_{if} = (8\pi^3/3h^2) \, R_{if}^2 \qquad (2.13)$$

Unlike atoms, the optical absorption spectrum for molecules consists of lines, bands and continuous portions with band absorption occurring as the closely spaced vibrational and rotational structure is broadened by natural mechanisms.

It is now necessary to consider what happens to the molecules once absorption has taken place. Perhaps the most useful result of absorption in terms of photochemistry is dissociation of the molecule. Dissociation will occur if the energy of the final state after absorption is greater than the dissociation limit of the final state, or if the final state is inherently repulsive. If dissociation is the result of the absorption process, the absorption spectrum will be continuous. Figure 2.3 shows an energy diagram illustrating photolytic dissociation.

It is important to realize that for a molecule the heat of dissociation and the photonic energy necessary for photolytic dissociation is not necessarily the same. Pho-

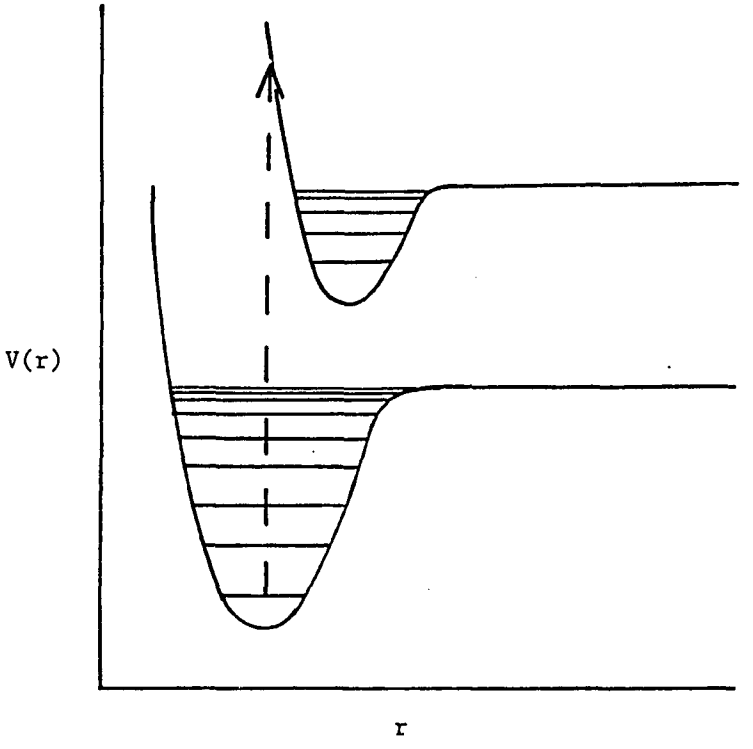

Figure 2.3 Energy Diagram Showing Molecular Photolytic Dissociation.

tolytic dissociation is determined not only by the energy of bonds that are to be broken in photolysis but also on the selection rules of absorption previously discussed. For this reason, the fragments of photodissociation often possess translational, electronic or vibrational energy above the ground state of the fragment. This differs from dissociation by pyrolysis where dissociation occurs by step-wise excitation of the vibrational energy states. Fragments of pyrolytic dissociation are, in general, in near thermal equilibrium with their surroundings.

Consider the case, shown in Fig. 2.4, where the electronic excitation occurs into a state below the dissociation limit of that excited electronic state. In addition, consider that this excited electronic state (1) is crossed by another energy curve (2). If the excited molecule "vibrates" into the region of the crossing, the possibility exists that the molecule will be transferred into this second excited state by a radiationless transfer. If the energy of the molecule exceeds the dissociative limit of this second excited state, molecular dissociation occurs. This process is known as predissociation.

One-dimensional energy diagrams offer a clear but oversimplified picture of the absorption process. This is especially true for polyatomic molecules where many degrees of freedom exist. When a polyatomic molecule absorbs a single photon, dissociation occurs only if the absorbed energy is redistributed to the proper dissociation channels. As such, dissociation or predissociation are not the only results possible when a molecule is excited. A molecule may undergo fluorescence, phosphorescence from a triplet state or bimolecular collision possibly resulting in a chemical reaction. The relative importance of each event depends, of course, on the rate constants involved.

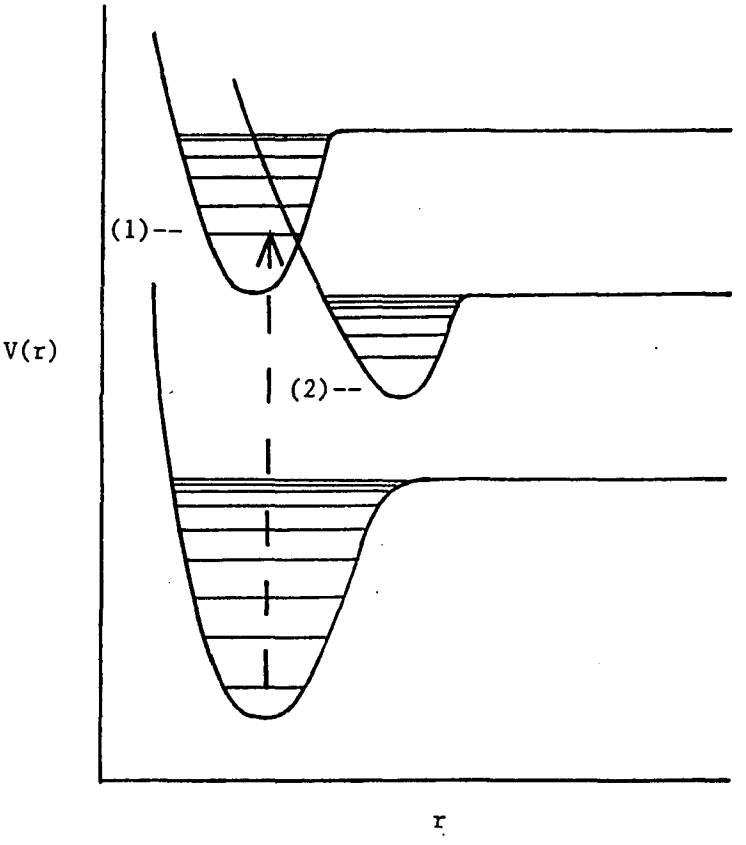

Figure 2.4 Energy Diagram Showing an Example of Predissociation.

In addition to the effects resulting from direct excitation of the molecule, it is also possible for photochemical change to occur from the interaction of an excited atom or molecule with an unexcited reactant molecule. When an atom becomes electronically excited through photon absorption, the possibility exists that the excited atom will collide with a molecule transferring all or part of this energy to the molecule. If a chemical change of the reactant molecule occurs due to this energy exchange, this process is known as photosensitization. Mercury atoms, for example, can be excited into the $6^3P_1^o$ state by resonant 2537.5 angstrom radiation.[24] This results in an excess energy of 4.86 eV above the ground state which can be transferred by collision to reactant molecules resulting in chemical change. In general, the photosensitization process can be understood by considering the reactions

$$A + h\nu \rightarrow A^* \tag{2.14}$$

$$A^* \rightarrow A + h\nu \tag{2.15}$$

$$A^* + Q \rightarrow A + Q^* \tag{2.16}$$

where A is the absorbing atom, Q is the quenching molecule, and A* and Q* represent the excited states. This reaction is governed by

$$\frac{d[A^*]}{dt} = I_{abs} - k_1[A^*] - k_2[A^*][Q] \tag{2.17}$$

where I_{abs} is the absorbed light intensity, k_1 is the emission rate constant for the atom and k_2 is the rate constant for the collision of the excited atom and molecule Q. The electronic energy of the atom can be transferred to the quenching molecule as electronic, vibrational, rotational or translational energy. For electronic to electronic transitions, the energy stored in the atom must be close to the energy taken by the molecule. In steady state, Eqn. (2.17) can be solved to yield the fraction of excited

atoms which transfer energy to the molecules as[25]

$$\frac{\text{no. of molecules excited}}{\text{no. of atoms excited}} = \frac{k_2/k_1[Q]}{1 + k_2/k_1[Q]} \tag{2.18}$$

As mentioned earlier, photonic interaction may involve surface-adsorbed species as well as the substrate itself. Optical excitation of the adsorbate-surface system may lead to photodissociation, photodesorption and photoreaction of the adsorbed species arising from thermal and non-thermal effects.[26] Photo-induced effects on the adsorbate may differ from those for gas phase species due to the interaction with the surface. Basically, either the adsorbate or the substrate can absorb the radiation with thermal and non-thermal processes possible with both.

The optical absorption by the adsorbed species closely resembles that of the gas phase species for weakly coupled adsorbate-surface systems. The electronic absorption spectra is generally shifted with most of the vibrational structure absent due to the reduced lifetime of the vibronic states as the adsorbed species interacts with the surface.[27] The direction of the spectral shift is determined by the interaction energy difference between the excited state and the ground state. If the excited state interacts more strongly with the adsorbent, the spectrum shifts to the red. Otherwise, a blue shift results. In addition, new absorption bands may appear for the adsorbed species indicating that a chemical change of the adsorbed species has taken place.

The result of excitation of the adsorbate depends on the nature of the interaction between the adsorbate and the substrate surface. For a metal substrate, energy transfer from the excited adsorbate to the substrate is rapid, quenching any possible fluorescence of the adsorbate, with substrate heating being the result. This rapid

energy transfer occurs as the metal has many available states corresponding to the same energy as the excited state of the adsorbate. For insulators and many semiconductors, the excited energy state of the adsorbed species lies within the energy gap of the substrate. As there are no available states at the appropriate energy, transfer will be inefficient with the result being the fluorescence or photochemical change of the adsorbate. In this case, little substrate heating due to energy transfer from the adsorbate to the substrate will occur. However, if the excited energy state of the adsorbate overlaps the conduction band of the substrate, interaction can readily take place. A similar situation results if an empty state of the excited adsorbate overlaps the valence band of the substrate.

It is clear that both thermal and non-thermal effects can result from adsorbate optical absorption. For substrate absorption, the most obvious result is simple heating. However, direct interaction between the photo-generated electron-hole pairs and the adsorbate-surface complex may also occur. This latter process, although not well understood, is generally viewed as being non-thermal in nature.

Each of these photo-induced processes occurring at the surface may produce similar photochemical results. These processes can, however, be distinguished by observing the time dependence as well as the wavelength dependence of certain photo-induced processes such as photodesorption.[28] Non-thermal processes are inherently faster than thermal processes allowing a distinction between them. In addition, the wavelength dependence of the process should be similar to either the optical absorption of the substrate or the adsorbate indicating which is absorbing the photons. Using these arguments along with ultra high vacuum analytical techniques such as

photo-induced desorption, thermal desorption and electron energy loss spectroscopy, these photo-induced processes have been observed and identified.[28]

2.3 Review of Photochemical Vapor Deposition of III-V Compound Semiconductors

In the previous sections of this Chapter, we have discussed the mechanisms involved in conventional organometallic chemical vapor deposition of GaAs as well as the physics of interaction of light with chemical systems relevant to OMCVD. In the remainder of this Chapter, discussion will be given to various efforts reported in the literature on the use of light to enhance or drive deposition processes. There are several reviews given in the literature discussing photochemical vapor deposition of various semiconductor elements and compounds as well as discussion of PCVD of insulators and metals relevant to semiconductor processing.[29–37] The discussion in this section, however, will be limited to the interaction of optical radiation with the growth and/or deposition of III-V compound semiconductors as well as the elements making up these compounds.

The optical absorption spectra of many reactants used in OMCVD of GaAs have been reported in the literature. The onset of absorption by AsH_3 has been reported to begin at 239 nm extending into the ultraviolet.[38] The maximum in absorption is at 183 nm resulting in predissociation of the molecule forming AsH_2.[39] A second electronic transition is given by

$$\nu(cm^{-1}) = 62{,}453 + 421.5n' + 5.94n'^2 \qquad (2.19)$$

$$(n' = 0,1,2,...,11)$$

At room temperature, the absorption was measured to be 4260 l/mole-cm at 190 nm with significant absorption extending to 210 nm.[40] In addition, the photolysis of AsH_3 has been studied using 193 nm excimer laser radiation along with photo- fragment excitation spectroscopy and is shown to produce AsH_2 detected by the $\tilde{A}^2A_1 \rightarrow \tilde{X}^2B_1^2$ emission (420 - 650 nm).[41] Decay time for the excited AsH_2 was found to be 130 ns at 20 mTorr AsH_3. It was shown that total photodecomposition of AsH_3 requires two 193 nm photons involving sequential two-photon absorption. The optical absorption for AsH_2 has also been measured and found to coincide with the expression[42]

$$\nu(cm^{-1}) = 19{,}905.9 + 854.5n' + 3.1n'^2 \qquad (2.20)$$

$$(n'=0,1,2,...,6)$$

The UV absorption spectra has also been measured for a number of useful organometallic compounds.[43,44] The UV absorption spectra for TMG, TEG, TMAs and TEAs have, in fact, been measured as a function of temperature.[43] The absorption cross-section for TMG at room temperature was found to be $9x10^{-17}$ cm^{-2} and $2.15x10^{-18}$ cm^{-2} at 193 and 248 nm, respectively. Little shift in the absorption spectrum is noted at higher temperatures. For TEG, the absorption cross-section was found to be $9x10^{-18}$ cm^{-2} and $5x10^{-18}$ cm^{-2} at 193 and 222 nm, respectively, with negligible absorption at 248 nm. Again, no shift in the absorption spectrum was noted at elevated temperatures. For TMAs and TEAs, a slight red shift in the absorption has been observed at elevated temperatures. For TMAs, absorption cross-sections of $4.46x10^{-17}$ cm^{-2} and $1.6x10^{-18}$ cm^{-2} were determined at 193 and 248 nm, respectively. For TEAs, the absorption cross-section was found to be $1.76x10^{-17}$ cm^{-2} and $1.2x10^{-18}$ cm^{-2} at 193 and 248 nm, respectively. The absorption spectra for certain

Al- and In- based organometallics have been determined as well.[44]

The first report of light-assisted chemical vapor deposition of GaAs involved the use of a Hg lamp.[45] Trimethylgallium and arsine were utilized with a radiation flux of 1 W/cm^2 for wavelengths between 240 and 320 nm. It was found that the growth rate was enhanced at 450°C with a substantial improvement in morphology. Similar work has been reported for OMCVD using TMG, TEG or triisobutylgallium with arsine utilizing a low pressure Hg lamp in which the majority of the radiation occurs at 254 nm.[15,46,47] Similar results were reported with improved morphology and crystal quality being the principle effects observed. The growth rate is significantly affected by the ultraviolet radiation only within the kinetically-controlled growth regime for all three gallium reactants. Interaction of the UV radiation with the reactants (gas-phase or surface-adsorbed) accounts for the enhanced deposition although the mechanisms for improved morphology are not known.

In and InP have been deposited using a Xe arc lamp.[48,49] The Xe arc lamp was found to have little effect on growth rate observed for InP grown at 550°C using trimethylindium and triethylphosphorus. However, morphology was greatly improved. Indium was photodeposited on pyrex and GaAs substrates from trimethylindium and indium cyclopentadienyl. Carbon was found to be present in the films. Gallium was also deposited with the Xe arc lamp utilizing trimethylgallium as the reactant.

Aluminum has been photodeposited with microwave-excited rare gas lamps, emitting in the vacuum UV, using trimethylaluminum.[50] Patterned deposition was obtained with masking. Application of an electric field perpendicular to the substrate enhanced deposition indicating that ionization was occurring.

For photolytically-driven chemical vapor deposition, the most useful laser source is the excimer laser. InP was first deposited using an ArF (193 nm) excimer laser with $(CH_3)_3InP(CH_3)_3$ and $P(CH_3)_3$ serving as the reactants.[51] Deposition was carried out with parallel, perpendicular and low-angle incidence geometry with quartz, InP and GaAs serving as the substrates. Growth was due to photolytic mechanisms with the substrate temperature below that necessary for pyrolytic decomposition. Emission from atomic In was observed for an unfocused laser beam presumably formed by sequential two-photon absorption by the reactant. With the laser focused, emission from CH is observed revealing multiphoton dissociation of hydrocarbons. The total dissociation of $P(CH_3)_3$ requires three 193 nm photons. Emissions from P, C and CH were detected only with focused laser irradiation with single photon absorption by $P(CH_3)_3$ yielding $P(CH_3)_2$ and CH_3. Stoichiometric InP was deposited on room temperature substrates for both perpendicular and glancing incidence beam geometry. Again, morphology of the deposited film was much better within the beam spot location than outside. In addition, no carbon was detected in photodeposited films in which the light was incident on the substrate. Outside the laser beam spot location, however, the carbon content was approximately 40% indicating that photodesorption of the hydrocarbons occurs. Although surface irradiation was necessary for good film quality, the thickness of the deposited film both inside and outside the beam spot was approximately the same indicating the importance of gas-phase photolysis. Characterization of the InP films photodeposited on InP substrates indicates that the region of the deposit directly exposed to the laser with an energy density per pulse of 0.1 J/cm^2 was single crystal as determined by Rutherford backscattering.[52] Outside the beam spot

location, the films were polycrystalline or amorphous. It appears that in-situ annealing of the growing film occurs with each laser pulse.

In a similar manner, GaAs has been deposited on GaAs and Si substrates using the ArF laser with trimethylarsenic and trimethylgallium serving as the reactants.[53] In-situ cleaning of the substrates was carried out by laser irradiation of the surface in either $As(CH_3)_3$ or BCl_3 atmospheres. It was found that, although the film morphology was greatly improved by direct irradiation of the substrate surface, single crystal growth did not occur for substrate temperatures up to 343°C with the carbon content for the deposited film being 1-3%. Sequential photon absorption by the reactants was assumed to be necessary for complete dissociation of the reactants.

Nishizawa et al. have studied the photodecomposition of trimethylgallium and arsine using an excimer laser at various wavelengths (193, 248, 308 and 351 nm) with infrared absorption spectroscopy utilized to identify changes in the gas-phase composition.[54] It was found that, with 193 or 248 nm radiation, photodecomposition of TMG produces ethane presumably from the recombination of methyl radicals produced. For AsH_3, decomposition occurs with 193 nm radiation. However, with 248 nm radiation, decomposition occurs only in the presence of silicon wafers suggesting a shift in the absorption spectrum for the surface-adsorbed species. For the TMG-AsH_3-H_2 system, photodecomposition of both reactants occurs with both 193 and 248 nm radiation with the generation of methane. The enhancement of the photodecomposition of AsH_3 in the presence of TMG suggests an interaction between the reactants.

Photodeposition of GaAs, AlAs and GaAlAs on Ge has been studied using the Lewis acid-base adducts trimethylgallium-trimethylarsenic and trimethylaluminum-

trimethylarsenic with 193 and 248 nm radiation.[55] Stoichiometric amorphous GaAs was deposited at 300°C with parallel 193 nm laser radiation. With 248 nm radiation, the films were arsenic deficient due to poor absorption by TMAs. Perpendicular incidence results in non-stoichiometric gallium-rich films with desorption of As competing with deposition. For perpendicular laser incidence, the maximum substrate temperature was estimated to be approximately 600°C. For AlAs, non-stoichiometric films resulted for all configurations although Al and As were deposited. Stoichiometric AlGaAs was possible only with parallel beam geometry at 193 nm. Auger electron spectroscopy revealed approximately 5% carbon in the films.

The interaction of excimer laser radiation (193, 222, 248, 308 and 351 nm) with chemical beam epitaxy of GaAs, Al and AlAs has also been studied.[56,57] Enhancement of the surface kinetics using a wide range of organometallic reactants has been achieved with no observable dependence on wavelength. When depositing Al from triisobutylaluminum, deposition occurred only at the laser beam location for substrate temperatures in the vicinity of 200°C.

The photodecomposition of trimethylaluminum leading to Al film deposition has been studied by several workers. A study comparing the fragmentation difference between photolytic and pyrolytic decomposition of trimethylaluminum using Fourier transform infrared spectroscopy has indicated that photolysis of trimethylaluminum yields C_2H_6 through the coupling of methyl radicals.[58] There is some debate, however, as to whether ethane is formed through direct extraction from the molecule or by recombination of the methyl radicals after photodecomposition. Studies reported by Motooka et al. on the photolysis of trimethylaluminum with 248 nm radiation suggests

that photodecomposition occurs by sequential absorption with subsequent elimination of methyl radicals.[59,60] Time-resolved fluorescence studies have indicated the presence of CH due to photolysis of hydrocarbons. The aluminum films were found to contain carbon for deposition temperatures of 30-200°C.

Selective nucleation of aluminum has been demonstrated through photolysis of adsorbed triisobutylaluminum with a 248 nm excimer laser.[61] Surface adsorbates are photochemically decomposed leaving highly reactive Al sites. With subsequent heating to 250°C in the presence of the reactant, growth proceeds only on these preferred sites in the absence of UV radiation. This technique has been applied to obtaining source, drain and gate metallization for a MOSFET. Post- annealing at 450°C was found to improve the quality of the aluminum films.

The photodecomposition of trimethylgallium with 248 nm radiation has been studied in detail using laser-induced fluorescence.[62] Using spatially-resolved and time-resolved fluorescence, it was found that, for the laser beam perpendicular to the substrate, decomposition of the surface-adsorbed molecules is the dominant process. There was also evidence that the decomposition involved thermal as well as photolytic mechanisms.

In addition to the interaction of excimer laser radiation with OMCVD systems, the enhancement of chloride-based vapor phase epitaxy with this light source has also been investigated.[63] Interaction of the radiation source with both the source and growth zones was studied with both enhanced and inhibited growth observed depending upon where in the reaction chamber the radiation interacts with the chloride-bearing species.

Another laser system which has been extensively used for III-V compound semiconductor deposition is the Ar ion laser. Bedair et al. have studied selective direct-writing of GaAs, InGaAs and GaAsP.[64,65] Deposition was achieved on Si and GaAs substrates with trimethylgallium, triethylindium, arsine and phosphine serving as the reactants. The Ar ion laser was focussed to a spot size of approximately 20-30 μm with deposition carried out at 350°C. Note that no deposition occurred in the absence of light with 1 watt of optical power necessary before deposition proceeds. Growth rate was found to be quite high due to three-dimensional mass transfer. Both photolytic and pyrolytic mechanisms appear to be involved in the deposition process with significant substrate heating occurring at the beam spot location. Similar results have been reported by other workers.[66] An interesting aspect of this work was that the growth rate depends on the carrier type of the substrate with the growth rate on n-type GaAs measurably higher than that obtained for semi-insulating or p-type substrates.[67,68] This suggests a mechanism involving the interaction of charge carriers in the substrate with the adsorbate. It was also indicated by experiments involving the sequential injection of the individual reactants that the laser radiation interacts with the TMG with little interaction of the radiation with the arsine molecules.

The first optical device fabricated using photochemical vapor deposition was a light-emitting AlGaAs bar deposited with an Ar ion laser.[69] It was found that the wavelengths emitted by the bar were position-dependent as the Al content was position-dependent. For the fabrication of this device, the laser was operated with an output of 1.2 watts with a 1.0 mm spot size.

Frequency-doubled Ar ion laser output producing 257.2 nm radiation has also

been utilized to deposit semiconductor material. In one study, photonucleation of Al was achieved on quartz using this light source.[70] Subsequent growth was carried out using a CO_2 laser to heat the quartz substrate leading to pyrolytic decomposition of tri-isobutylaluminum. Gallium has also been deposited utilizing this light source.[71]

A frequency-doubled Nd-YAG laser (530 nm) has also been utilized to study light-assisted OMCVD of GaAs.[72,73] Single crystal GaAs was grown at 450°C. Trimethylgallium and AsH_3 served as reactants. Surface adsorption of the reactants between laser pulses was found to be quite important in this growth regime. A mesa diode and a photoconductive detector were fabricated using this technique.

In addition to the above mentioned light sources, a limited amount of work has been reported on the use of a CO_2 laser for photodeposition of GaAs.[74] In this study, a pulsed CO_2 TEA laser was used with TMG and AsH_3 serving as the reactants. The laser was tuned to the AsH_3 P(12) line of the 9.6 μm branch. The substrate temperature was varied between 500 and 700°C. For the kinetically-controlled growth regime, morphology improved and electronic properties degraded in the presence of the radiation during growth.

CHAPTER 3

EXPERIMENTAL APPARATUS AND PROCEDURE

The experimental apparatus used in this work is shown in Fig. 3.1. It primarily consists of a modified version of a Tylan PVD 1000 reactor. The gas handling system as well as the reactor chamber was constructed of stainless steel. A 27 CFM rotary pump provided for a pressure range of 20 to 3000 mTorr with pressure controlled by flowing N_2 into the vacuum side of the rotary pump very near the pump intake. Pressure was measured using a thermocouple gauge as well as a capacitance manometer. Flow rates were controlled by electronic mass flow controllers. The Hg bubbler was held at room temperature while the organometallic bubbler temperature could be varied from -30 to 50°C. The details of the deposition chamber will be discussed within each Chapter as significant modifications of the chamber were necessary for different experiments performed. Also, the safety system pertaining to these experiments is described in Appendix A.1.

The reactants used in these experiments were 10% arsine mixture in 99.995% pure hydrogen, 99.999% pure triethylgallium and 99.995% pure Hg. Ultra high purity nitrogen was used as the carrier gas for the triethylgallium with ultra high purity hydrogen serving as the carrier gas for the Hg vapor unless stated otherwise. Window purging when utilized was performed using ultra high purity nitrogen unless specified otherwise.

A variety of substrate materials were utilized for the various experiments including commercial grade quartz and synthetic fused silica of 1.6 mm thickness,

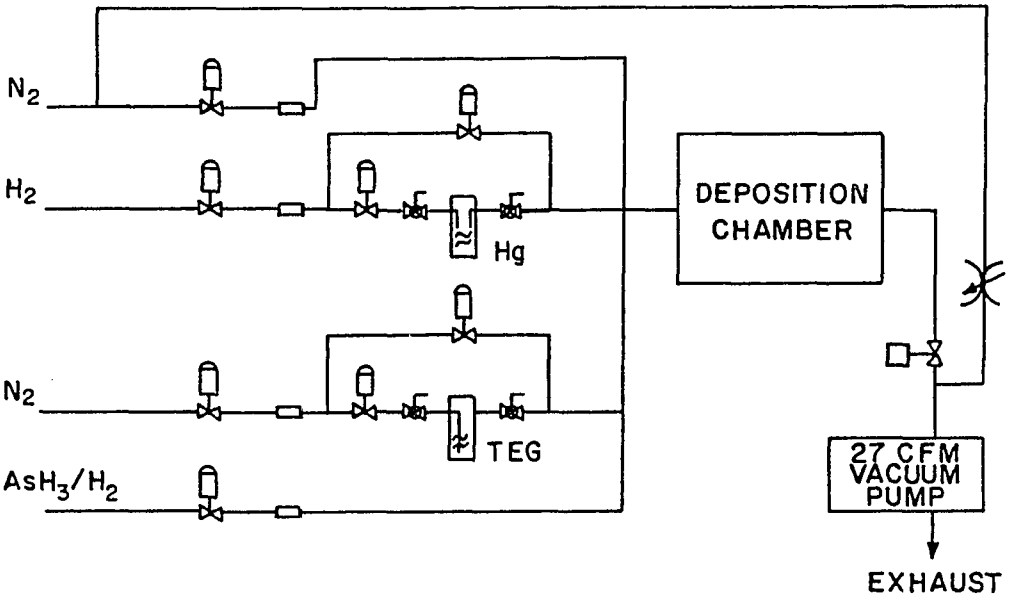

Figure 3.1 Schematic of Experimental Apparatus.

(100) Cr-doped GaAs of 0.4 mm thickness as well as (100) and (111) n-type silicon of 0.31 mm thickness. All of the substrates were degreased in hot trichloroethylene and acetone baths. For the quartz and fused silica substrates, this was followed by successive ultrasonic cleaning in laboratory detergent, deionized water, methanol, acetone, trichloroethylene, acetone and methanol baths. The substrates were stored in methanol and blown dry with prepurified nitrogen prior to loading into the reactor. For the GaAs substrates, the trichloroethylene and acetone baths were followed by a 5 minute etch in H_2SO_4:H_2O_2:H_2O in ratio of 8:1:1 by volume. This was followed by rinsing in distilled water and methanol. Again, substrates were blown dry prior to loading into the reactor. A similar treatment was afforded the Si substrates except that a 10% HF solution was chosen as the etchant.

For each deposition experiment, the deposition system was flushed with ultra high purity nitrogen for 30 minutes and subsequently vacuumed to a low pressure for 30 minutes. At this point, the reactant gas flows were initiated and light sources switched on. As will be described in later chapters, three different light sources were utilized at various stages of this work. For the mercury-photosensitized experiments, a low pressure Hg grid lamp was utilized. This light source emits a line spectrum with the majority of its output at a wavelength of 254 nm making it ideal for the excitation of Hg atoms. A Hg-Xe arc lamp was also used in some portions of this study. The Hg-Xe arc lamp, whose optical output as a function of wavelength is shown in Fig. 3.2, is a broadband light source emitting continuous radiation from approximately 210 nm through the near-infrared. In addition to the above mentioned continuous-wave light sources, an ArF excimer laser (193 nm) was utilized for some of the work

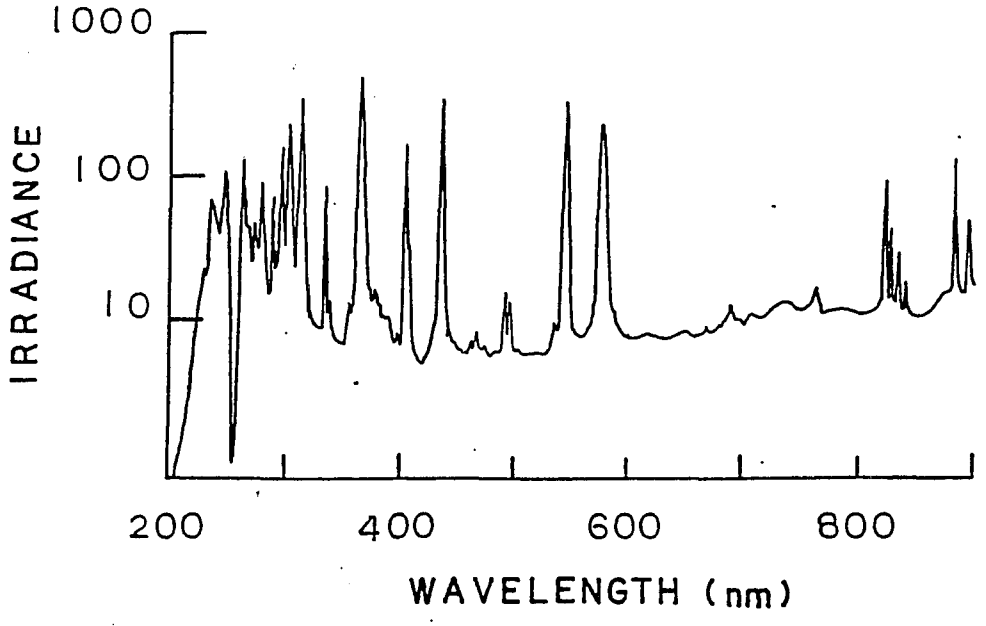

Figure 3.2 Relative Spectral Output of the Hg-Xe Arc Lamp.

reported in Chapter 6.

A sub-microgram electro-balance was used to obtain the deposition rate by means of mass gain of the substrate. A stylus surface profiler was also utilized to determine film thickness. For the GaAs thin films deposited on GaAs substrates, film thickness was determined with an optical microscope using a cleave and stain technique. The film thickness for the GaAs deposited on silicon was determined using a scanning electron microscope image of the film cross-section. The electrical properties of the films on insulating substrates were determined using van der Pauw mobility and carrier concentration measurements. In addition, the deposited films were also characterized using scanning electron microscopy (SEM), energy-dispersive spectrometry (EDS), Auger electron spectroscopy (AES), X-ray photoelectron spectroscopy (XPS), cold vapor atomic absorption spectroscopy, optical transmittance and X-ray diffraction.

CHAPTER 4

MERCURY-PHOTOSENSITIZED CHEMICAL VAPOR DEPOSITION OF ARSENIC THIN FILMS

4.1 Introduction

Mercury-photosensitized decomposition of arsine resulting in the formation of arsenic on the chamber walls was first reported by Simmons and Beckman in 1936.[75] Since then, however, little work has been done to understand the processes involved in the deposition of arsenic using this technique. Although extensive studies have been reported on the properties of arsenic thin films deposited by other techniques such as sputtering or evaporation,[76,77] an extensive literature search failed to reveal any work reporting on the properties of arsenic films deposited by means of mercury-photosensitization of arsine. In this Chapter, the preparation of arsenic thin films on quartz substrates by means of mercury-photosensitized decomposition of arsine is examined. The properties of the arsenic films obtained using this technique are measured and discussed. The motivation in looking at Hg-photosensitization of arsine stems from its potential use as a technique in low temperature deposition of gallium arsenide as will be discussed in Chapter 5.

The reactor chamber, shown in Fig. 4.1, is made of stainless steel with a commercial-grade fused quartz plate serving as an optical window. The substrate holder was heated by four internal infrared lamps. The ultraviolet light source consisted of six 100 watt low pressure mercury lamps arranged in a grid. These lamps possess strong spectral output at 253.7 nm with virtually no output at 184.5 nm.

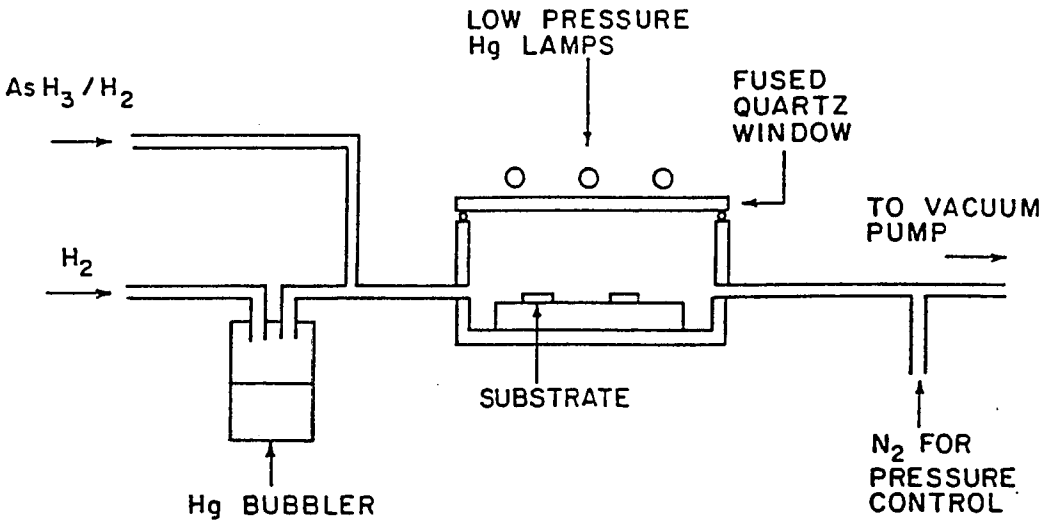

Figure 4.1 Schematic of Reactor Chamber Utilized for Hg-Photosensitized Chemical Vapor Deposition of Arsenic Thin Films.

Attenuation of the light by arsenic deposition on the window was effectively controlled by applying a thin coating of perfluorinated polyether fluid to the inside of the window prior to film deposition. A 10% arsine in ultra high purity hydrogen was used as the arsenic source. The mercury bubbler was maintained at room temperature. Commercial-grade quartz was used as the substrate material.

4.2 Arsenic Film Preparation

Hg-photosensitization of arsine involves dissociation of arsine molecules through collisions with the photo-excited Hg atoms. Since the principal mechanism for dissociation does not involve thermal energy, arsenic deposition is possible at low temperatures. The substrate temperature is not expected to significantly affect the Hg-photosensitized process. However, since collisions are necessary between the excited mercury atoms and the arsine molecules for energy transfer, pressure will affect the molecular decomposition process. Figure 4.2 shows the deposited arsenic film thickness as a function of total chamber pressure. The fractional composition of the reactants was held constant during these measurements while the total pressure was varied by changing the pumping rate of the mechanical pump. This plot clearly indicates an increase in the deposition rate with increasing chamber pressure. This can be attributed to a decrease in the mean free path for arsine molecules colliding with excited mercury atoms as well as an increase in the arsenic-bearing radicals colliding with the substrate with an increase in pressure. In addition, a decrease in the fluorescence of excited mercury atoms with increase in pressure can also contribute to an increase in the arsine decomposition rate.[75,78]

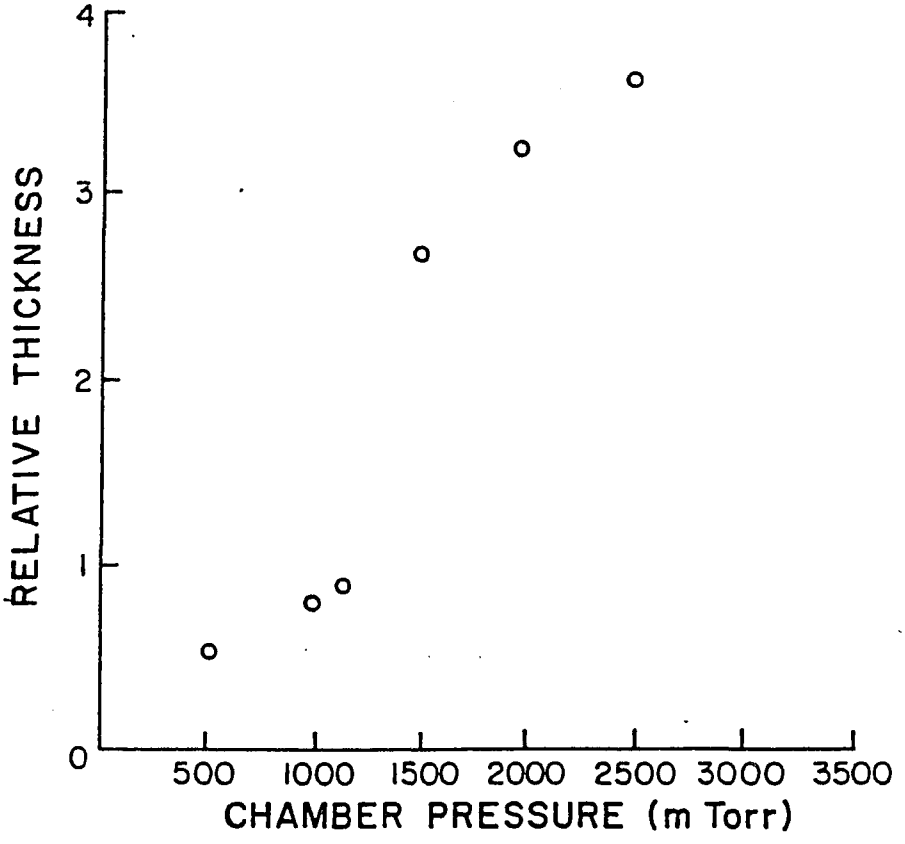

Figure 4.2 Arsenic Film Thickness as a Function of Total Chamber Pressure. Substrate Temperature Equals 50°C with 10% AsH_3 in H_2 Flow Rate Maintained at 41 sccm. Deposition Time is 60 Min.

Dependence of the deposition rate on the arsine partial pressure, P_{AsH_3}, with the total pressure held constant is shown in Fig. 4.3. The dashed curve represents the experimentally observed values. As seen from this figure, for the range of P_{AsH_3} values considered, the arsenic deposition rate increases as the arsine partial pressure decreases. With total pressure held constant, the Hg partial pressure increases as the arsine partial pressure decreases. The deposition of arsenic by this technique results from the surface-catalytic decomposition of AsH_2.[9,75] The AsH_2 is formed by AsH_3 dissociation due to collisions with the excited Hg atoms. The behavior seen in Fig. 4.3 can be understood by considering the collision rates between gas-phase atoms and molecules as a function of pressure. If the rate-limiting step in the arsenic deposition is due to the gas phase kinetics, then the arsenic deposition rate should be linearly proportional to the partial pressure of AsH_2. If the reaction

$$AsH_3 + Hg^* \rightarrow AsH_2 + H + Hg \tag{4.1}$$

is the principal means by which AsH_2 is formed by the gas phase collisions, it follows that the deposition rate should be linearly proportional to the collision rate of the arsine molecules with the excited mercury atoms, Hg*. The collision rate, R_1, is given by[79]

$$R_1 = \sigma_{AsH_3-Hg^*}(8/\pi\mu)^{1/2}(1/kT)^{3/2}P_{AsH_3}P_{Hg^*} \tag{4.2}$$

where k is the Boltzmann constant, $\sigma_{AsH_3-Hg^*}$ is the effective collision cross-section, μ is the reduced mass, T is the absolute temperature and P_{Hg^*} is the partial pressure of Hg*. For low Hg partial pressure, P_{Hg^*} is linearly related to P_{Hg}. Although no reliable value for $\sigma_{AsH_3-Hg^*}$ is available, we can assume it to be of the same order of magnitude as for phosphine which is given by $26.2 \times 10^{-16} cm^2$.[78]

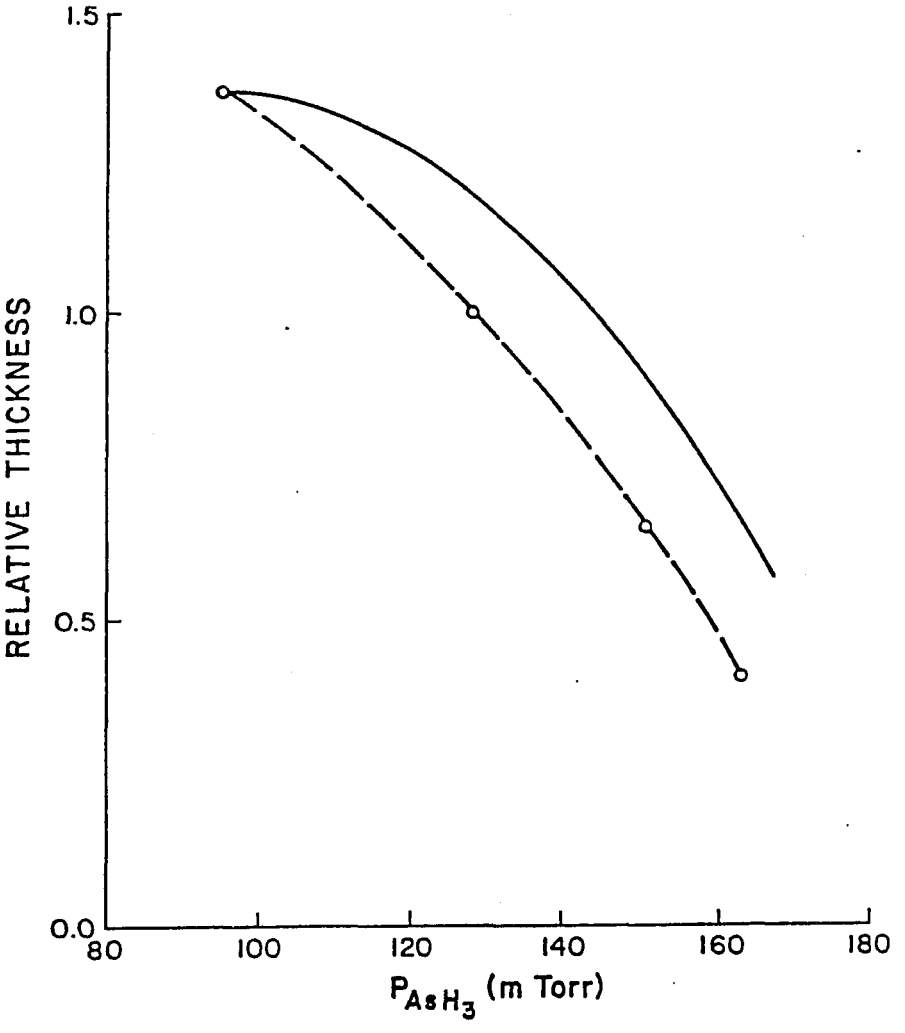

Figure 4.3 Arsenic Film Thickness as a Function of Arsine Partial Pressure. Total Pressure is maintained at 1900 mTorr. Substrate Temperature is 50°, and the Deposition Time is 1 Hour. The Solid Curve is for Calculated Values with the Dashed Curve Representing the Experimental Values.

The solid curve in Fig. 4.3 shows the calculated results based on the model described by Eqn. (4.1) taking into account the changes in both P_{AsH_3} and P_{Hg}. The total pressure is held constant for these calculations. The experimentally determined value of the deposition rate at P_{AsH_3} equal to 96 mTorr is chosen to empirically evaluate the constant of proportionality between Eqn. (4.2) and the deposition rate. The film thickness ratio as a function of P_{AsH_3} predicted by this simple model is seen to be in good qualitative agreement with the experimentally observed values. The fact that the slope of the experimental curve is slightly higher in magnitude than that predicted by the model can be explained by considering mechanisms for forming AsH_2 other than that given in Eqn. (4.1). Consider the reaction

$$H_2 + Hg^* \rightarrow 2H + Hg \tag{4.3}$$

$$H + AsH_3 \rightarrow AsH_2 + H_2 \tag{4.4}$$

The collision rate between H_2 and Hg* under the same deposition conditions as those described for Fig. 4.3 is more than 20 times that found for excited mercury atoms and arsine. This result is obtained by taking the collision cross-section of H_2 with Hg*, $\sigma_{H_2-Hg^*}$, to be $9.8 \times 10^{-16} cm^2$.[80] Significant formation of AsH_2 may result from this reaction. In the work previously reported by Simmons et al., atomic hydrogen did not appear to play a significant role in the formation of As as the ratio P_{H_2}/P_{AsH_3} in their work was much smaller than the values obtained in the work reported here.[75]

Another possible explanation for the differences between the predicted and observed values in Fig. 4.3 is given by considering the reactions

$$Hg^* + H_2 \rightarrow HgH^* + H \tag{4.5}$$

$$HgH^* + AsH_3 \rightarrow AsH_2 + H_2 + Hg \tag{4.6}$$

as first postulated by Compton and Turner.[80] Here, mercury hydride molecules interact with AsH_3 to produce AsH_2. However, as the lifetime of the HgH molecule is extremely short, it seems unlikely that this mechanism could account for the behavior noted.

Figure 4.4 shows the film thickness obtained as a function of deposition time for three different values of substrate temperature. As seen from this figure, the deposition rate decreases with increasing substrate temperature. This behavior is expected as the vapor pressure of arsenic is relatively high for the higher substrate temperatures considered. At these temperatures, the thermal decomposition of AsH_3 is not expected to be significant.[9] From Fig. 4.4, it is seen that the deposition rate is fairly constant after an hour of growth. The growth rate during the initial period, however, is seen to be higher than the rate obtained for times greater than one hour. This appears to be especially true for the 240°C substrate temperature case.

4.3 Film Characterization

The arsenic films were characterized using a variety of techniques including X-ray diffraction, X-ray photoelectron spectroscopy (XPS) and optical absorption. The crystallinity of the thin films as a function of deposition temperature was studied using a thin film diffractometer. The film deposited at 240°C consists of polycrystalline rhombohedral arsenic as seen from Fig. 4.5. The Miller indices of the peaks are given in this figure. The broad peak at 2θ value of approximately 21 degrees is from the quartz substrate. As seen from this figure, as the deposition temperature decreases, the presence of the rhombohedral phase diminishes with broad peaks appearing at approxi-

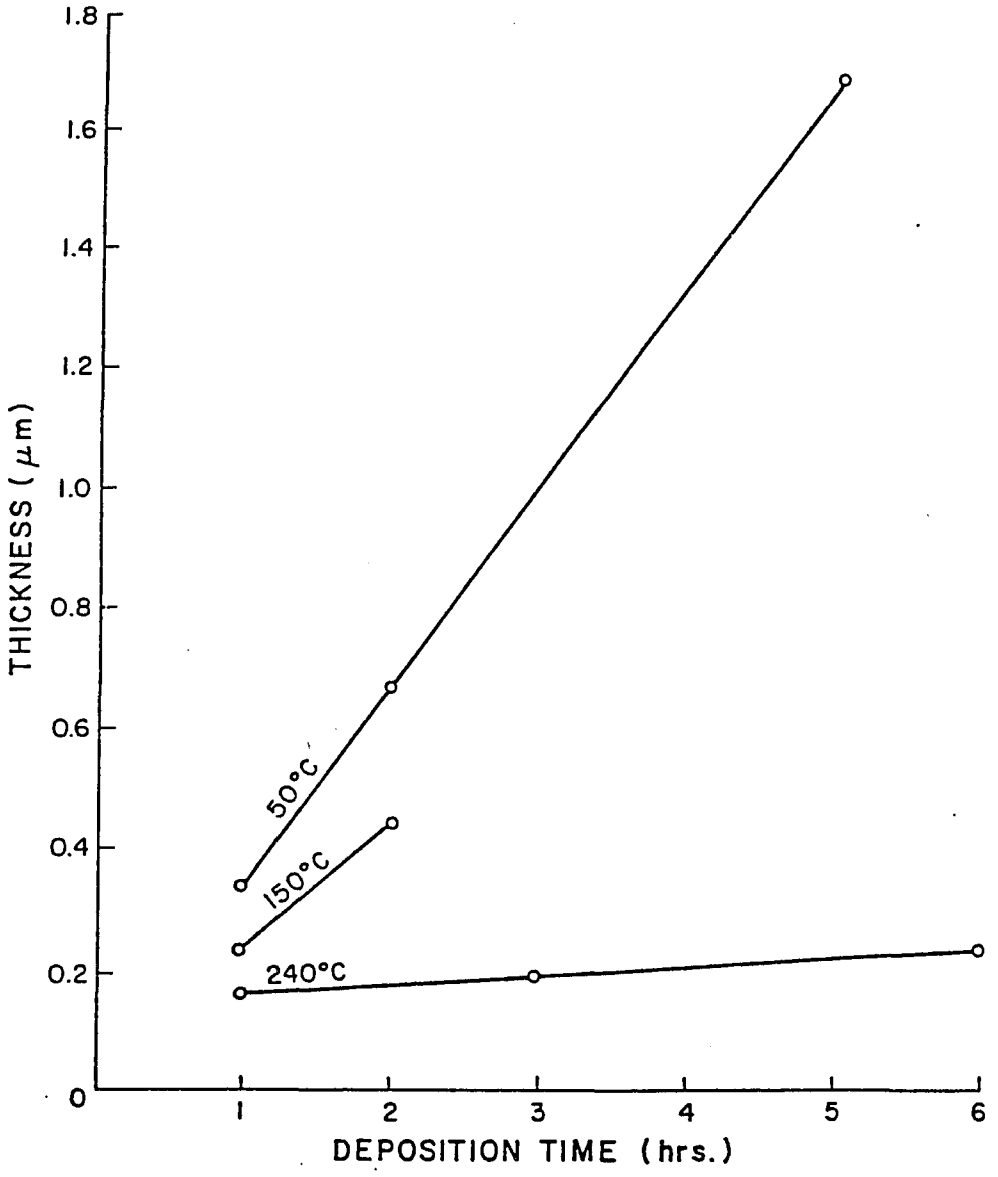

Figure 4.4 Arsenic Film Thickness as a Function of Deposition Time for Various Substrate Temperatures. Partial Pressure of AsH_3 and Total Pressure Equals 0.1 and 2 Torr, Respectively.

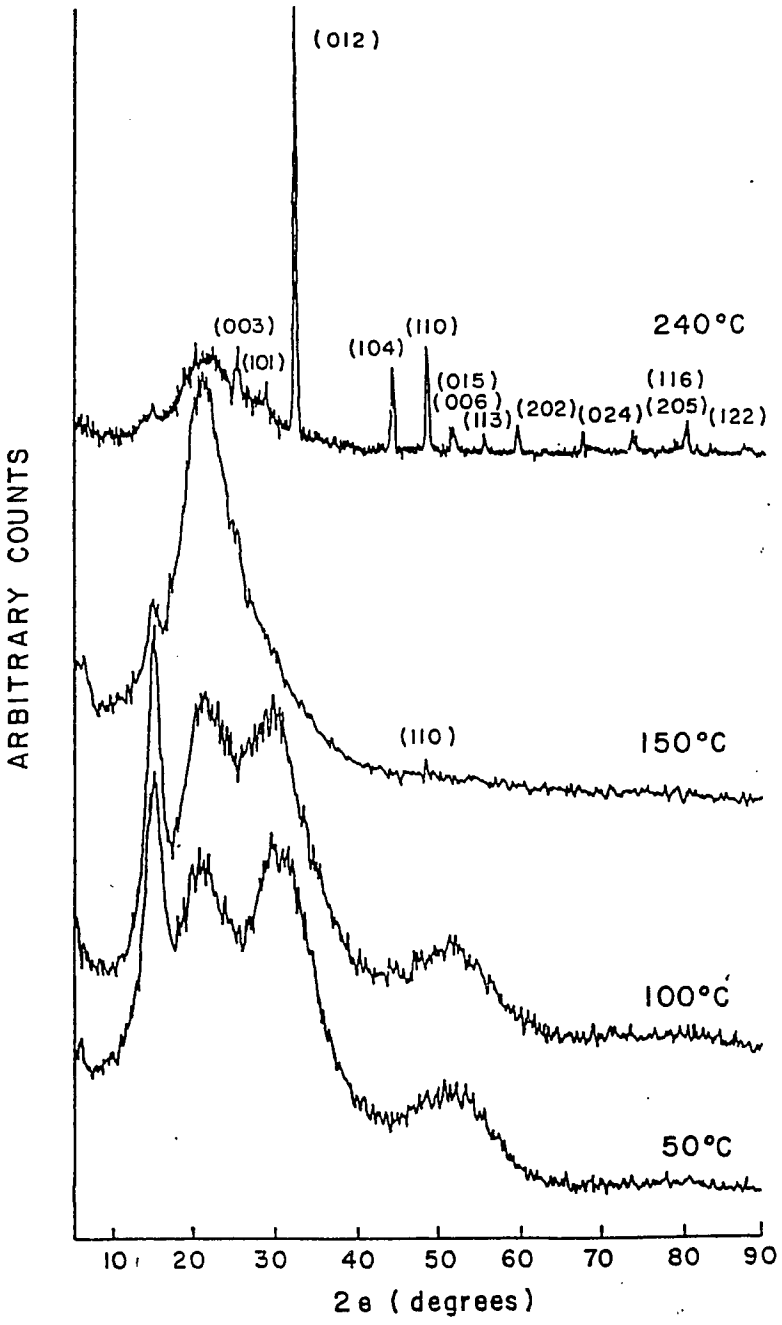

Figure 4.5 X-ray Diffraction Patterns for Arsenic Films Deposited at Various Temperatures. The Diffraction Patterns are Shifted Vertically and the 240°C Pattern is Compressed by a Factor of 3 for Clarity.

mate 2θ values of 15°, 31° and 52° which are characteristic of amorphous arsenic.[81,82] No rhombohedral peaks were observed for films deposited at temperatures of 100°C or less.

Films deposited at substrate temperatures of 150°C or less were highly specular with virtually no features present on the surface. However, films deposited at substrate temperatures of 200°C or more were not specular with some features present on the surface. Figure 4.6 shows a scanning electron microscope (SEM) image of the structures typical for arsenic films deposited at 200°C or higher. These structures appear to represent the rhombohedral phase indicated from the X-ray diffraction data. These column-like structures were several micrometers in height, as seen in the surface profile measurement in Fig. 4.7, even though the majority of the arsenic films were less than 1 μm in thickness. It appears that, once nucleated, the rhombohedral phase grows much faster than the amorphous phase. Although the X-ray diffraction data was inconclusive about the formation of rhombohedral arsenic at 200°C, the SEM micrographs suggest that the crystalline phase does begin to form at 200°C.

When left exposed to the air for a period of several days, As_2O_3 crystallites formed spontaneously on the surface of the arsenic films. Figure 4.8 shows a SEM micrograph of the oxide crystallites on the film surface. X-ray diffraction data confirm that these As_2O_3 are cubic in structure. From the stylus profile of the surface shown in Fig. 4.9, the oxide crystals are seen to be several micrometers in height. Similar results have been reported by Lau et al. for the formation of arsenic oxide on GaAs and arsenic-coated InGaAs.[83]

The arsenic thin films were also studied using X-ray photoelectron spectroscopy

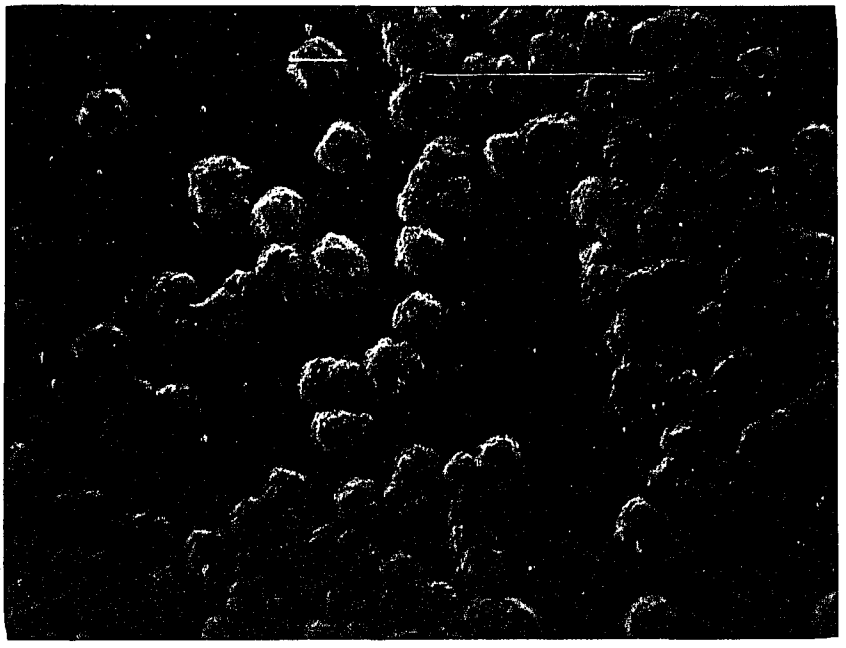

Figure 4.6 SEM Micrograph of Rhombohedral Phase Seen on the Film Surface. Longest Line Equals 10 μm.

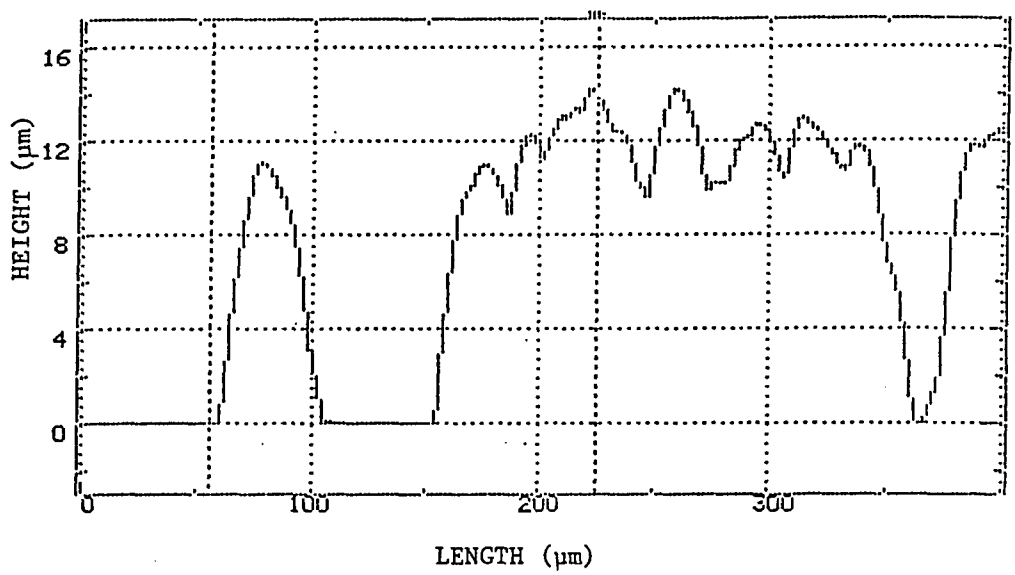

Figure 4.7 Surface Profile of Rhombohedral Arsenic Structures Present on Film Surface.

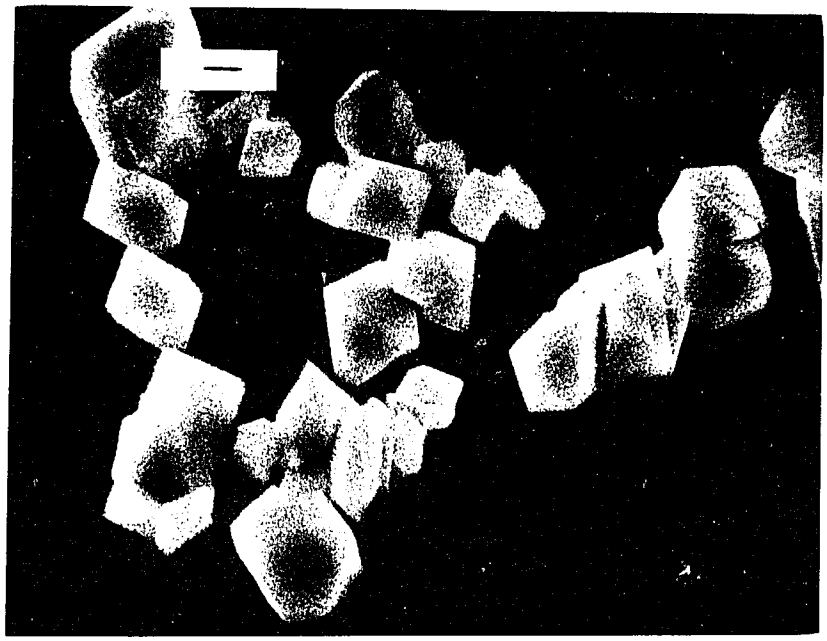

Figure 4.8 SEM Micrograph of As_2O_3 Crystals on the Arsenic Film Surface. Longest Line Equals 1 μm.

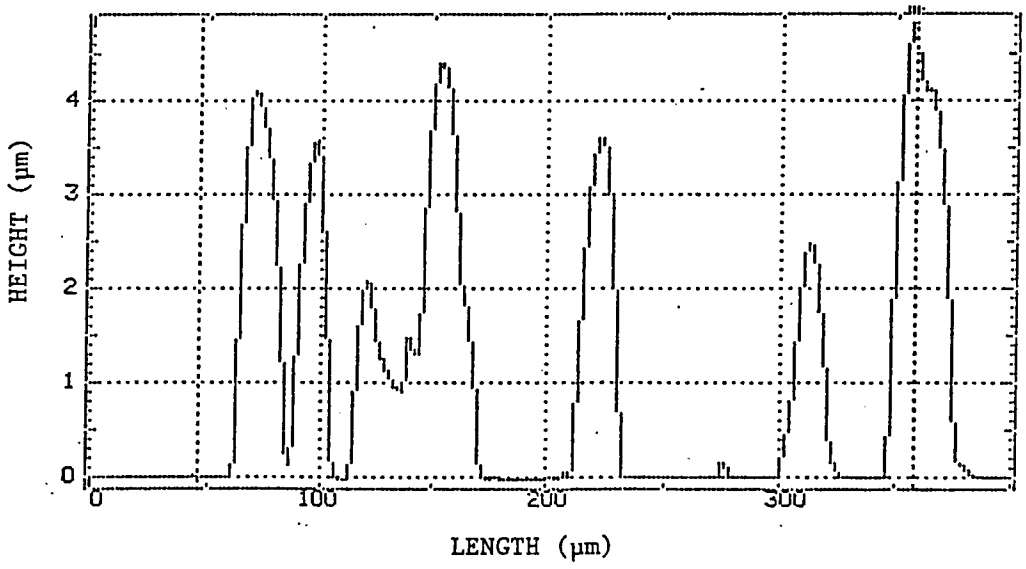

Figure 4.9 Surface Profile of As_2O_3 Crystals Formed on the As Surface After Prolonged Exposure to Air.

(XPS) measurements. Table 4.1 shows the location of the various peaks. In this work, 1253.6 eV MgKα radiation was used with the 284.6 eV carbon C1s peak used for calibration. The thin films were maintained in an ultra-high vacuum for several hours to allow desorption of the arsenic oxide prior to obtaining the spectra.[84] The values for the binding energies are in good agreement with those reported by Bahl et al.[85] There was no noticeable difference in binding energies for amorphous films as opposed to the rhombohedral films obtained at higher substrate temperatures.

An interesting observation was made in examining the structure of the valence band of the arsenic films using XPS. Figure 4.10 shows the three discernible peaks at approximately 1.3, 9.6 and 11.8 eV present in the XPS spectrum of an amorphous film. This differs somewhat from results reported by Ley et al. where discernible peaks are found at 3.53, 10.64 and 13.26 eV for the polycrystalline phase with the amorphous phase possessing a peak at 3.53 eV and a broad plateau extending from 12.5 eV to 9.5 eV with virtually no dip in intensity between the end points of the plateau.[86] The reason for this difference in the amorphous films is not clear.

Figure 4.11 shows a plot of the optical absorption coefficient, α, as a function of photon energy for the amorphous As films deposited by means of Hg-photosensitization of arsine. Substrate deposition temperature was maintained at or below 150°C to insure that the films were amorphous. Thin film interference effects were utilized to obtain absolute absorbance with a conventional transmittance spectrometer. The optical absorption coefficient for these films was found to be independent of the substrate deposition temperature for substrate temperatures of 150°C or lower. The absorption coefficients for these films were found to be less than those

Level	3s	$3p_{1/2}$	$3p_{3/2}$	3d
Binding Energy (eV)	205.0	145.5	140.8	42.0

Table 4.1 Experimentally Determined Binding Energies. Estimated Uncertainty is ± 0.3 eV.

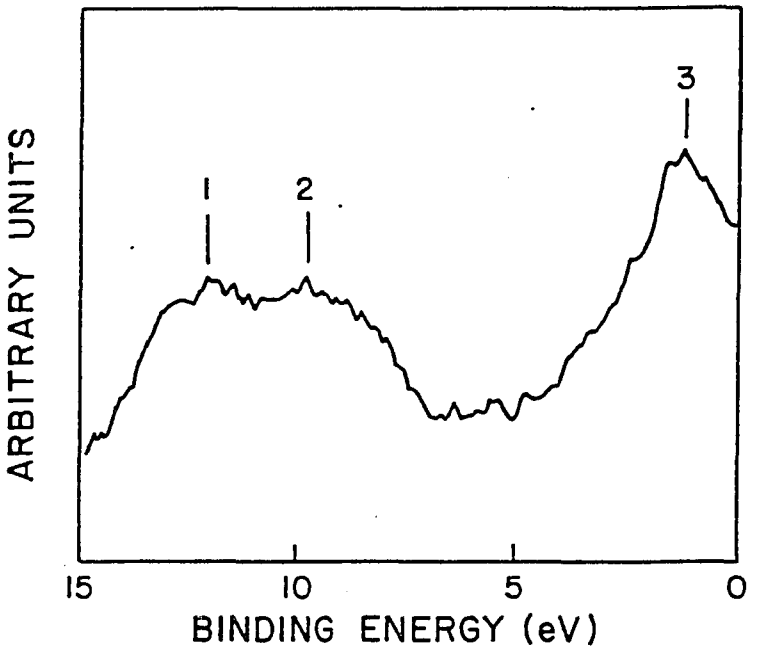

Figure 4.10 XPS Spectrum of Amorphous Arsenic Film Deposited at 50°C

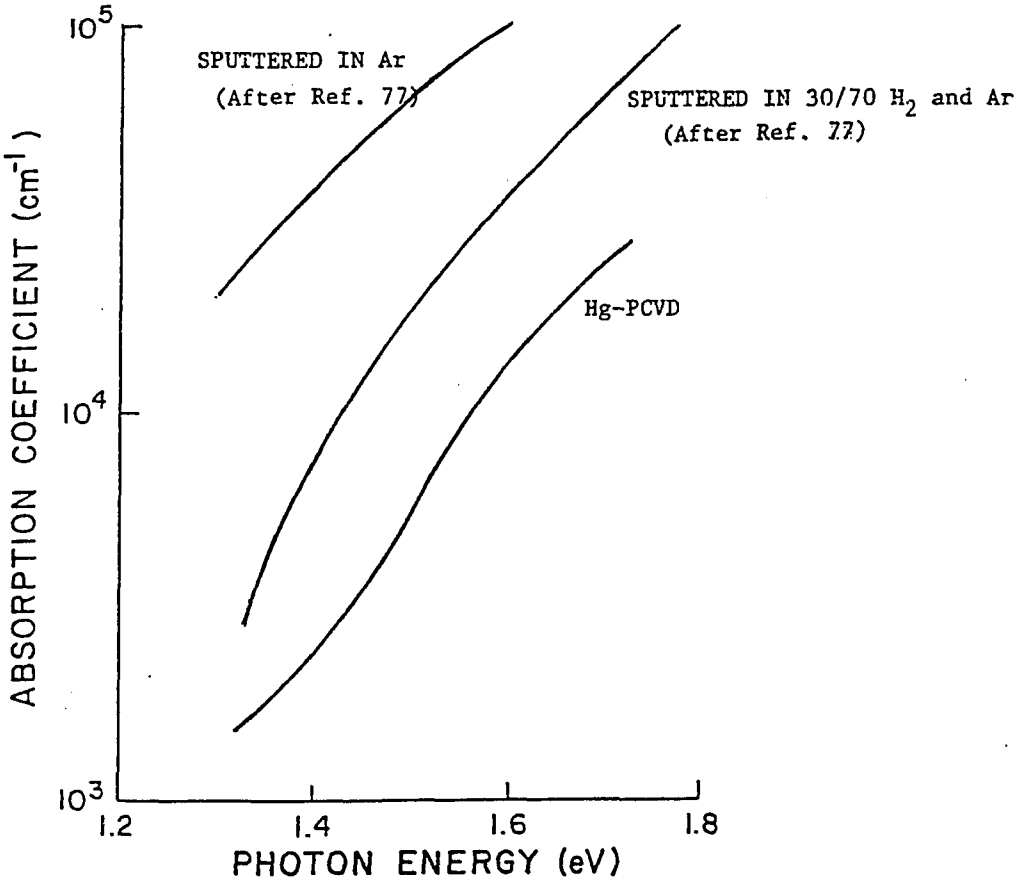

Figure 4.11 Optical Absorption Coefficient as a Function of Photon Energy for Amorphous Arsenic Thin Films.

reported for sputtered or evaporated amorphous arsenic thin films for the photon energies considered.[76,77] The reasons for this difference is not clear.

As mercury vapor is necessarily present in the deposition chamber during Hg-photosensitization, it is of interest to know the mercury content of the deposited arsenic thin films. From the XPS measurements, there were no indications of the Hg4f or Hg4d peaks. Using cold vapor atomic absorption spectrometry techniques, it was determined that the films deposited at 50°C contained approximately 0.1% Hg while the films deposited at 240°C contained only 40 parts per million Hg. This drastic decrease in the Hg content with increasing deposition temperature can be attributed to the high Hg vapor pressure values at moderately high temperatures. The fact that the Hg content was so low at only moderately high substrate deposition temperatures suggests that Hg-photosensitization may be useful in decomposing AsH_3 in arsine-based chemical vapor deposition of arsenic-bearing III- V semiconductor compounds.[87]

In conclusion, the preparation and properties of arsenic thin films obtained by means of mercury- photosensitized chemical vapor deposition have been reported here. X-ray diffraction studies of these films indicate that arsenic films obtained at 240°C are polycrystalline rhombohedral-phase with scanning electron microscopy images indicating the presence of rhombohedral-phase structures for films deposited at a temperature of 200°C and above. Our results show that deposition process behavior can be explained by considering the formation of AsH_2 as the rate-limiting step with the principal mechanism for obtaining AsH_2 being the gas phase collisions of excited mercury atoms with arsine molecules. In addition, the films obtained using this technique have been extensively characterized showing only minor differences between arsenic thin

films prepared by the method described here as compared to those obtained by other deposition techniques. The XPS spectrum of the valence band for the amorphous films obtained in this work contained slightly more structure than films deposited by other methods. In addition, it appears that the optical absorption coefficient for the amorphous arsenic films obtained by mercury-photosensitized chemical vapor deposition is lower than that for films obtained by means of sputtering or evaporation over the range of photon energy considered.

CHAPTER 5

HG-SENSITIZED PHOTOCHEMICAL VAPOR DEPOSITION OF GALLIUM ARSENIDE ON QUARTZ

5.1 Introduction

In this Chapter, we report on the deposition of GaAs on quartz substrates by photochemical means using Hg- photosensitization and photolysis. Although some work has been reported on the use of Hg-photosensitization to deposit silicon,[88,89] this is the first time that similar work has been reported for the deposition of GaAs. The particular technique developed here, referred to as Hg- sensitized Photochemical Vapor Deposition (Hg-PCVD), utilizes both Hg-photosensitization and photolysis to achieve deposition. Attempts to deposit GaAs by Hg-photosensitization alone were unsuccessful as will be discussed later. Polycrystalline GaAs deposition on quartz is accomplished at chamber temperatures below that necessary for any deposition to occur in the absence of light.

These experiments were carried out in the reactor chamber shown schematically in Fig. 5.1. This reactor is the same as that used for the work reported in Chapter 4 except that the substrates were mounted to the underside of the window with support from braided ceramic high temperature sleeving. The 1000 watt Hg-Xe arc lamp and 500 watt low pressure Hg grid lamp could be used simultaneously. The arc lamp output was focussed to a 0.64 cm diameter spot size using two ultraviolet(UV)-grade plano-convex lenses. A 10% mixture of arsine in 99.999% pure hydrogen and 99.999% pure triethylgallium (TEG) were used as the reactants. The triethylgallium

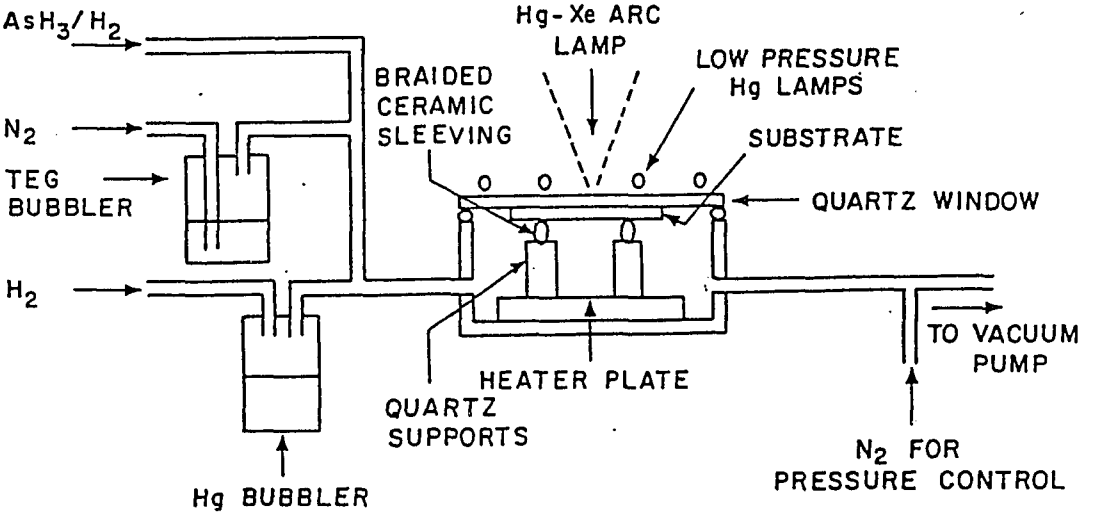

Figure 5.1 Schematic of Deposition Chamber Used to Deposit GaAs Utilizing Hg-Sensitized Photochemical Vapor Deposition.

was kept in a bubbler at -17°C. Mercury was kept in a bubbler at room temperature. Experiments were carried out with a total chamber pressure of 2 Torr. The gas flow rates were 10 sccm H_2 through the Hg bubbler and 5 sccm for N_2 through the TEG bubbler unless specified otherwise. The heater plate was maintained at 240°C for all experiments involving the use of both the arc lamp and the low pressure Hg lamps. Commercial grade quartz substrates were used.

5.2 Hg-Photosensitization

Initial experiments carried out to determine the effects of Hg-photosensitization on the AsH_3-TEG system used only the low pressure Hg lamps. It has been demonstrated in the preceding Chapter that the Hg-photosensitized decomposition of arsine proceeds as follows:[75]

$$Hg + h\nu(253.7nm) \rightarrow Hg^* \quad (5.1)$$

$$Hg^* + AsH_3 \rightarrow AsH_2 + H + Hg \quad (5.2)$$

$$AsH_2 \rightarrow As + H_2 \quad (5.3)$$

leading to the formation of As films. Here, Hg* represents the excited Hg atom and hν represents the photon energy. No experimental data are available, to our knowledge, on the effects of Hg-photosensitization on triethylgallium.

Experiments were carried out on the Hg-photosensitization of the AsH_3–TEG system for a variety of conditions including those found optimal for the Hg-photosensitized deposition of arsenic from AsH_3. The later experimental conditions include 2 Torr total pressure, 10 sccm flow rate for the 10% AsH_3 mixture in H_2 and 10 sccm flow rate for the H_2 through the Hg bubbler. The perfluorinated polyether

fluid could not be used to prevent window fogging as TEG reacts with this vacuum oil. It was found that the addition of triethylgallium flow to the chamber inhibited the film deposition rate significantly. The film thickness was estimated by measuring the mass gain of the substrate on a microbalance. For very thin films, optical transmittance was used to estimate the relative thickness values. From Beer's Law, the film thickness ratio is given by

$$\frac{x_1}{x_2} = \frac{\ln(I_1/I_0)}{\ln(I_2/I_0)} \tag{5.4}$$

where I_0 is the light intensity entering the samples and I_1 and I_2 are respectively the transmitted intensities from the two samples of thicknesses x_1 and x_2. The value for I_0 is determined from the incident light after taking into account the reflected component.

The film deposition rate from these thickness estimates did not exceed 10 nm/hr for the AsH_3-TEG system. This was at least five times less than the rate obtained for the deposition of arsenic from arsine under otherwise similar experimental conditions. Similar results were also obtained when the 10% AsH_3 in H_2 mixture flow rate was varied from 10 to 60 sccm. In addition, the deposition rate for the AsH_3-TEG Hg-photosensitized system was highest for a substrate temperature of 240°C with the substrate placed on the heater plate and nearly zero for a substrate temperature of 50°C. This behavior of increasing deposition rate with increasing temperature is opposite to that obtained for the Hg-photosensitized deposition of arsenic from arsine as shown in Fig. 5.2 where the deposition rate decreased with increasing substrate temperature. The deposition conditions for the points shown in Fig. 5.2 were 2 torr total pressure, 10 sccm flow rate for the 10% AsH_3 in H_2 mixture, 10 sccm flow rate for the H_2

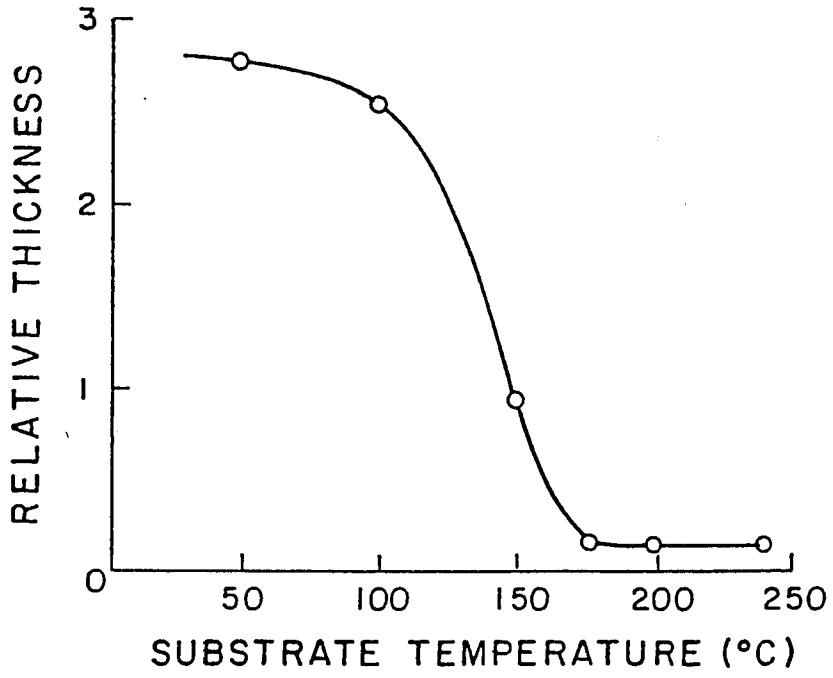

Figure 5.2 Arsenic Film Thickness as a Function of Substrate Deposition Temperature Obtained by Means of Hg-Photosensitization of Arsine.

through the Hg bubbler and 30 minutes deposition time. Optical transmittance through the deposited films was utilized to estimate the thickness ratios of these extremely thin films.

Energy-dispersive spectrometry was performed on these films obtained by means of Hg-photosensitization of the AsH_3-TEG system to obtain an approximate value for the composition of these very thin films. Results showed that the films obtained at a substrate temperature of 240°C were at least 80% arsenic by atomic concentration. This inhibition of the deposition rate with the addition of triethylgallium strongly suggests the formation of a volatile complex probably involving AsH_2 and TEG. This complex formed by means of the Hg-photosensitization process is apparently stable at temperatures less than 240°C and is unaffected by the low pressure Hg lamp radiation.

5.3 Hg-Photosensitization and Photolysis

The output of a 1000 watt Hg-Xe arc lamp was used in order to increase the film deposition rate. The Hg-Xe arc lamp possesses an optical output over the entire wavelength range from approximately 210 nm in the ultraviolet up through the near-infrared making it a good candidate in attempting photolytic processing on species with unknown spectral absorption properties. The quartz window used in this work, however, absorbed at least 70% of the radiation below 240 nm. In this portion of the study, the quartz substrates were mounted to the underside of the window as shown in Fig. 5.1. For this configuration, the radiation from the arc lamp must pass through the depositing film before participating in the photodecomposition process. In this case,

deposition due to photolysis in the gas phase will be determined by

$$\frac{dx}{dt} = KI'_o(1-R)\exp(-\alpha x) \tag{5.5}$$

where x is the film thickness, I'_o is the incident intensity, R is the film reflectance and α is the film optical absorption coefficient. Integrating this equation yields

$$x = \alpha^{-1}\ln(\alpha tKI'_o(1-R) + 1) \tag{5.6}$$

with the initial condition that x = 0 for t = 0. The temperature of the window-mounted substrates was not measured directly but was less than the heater plate temperature of 240°C at the onset of film growth. The introduction of the optical output from the arc lamp resulted in a substantial increase in the deposition rate compared to that obtained from using Hg-photosensitization only. The films were as thick as 40 μm for a deposition time of one hour. The size of the deposit was somewhat smaller than the Hg-Xe optical beam which was 0.64 cm in diameter. A surface profile measurement of a typical film is shown in Fig. 5.3. The dip in the deposit at the center of the deposit may be due to reactant depletion. Mass gain is used most of the time in this Section as a measure of the average deposition rate. Film thicknesses estimated from mass gain by assuming the density of the deposited films to be that of bulk GaAs gives results which are approximately four times smaller than that measured with a surface profiler indicating that the films are quite porous. Radiation from the low pressure Hg lamp remains necessary in this case since the Hg-Xe arc lamp has very little output at 253.7 nm necessary for the excitation of the Hg atoms for Hg-photosensitization of arsine.

A scanning electron microscope (SEM) image of one of the films obtained on quartz utilizing both Hg-photosensitization and photolysis simultaneously is shown in

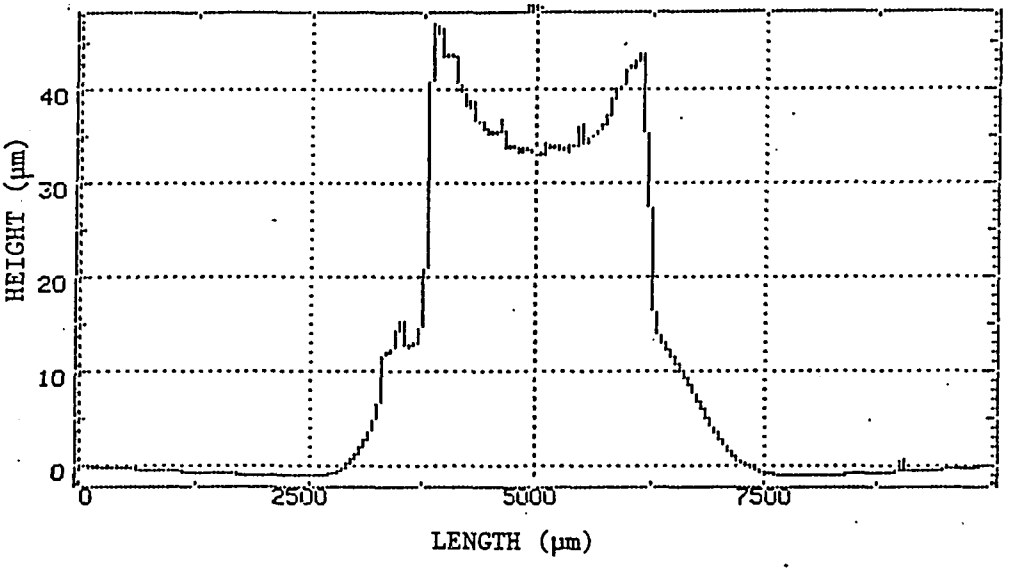

Figure 5.3 Surface Profile of GaAs Film Photodeposited on Quartz Utilizing Hg-Photosensitization.

Fig. 5.4. This figure shows the film area near the periphery of the Hg-Xe lamp beam. The surface morphology for these films ranged from nearly featureless to columnar and needle-like. Figure 5.4 shows a sample which demonstrates the four main surface morphological features of these films, although this was one of the few samples which possessed all of these four features simultaneously. Energy-dispersive spectrometry (EDS) measurements of the films indicated that the film surface morphology changed with composition with the featureless or somewhat roughened surface being near stoichiometric. The needle-like structures were arsenic deficient being approximately 47% arsenic and 53% gallium in composition while the column-like structures were arsenic rich being approximately 53% arsenic and 47% gallium in atomic composition. The composition of the deposited films as a function of lateral distance from the center of the deposit was determined using EDS. Figure 5.5 shows the results of these measurements for which the partial pressure of arsine, P_{AsH_3}, was varied by varying the 10% AsH_3 in H_2 flow rate from 20 to 80 sccm. The area used in these EDS measurements was large enough to obtain an average compositional measurement for the selected location. The total pressure in the growth chamber is denoted by P_{Tot} which was 2 Torr in this case. The deposition time was kept fixed at 30 minutes and the heater plate temperature was 240°C. The initial temperature of the substrate, being mounted onto the window, was less than 240°C although this temperature could not be measured directly. Figure 5.5 shows that these films were stoichiometric GaAs at the center. At a distance from the center of approximately 70% of the radius of the deposit, the composition becomes As rich. The radius of deposit is defined as the distance from the center of the deposit to the point where the thickness drops to 10% of the

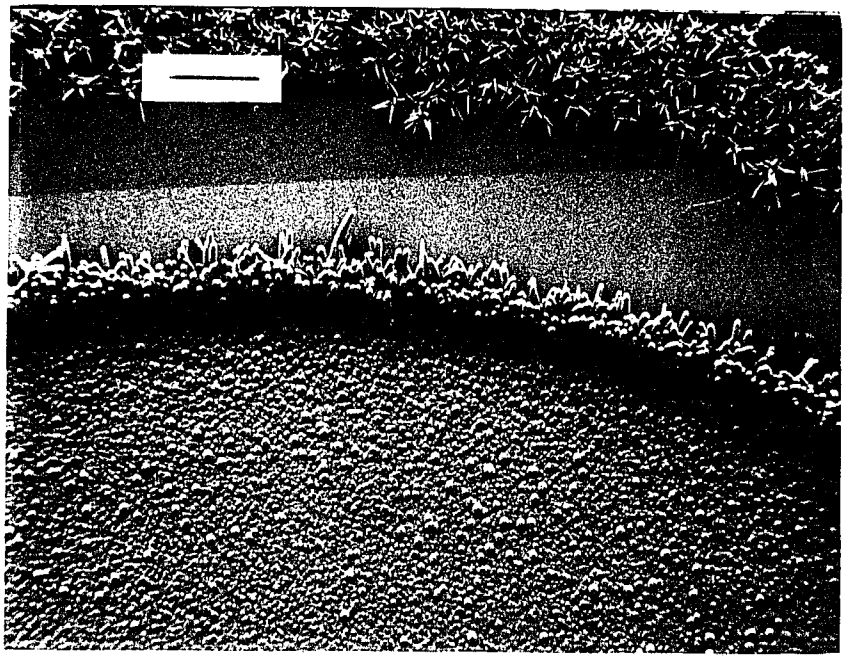

Figure 5.4 SEM Micrograph of a GaAs Film Deposited on Quartz by Means of Hg-Sensitized Photochemical Vapor Deposition (Hg-PCVD). Longest Line Equals 100 μm.

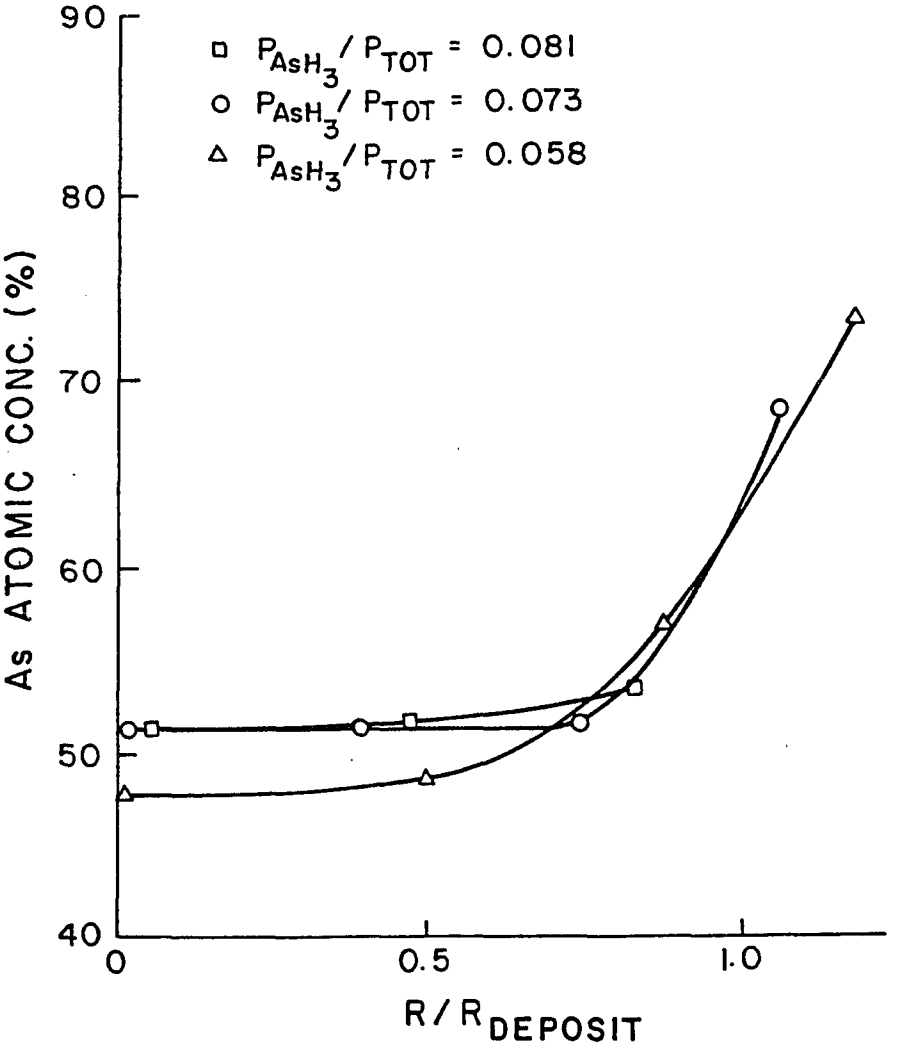

Figure 5.5 Arsenic Atomic Concentration as a Function of Distance from the Center of the Deposit for Films Deposited Without the Use of the Distilled Water Filter.

thickness at the center. This variation in the composition with lateral distance may be directly attributed to the temperature gradient which exists during film deposition due to the incident light beam as the intensity of the arc lamp beam decreases away from the center of the beam. The temperature at the center of the deposit will be higher and cause desorption of any excess arsenic. The actual temperature of the depositing GaAs film is difficult to estimate as the temperature varies both temporally and spatially. Temperature rise measurements performed on square 15 mil thick 2 cm^2 GaAs wafers mounted on a ceramic with heat conductivity similar to that of quartz indicated a temperature rise of 300°C using the same arc lamp light source and focusing lenses. From this measurement, the temperature of the deposited film is expected to be higher than 300°C.

For the samples where the full spectral output of the arc lamp was utilized with total optical power of 14.3 watts, severe cracking of the films was observed probably due to the difference between the thermal expansion coefficient of the film and that of the substrate. This suggests that upon nucleation, heating of the GaAs film occurs through absorption of the arc lamp output. The output from the Hg-Xe arc lamp was then reduced by approximately 30% to 10 watts by placing a distilled water optical filter in the path of the arc lamp output. This filter removes approximately 90% of the infrared radiation greater than 950 nm in wavelength and reduces by 25% wavelengths below 300 nm in the UV range. It does not greatly affect the radiation in the visible 300 nm to 800 nm range. The film deposition rate was reduced by a factor of seven with an 80% reduction with the filter but the cracking of the film was eliminated. The surface morphology of the films obtained with the use of the distilled water filter

was also improved with little or no features observed on the surface as indicated in Fig. 5.6. The diameter of the arc lamp beam was maintained at 0.64 cm.

Measurements on film composition as a function of lateral position were also performed on the films obtained utilizing the distilled water filter. Figure 5.7 shows the results of these measurements. The deposition conditions were the same as those for Fig. 5.5. As seen by comparing Figs. 5.5 and 5.7, the variation in composition as a function of lateral distance from the center was basically the same with or without the use of the water filter except for the sample deposited at the AsH_3 partial pressure ratio of 0.081. In the later case, the center portion of the film was also found to be arsenic rich for the case when the distilled water filter was used. This film was also somewhat thinner than the others and, hence, absorbed less incident light and subsequently was less heated. This decrease in film temperature results in a smaller amount of desorption of excess arsenic thereby resulting in higher arsenic content. For the experimental conditions considered here, it was observed that thin films less than 20 nm in thickness were consistently arsenic rich. Hence, the composition of the initial film responsible for nucleation and initial growth using this technique is likely to be rich in arsenic. However, subsequent heating of the film by absorption of the optical output results in desorption of excess As and may even result in slightly arsenic deficient film at the film interface.

It was also found that gallium could be deposited on quartz from TEG by photochemical means. Deposition was obtained both with and without Hg vapor present indicating that photolysis of triethylgallium is taking place even though the quartz window absorbs much of the radiation from the arc lamp which overlaps the absorption

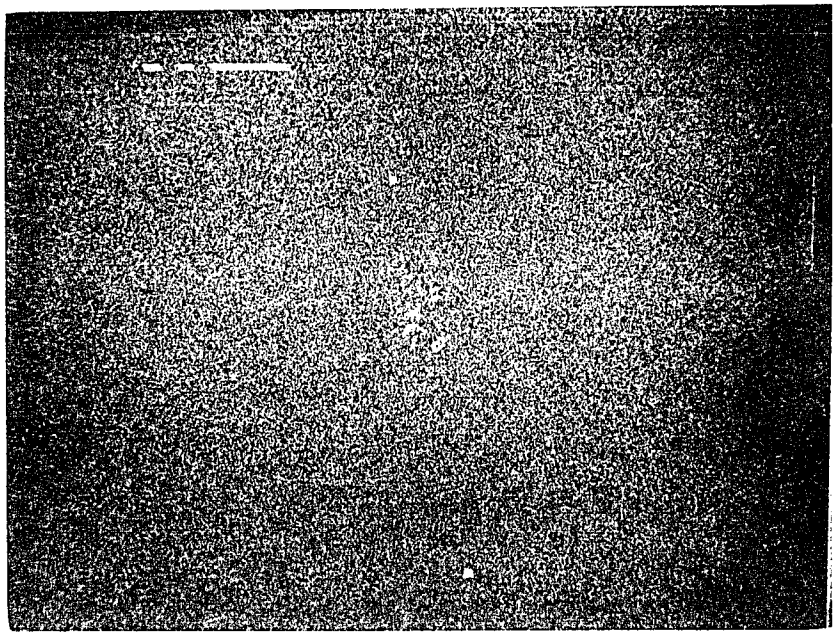

Figure 5.6 SEM Micrograph of a Film Deposited with the Use of the Distilled Water Filter. Longest Line Equals 10 μm.

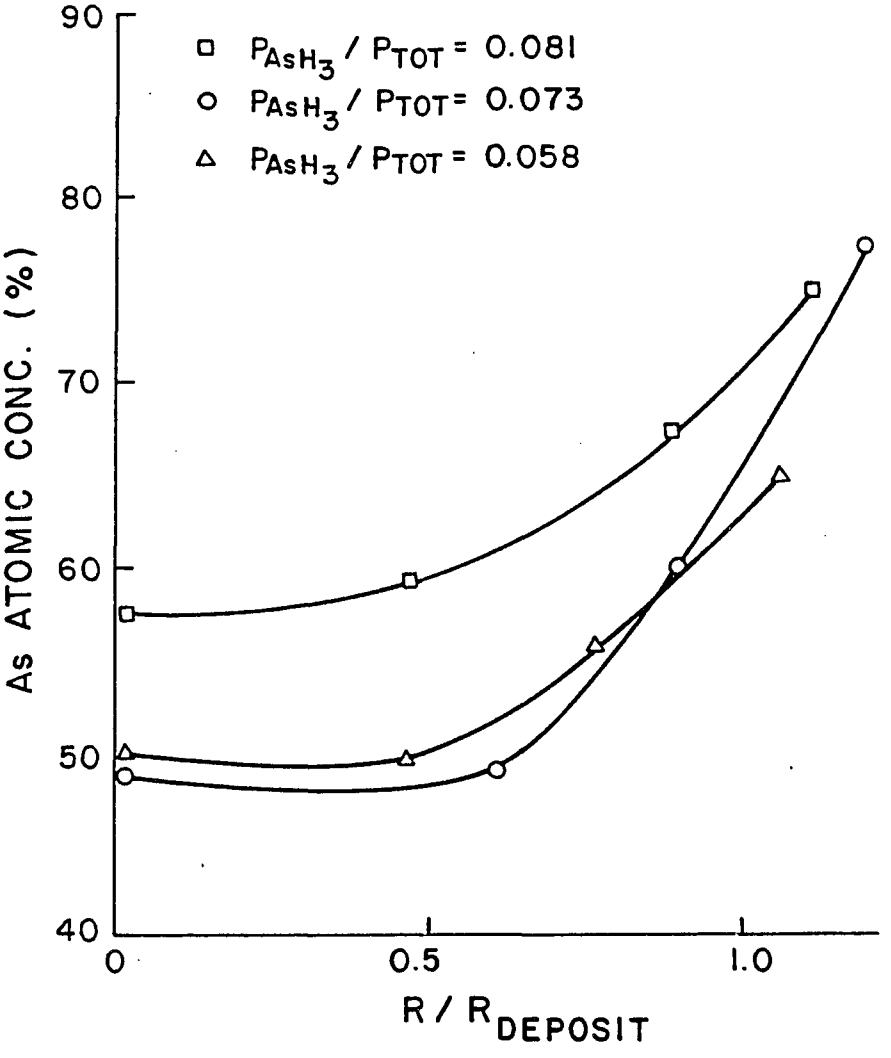

Figure 5.7 Arsenic Atomic Concentration as a Function of Distance from the Center of the Deposit for Films Deposited with the Use of the Distilled Water Filter.

spectra of the reactant. The appearance of the deposited film varied with optical intensity. A brown film was deposited for an arc lamp beam spot diameter greater than 6 mm with total optical power equal to 12 watts. For smaller beam spot diameters with the same total power, gallium droplets formed on the quartz substrates at the center of the beam spot location. Figure 5.8 shows an SEM micrograph of these droplets. A brown film surrounded this region with both regions of deposition containing high concentrations of carbon as determined using Auger electron spectroscopy.

The mercury content of the GaAs films was investigated by means of cold vapor atomic absorption. Using this technique, no Hg was detected in the films deposited utilizing both the low pressure Hg lamps and the Hg-Xe arc lamp with a detection limit of less than 10 ppm. It is highly probable that the high vapor pressure of Hg inhibits the incorporation of this impurity into the depositing film. Further investigation of the question of Hg incorporation into the film is needed to determine if the purity of the material obtained by this technique can be high enough for electronic device application.

Figures 5.9 and 5.10 show the deposition rate measured by mass gain as a function of the partial pressure ratio of AsH_3. Figure 5.9 is for the case where the total optical output power of 14.3 watts was used from the arc lamp. Figure 5.10 is for the case where the water filter was used with an optical power output of 10.0 watts. The deposition conditions were otherwise the same as those described for Fig. 5.5. Although the deposition rates are not the same in both figures, the general behavior of the curves is similar. The mass gain for a sample deposited by photolysis only with partial pressure of Hg, P_{Hg}, equal to zero obtained by excluding the use of

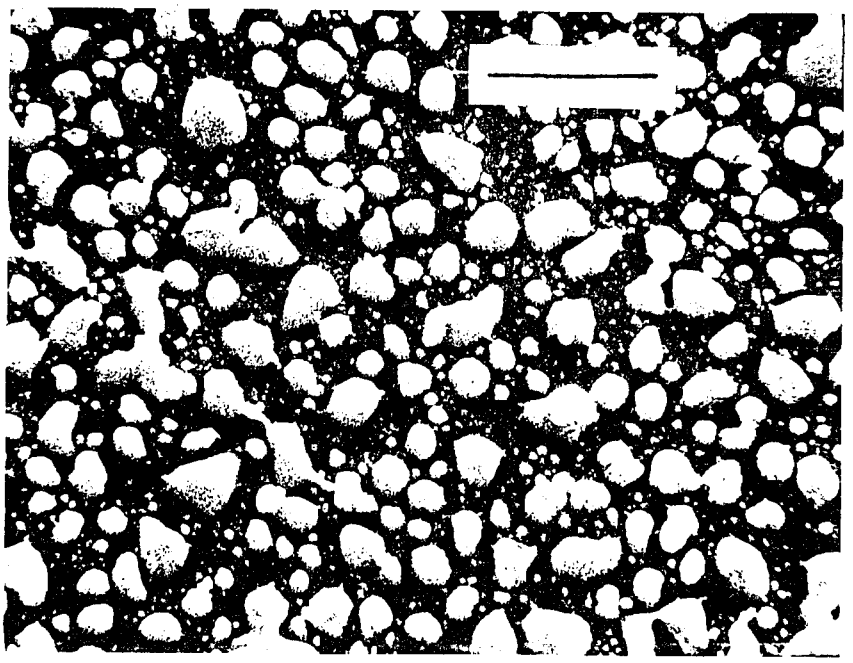

Figure 5.8 SEM Micrograph of Gallium Droplets Photodeposited on Quartz. Longest Line Equals 10 μm.

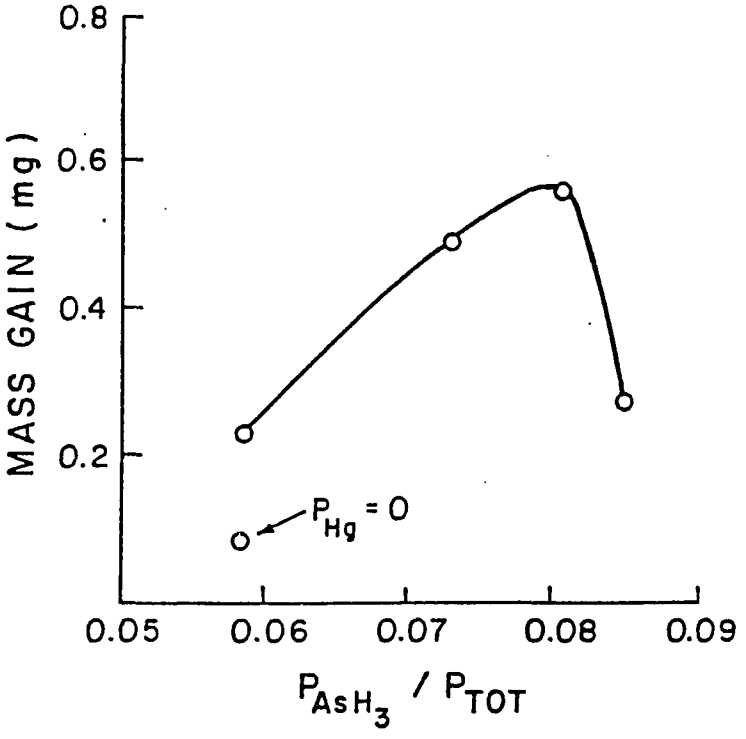

Figure 5.9 Mass Gain as a Function of Arsine Partial Pressure Ratio for the Case Where No Distilled Water Filter Was Used. Deposition Time Was 30 Minutes.

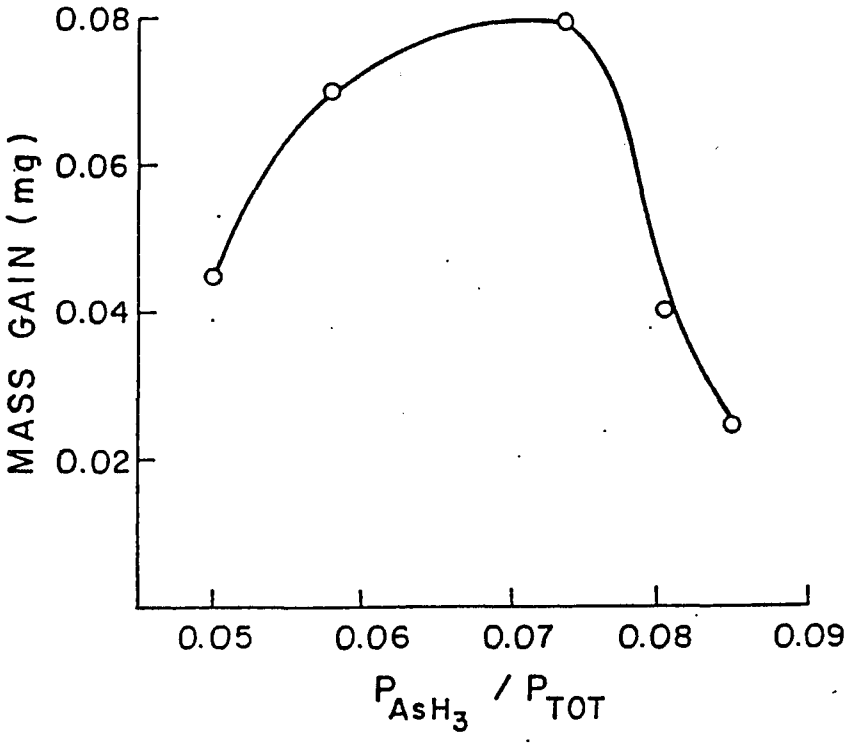

Figure 5.10 Mass Gain as a Function of Arsine Partial Pressure Ratio for the Case Where the Distilled Water Filter Was Used. Deposition Time Was 30 Minutes.

Hg-photosensitization is also shown in Fig. 5.9. As seen from this figure, the mass gain was significantly reduced when Hg vapor was excluded from the chamber. In fact, for other samples deposited without Hg vapor present, the reduction in the mass gain, and hence deposition rate, was greater than that indicated in the figure. This is not unexpected as the quartz optics attenuates most of the radiation useful in the photolysis of triethylgallium and arsine.[38,44]

Figure 5.11 shows the deposition rate, as measured by mass gain, as a function of the optical power of the arc lamp. In this case, the output power was varied by varying the input power to the arc lamp. No distilled water filter was used in this case. The deposition conditions for Fig. 5.11 were similar to those used in Fig. 5.5 with P_{AsH_3}/P_{tot} ratio maintained at 0.08. Since the origin of Fig. 5.11 denoting zero mass gain for no optical power input is also an observed data point, the mass gain and hence the deposition rate is seen from this figure to be a non-linear function of the optical power. This suggests the relative importance of pyrolytic effects on the deposition rate due to optical heating of the film as the film is being deposited.

In addition to the lateral variation, the film composition as a function of depth was also studied using sputtered Auger electron spectroscopy (AES). One of the major points of interest in this work was to investigate the conditions necessary for obtaining stoichiometric thin films of GaAs using photochemical means. Figure 5.12 shows the results obtained for a sample which, from EDS measurements, was determined to be stoichiometric GaAs at the center. The AES spectra shown here were obtained from the center of the sample. Curve A represents the spectrum obtained before sputtering. The relative intensities of the gallium and arsenic peaks indicate the

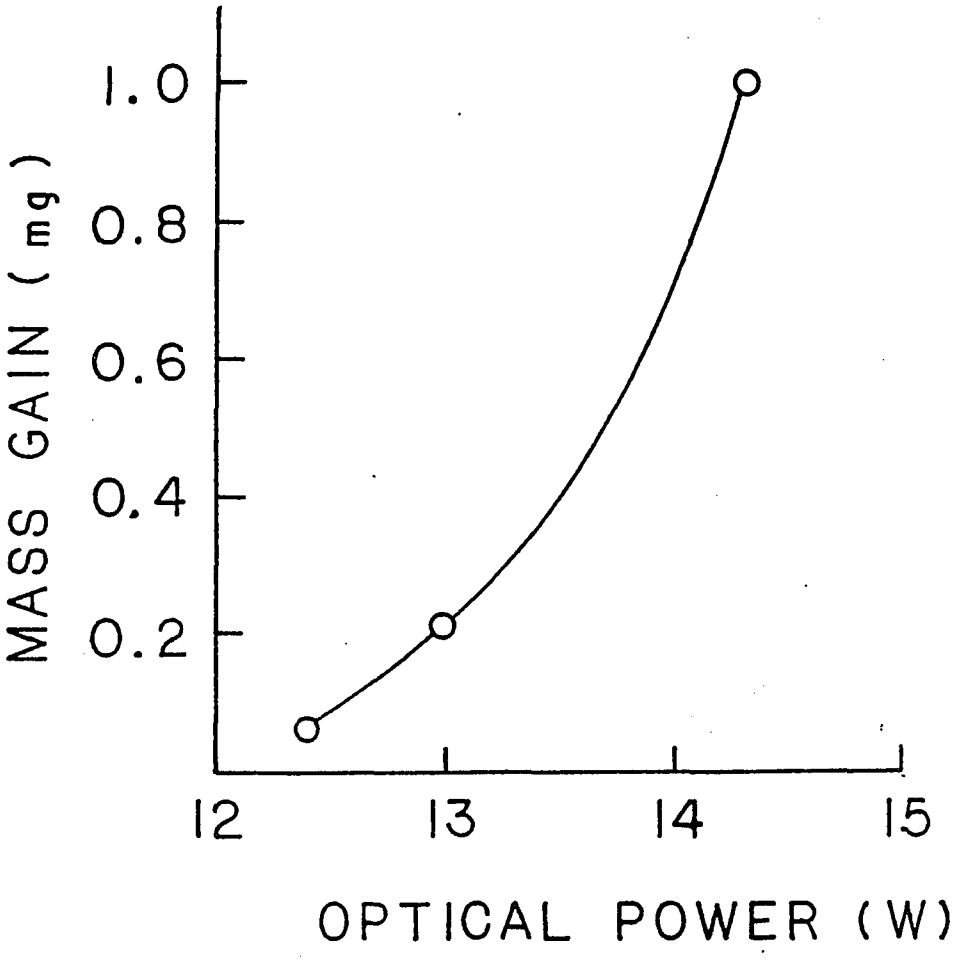

Figure 5.11 Mass Gain as a Function of Arc Lamp Optical Power. No Distilled Water Filter Was Used in this Case. Deposition Time was 30 Minutes.

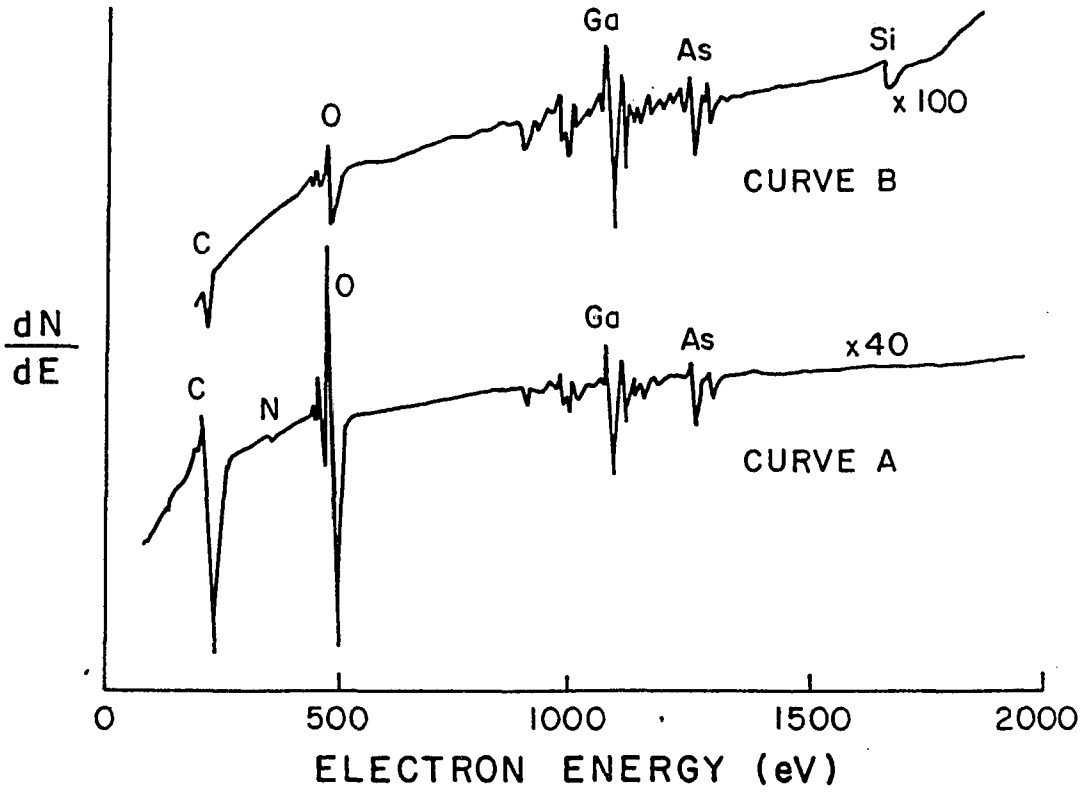

Figure 5.12 Auger Electron Spectra Obtained for a Hg-Sensitized Photodeposited GaAs Film. Curve A is for the Sample Before Sputtering; Curve B is for the Film After Sputtering Until the Substrate Material Peak is Observed.

presence of stoichiometric GaAs. Curve B in Fig. 5.12 was obtained after sputtering for a sufficient time to begin to see the silicon peak from the quartz substrate. It can be seen from the relative peak intensities that the lower portion of the GaAs film becomes slightly gallium rich with an approximate concentration of 53% gallium and 47% arsenic. The portion of the film near the GaAs-quartz interface also experiences the greatest temperature rise during deposition due to optical absorption. The carbon peak present in curve B after sputtering is of the same intensity as the carbon peak obtained on a carbon-free single crystal GaAs wafer using the same AES system. This sets a lower limit of 2% on the sensitivity for carbon detection from the background for the AES system used in this work. In the photodeposited films, the carbon concentration was below this background limit of 2%. In addition to the compositional studies of the films, the crystalline structure was also studied using X-ray diffraction. Figure 5.13a) shows the diffraction pattern obtained for a typical sample deposited utilizing Hg-sensitized photochemical vapor deposition using the total optical output of 14.3 watts from the Hg-Xe arc lamp. The Miller indices for each identified GaAs peak are indicated on the figure. From the peak width, the grain size was estimated to be approximately 80 nm using the Scherrer formula.[90] From the relative intensities of the peaks, the film was found to be randomly oriented. Figure 5.13b) shows the diffraction pattern obtained for a GaAs film deposited utilizing the distilled water filter. As seen from this figure, the (220) peak is much greater in magnitude than any other peak indicating that the polycrystalline film in this case exhibits some preferred orientation. From the peak width, the grain size was estimated to be approximately 50 nm.

Figures 5.14a) and 5.14b) show the optical transmittance as a function of

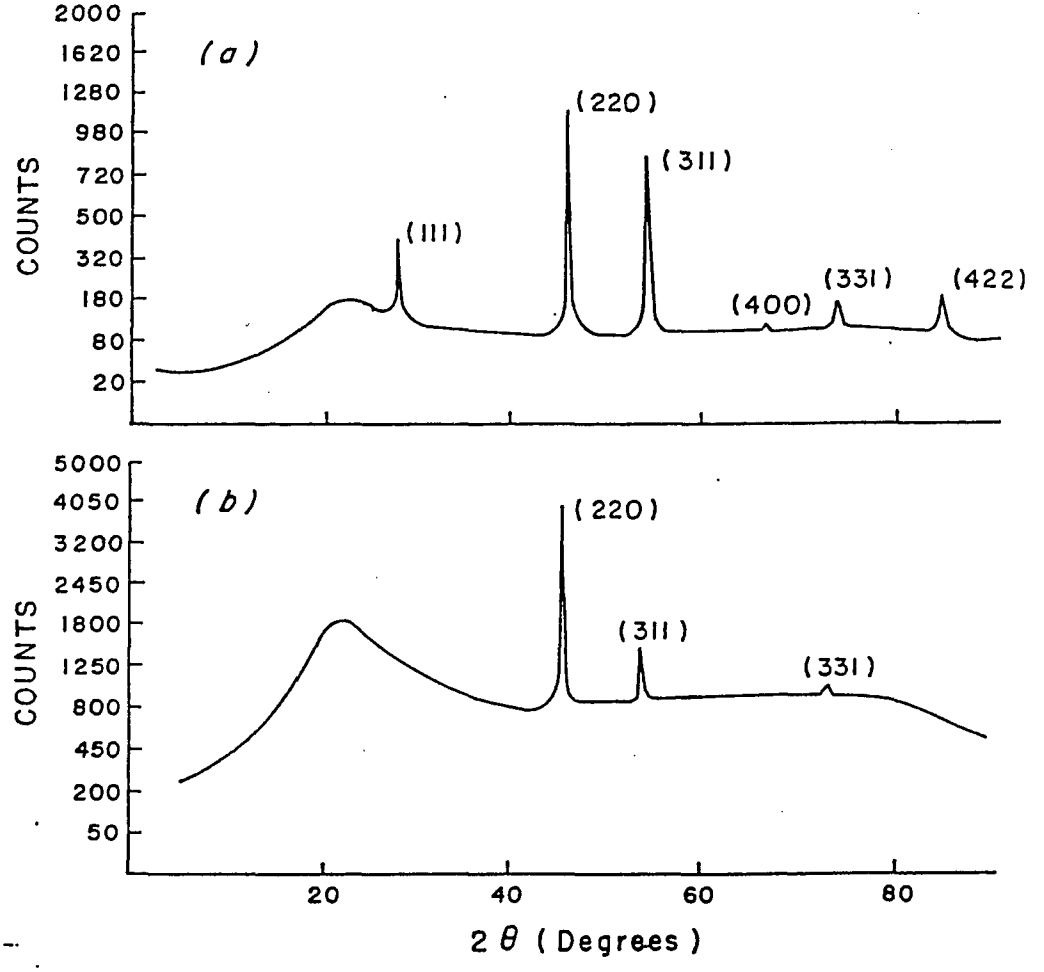

Figure 5.13 X-ray Diffraction Pattern of a Photodeposited GaAs Film Obtained (a) Without the Use of and (b) with the Use of the Distilled Water Filter.

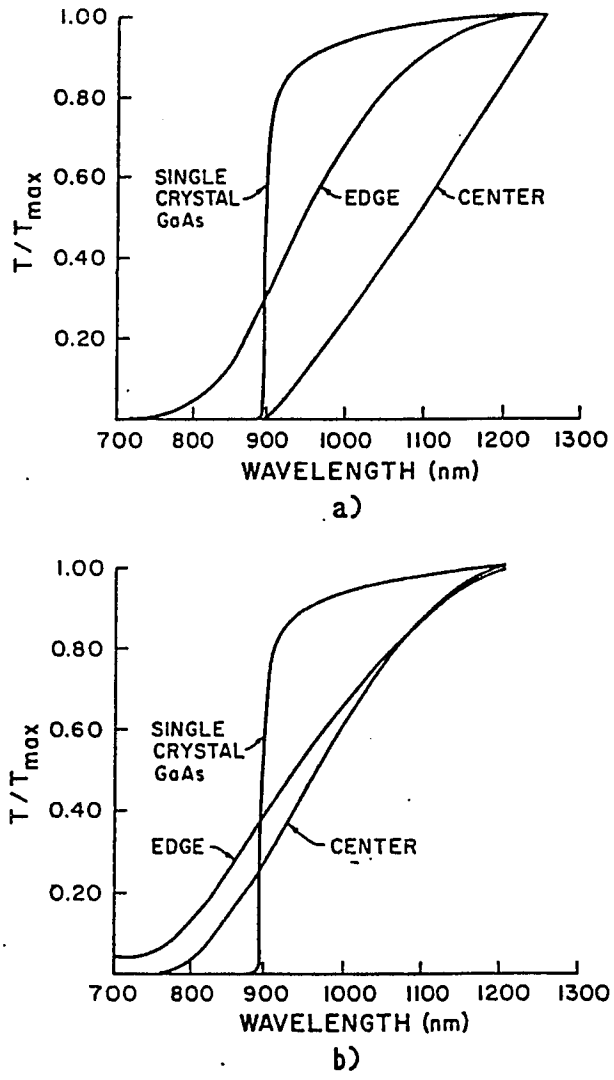

Figure 5.14 Normalized Transmittance T/T_{max} of a Photodeposited Film Obtained (a) Without the Use of and (b) With the Use of the Distilled Water Filter. The Transmittance of a Polished 0.4 mm Thick Single Crystal GaAs Wafer is Shown for Reference.

wavelength for two polycrystalline GaAs samples. The transmittance for a polished single crystal GaAs wafer is also shown for reference. Figure 5.14a) shows the normalized transmittance for a sample deposited by Hg-sensitized photolytic means utilizing the total optical output of the arc lamp. Transmittance was measured both at the center and away from the center near the edge of the deposited sample. The onset of transmittance with wavelength occurs very near that for single crystal GaAs for the center of the deposit for the case shown in Fig. 5.14a). However, for the region of deposit removed from the center, the onset of transmittance appears to occur at a shorter wavelength than that for the center. Energy-dispersive spectrometry of the edge and center regions used to obtain the transmittance indicated that both regions were near-stoichiometric GaAs, although the edge region used was very near the point of transition to the As-rich composition. Figure 5.14b) shows a similar plot of normalized transmittance versus wavelength for a Hg-sensitized photodeposited film utilizing the distilled water filter. The EDS measurements indicate that both regions in this case are also near-stoichiometric GaAs in composition. The high relative transmittance in these films below cut-off wavelength compared to the thicker single crystal sample may be an artifact of the deposited film thickness. The deposited films were thinner at the edge for all samples. The deposited films utilizing the water filter were thinner than those deposited without its use. The thinner films show some transmittance below the cut-off wavelength.

The deposition process used in this work can be qualitatively described as shown in Fig. 5.15. Initial nucleation of the film proceeds by a process involving both photolysis and Hg-photosensitization of the reactant gases. The substrate temperature

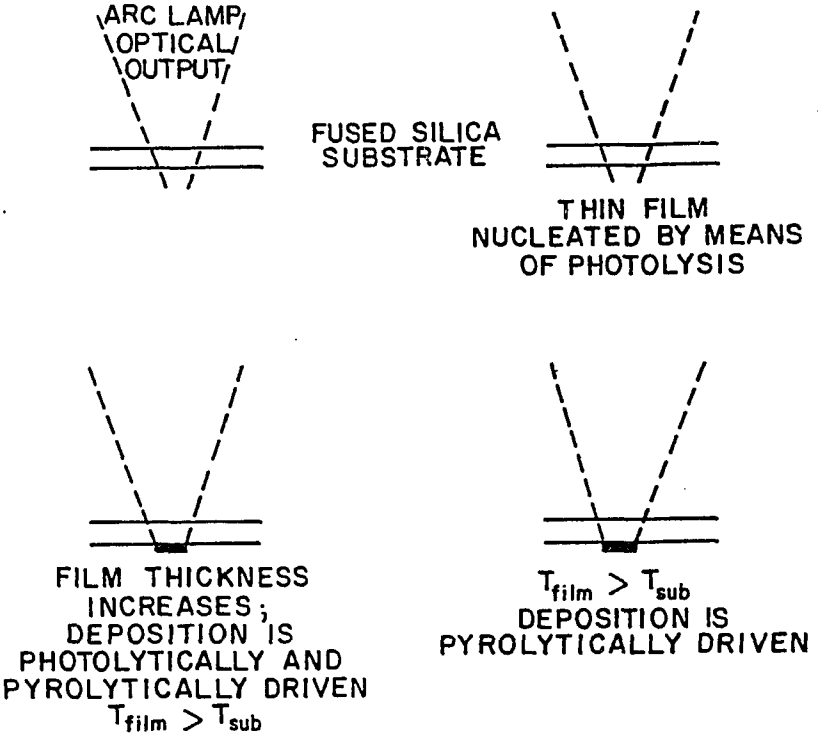

Figure 5.15 Model for Film Deposition for the Case Where Window Fogging is Utilized to Achieve Deposition.

is below that necessary to carry out pyrolysis of the reactants. As the nucleated film thickness increases, the temperature of the film also increases due to absorption of the optical output of the arc lamp while the amount of light transmitted into the reaction chamber decreases. The process is self-limiting and at some point the photolysis for gas-phase species will cease to occur due to attenuation of the light by the depositing film assuming that the radiation useful for photolysis is absorbed by the film. Film growth beyond this will have to be driven by pyrolytic means and will depend on the film surface temperature achieved through heat transfer from the substrate-interface end of the film.

In conclusion, we have demonstrated that selective deposition of polycrystalline GaAs on transparent quartz substrates is possible with Hg-sensitized photochemical vapor deposition utilizing a low pressure Hg lamp and a Hg-Xe arc lamp. These films were deposited for conditions in which no deposition occurs in the absence of the light sources. The results show that for the conditions investigated here, the temperature of the depositing film has to be sufficiently high for the desorption of excess arsenic in order to obtain stoichiometric GaAs films using this technique.

CHAPTER 6

DIRECT PHOTOCHEMICAL VAPOR DEPOSITION OF GALLIUM ARSENIDE

6.1 Photochemical Vapor Deposition of GaAs on Synthetic Fused Silica

A much more attractive mechanism for decomposing the reactants necessary for deposition of GaAs is by direct photolysis as this does not involve the use of Hg with its associated problems as an impurity. In this section, we report on the deposition of thin-film polycrystalline GaAs on synthetic fused silica by direct photochemical means. Use of a transparent substrate allows for some distinction between photolytic and pyrolytic deposition mechanisms during growth. A focused 1000 W Hg-Xe arc lamp is used as the light source with triethylgallium and arsine serving as the reactants. Unlike the previous work by Balk et al.[47] in which ultraviolet radiation is used to enhance an already existing deposition rate for the AsH_3–$(C_2H_5)_3Ga$ system, no GaAs deposition occurs in the absence of light for the work reported in this section.

Film deposition is carried out in the low pressure chemical vapor deposition system described in Chapter 5 equipped with a 1000 W Hg-Xe arc lamp. A schematic of the deposition system is shown in Fig. 6.1. The main difference is that the top plate is made of synthetic fused silica which, unlike quartz, is transparent to ultraviolet radiation down to approximately 185 nm. A needle valve at the output of the organometallic bubbler was used to keep the flow at 5 sccm. Total triethylgallium flow into the reactor was controlled with the bubbler temperature. The substrates used were nominally 1/16 in. thick plates of synthetic fused silica. As the fused silica sub-

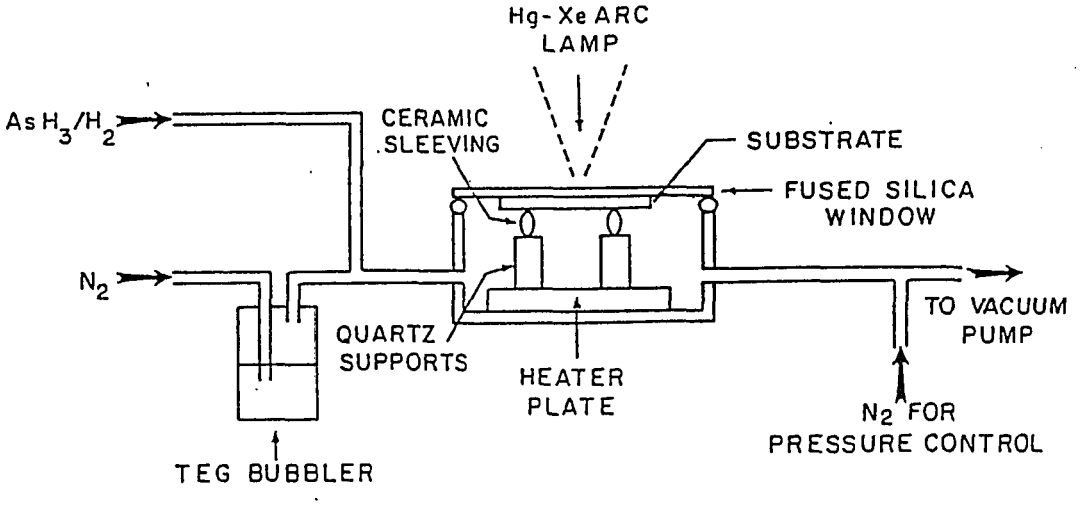

Figure 6.1 Schematic of Deposition Chamber Utilized for Photodeposition of GaAs on Fused Silica.

strates were transparent to the arc lamp output, the window fogging mechanism could in fact be utilized as in the previous Chapter to obtain film deposition. GaAs thin films were obtained using this technique. Deposition proceeds in much the same way as described in Fig. 5.15 with only photolysis being involved in the initial nucleation process.

Figure 6.2 shows the absorption spectra for AsH_3 and TEG as a function of photon energy.[38,44] Also shown is the optical output of the Hg-Xe arc lamp. As is seen in the figure, some overlap occurs at the extremes of both the absorption spectra of the reactants and the emission spectra of the lamp. Also shown is the first bond energy for AsH_3 and TEG indicating that dissociation of at least one bond is possible with the optical absorption indicated. However, the degree of dissociation which the molecule undergoes depends upon how the photonic energy is coupled into the molecule.

Polycrystalline GaAs thin films were photochemically deposited on synthetic fused silica with film thickness up to 3.3 μm measured with the surface profiler. Figure 6.3 shows the surface profile of a typical film obtained in this work. Figure 6.4 shows a scanning electron microscope (SEM) image of the same film. The thickness of the film shown is 3.3 μm. Mass gain measurements, when compared to the surface profile, indicate that these films are somewhat porous. This sample was deposited in 60 min with a 62 sccm flow rate for the 10% AsH_3 in H_2 mixture and a 5 sccm N_2 flow rate through the triethylgallium bubbler maintained at 0°C. The heater plate temperature was maintained at 240°C. The substrate temperature was not measured directly but was less than the heater plate temperature at the start of the deposition.

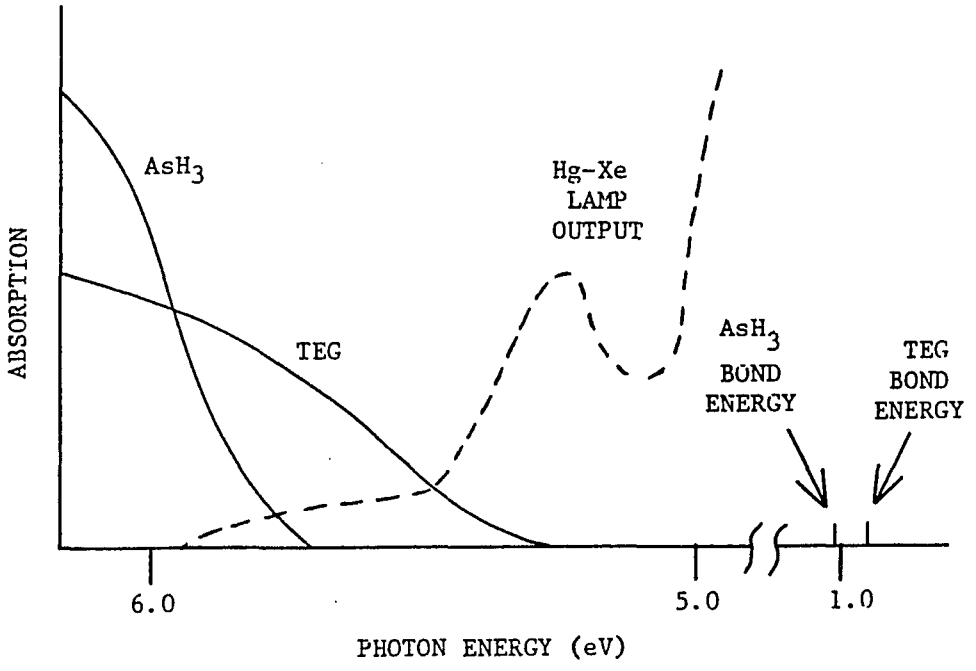

Figure 6.2 Comparison of Optical Absorption Spectra of AsH_3 and TEG with the Optical Output of the Hg-Xe Arc Lamp.

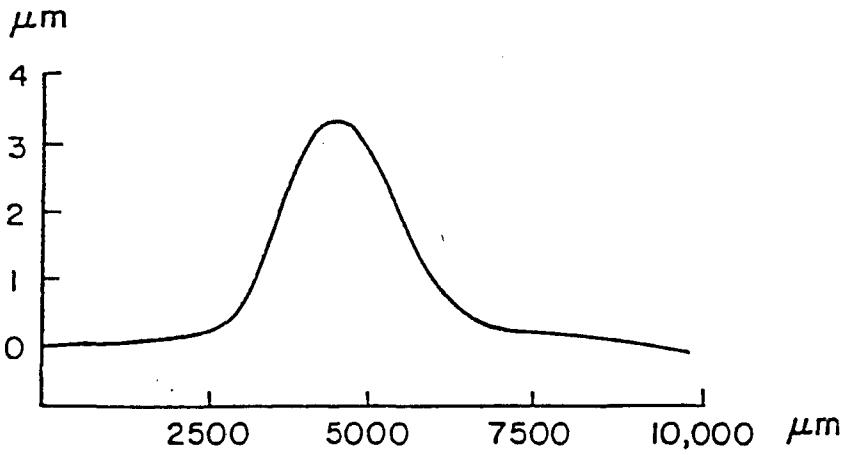

Figure 6.3 Surface Profile of GaAs Photodeposited on Fused Silica.

The total chamber pressure was 2 Torr. Total optical output used for this deposition was 14.3 W for a spot size of 6.4 mm in diameter. The surface of the deposit was somewhat bumpy with cracks apparent in the film as shown in Fig. 6.4. These cracks are attributed to the difference between the thermal expansion coefficients of GaAs and fused silica since during growth, the deposited film absorbs the arc lamp radiation and heats up.

A distilled water optical filter was then introduced into the optical beam path. The insertion of the water filter eliminates approximately 90% of the arc lamp radiation above 950 nm wavelength (1.30 eV) which is assumed to be unimportant in terms of the photolytic processes and marginally important in terms of pyrolytic effects as the photon energy of this radiation is less than the band-gap energy of GaAs. The filter reduces the ultraviolet radiation of wavelength less than 240 nm (5.17 eV) by approximately 35% which is important in terms of photolytic decomposition of triethylgallium and arsine based on the optical absorption data shown in Fig. 6.2. The total optical output of the arc lamp below 240 nm without the use of the distilled water filter is estimated to be approximately 40 mW. The distilled water filter has little effect on the radiation between 300 and 950 nm. Insertion of the filter reduced the total optical output to 10 W. Figure 6.5 shows a SEM micrograph of a GaAs film obtained using the distilled water filter. The conditions for deposition were the same as those for Fig. 6.4. The deposition rate was reduced with the use of the filter resulting in a sample thickness of 0.57 μm as estimated from mass gain. For this case the cracks do not appear in the film and the morphology of the film is significantly improved.

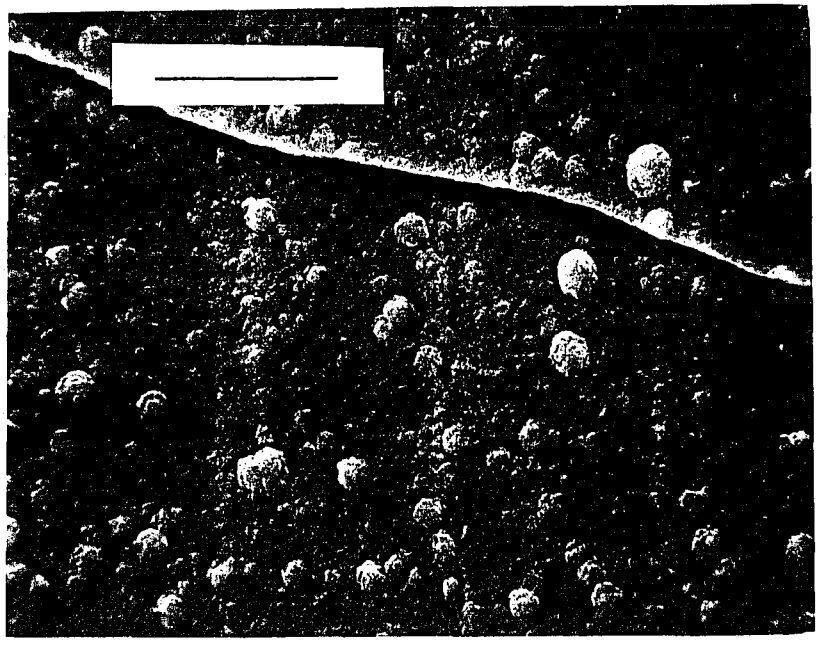

Figure 6.4 SEM Micrograph of GaAs Deposited on Fused Silica Without the Use of a Distilled Water Filter. Longest Line Equals 10 μm.

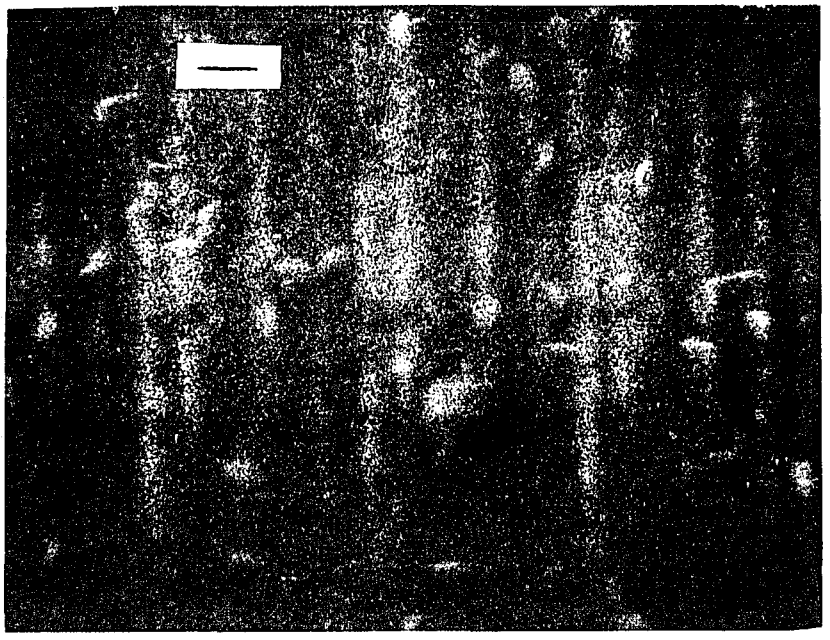

Figure 6.5 SEM Micrograph of GaAs Deposited on Fused Silica with the Use of the Distilled Water Filter. Longest Line Equals 1.0 μm.

The chemical composition of the GaAs films was examined using energy dispersive spectrometry. For spatially selective deposition of compounds such as GaAs, the question of uniformity of composition of the deposited film must be addressed. If the composition of the deposit, whether photolytically or pyrolytically obtained, is dependent on the light intensity, the deposit obtained will vary in composition as the light intensity varies with position in the beam. This does appear to be the case for the deposits obtained on fused silica as shown in Fig. 6.6. This figure shows the results for the two cases shown in Figures 6.4 and 6.5. In Fig. 6.6, r is the radial distance from the center of the deposit. The edge of the film ($r/r_{sample} = 1$) is defined as the position where the film thickness drops to 10% of the thickness at the center. As seen from Fig. 6.6, the center of the deposit is composed of near-stoichiometric GaAs. However, as the edge of the sample is approached, the deposited film becomes As-rich. This characteristic was observed in films deposited with or without the water filter. It appears that the center region of the film is heated sufficiently by the arc lamp to promote desorption of any excess arsenic while the film deposited near the edge is heated less resulting in greater arsenic incorporation. These results showing excess arsenic content illustrate that photolysis can introduce very different deposition mechanisms as thermal organometallic chemical vapor deposition of GaAs rarely yields arsenic rich films. In addition, a study of the deposition of arsenic on fused silica utilizing the photolysis of arsine with a Hg-Xe arc lamp yields a deposition rate which is two orders of magnitude less than that obtained for GaAs thin films. This result suggests that interaction of the reactants and photofragments may result in further decomposition of the reactants.

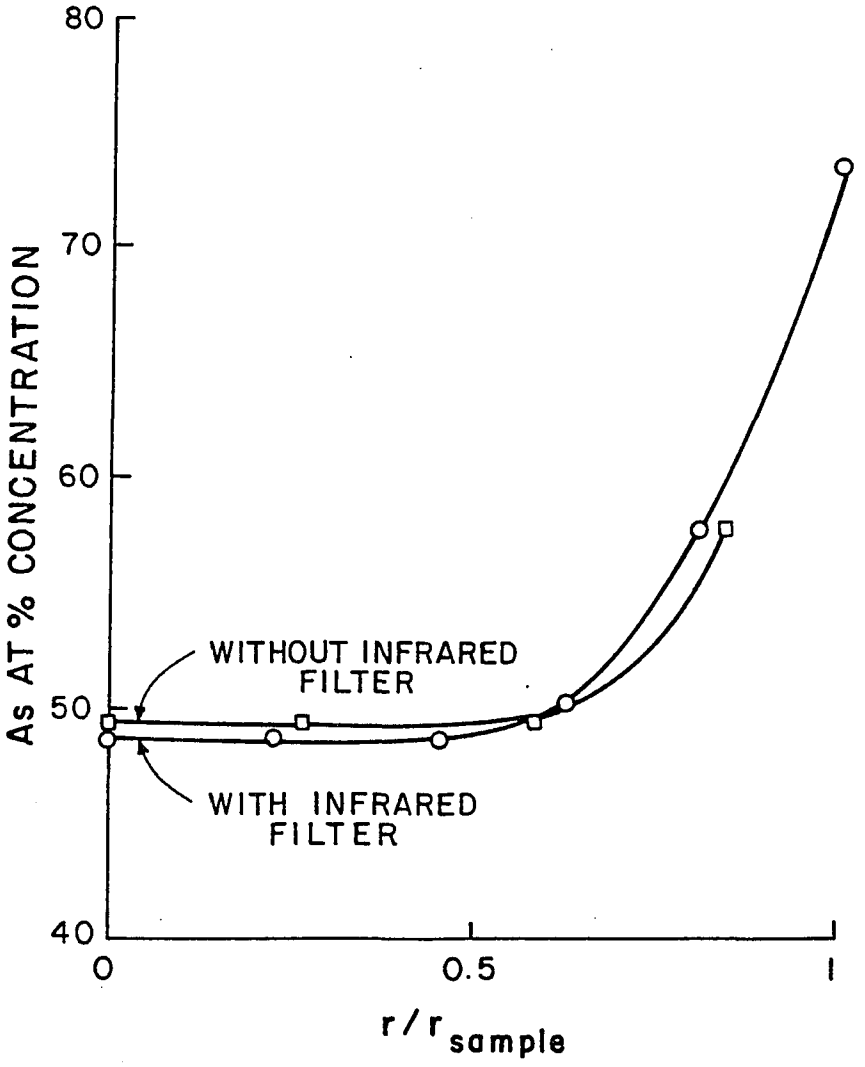

Figure 6.6 Atomic Percentage Concentration of Arsenic as a Function of Distance from the Center of the Deposit.

Figure 6.7 shows the X-ray diffraction patterns obtained from the stoichiometric regions of the films shown in Figs. 6.4 and 6.5. The Miller indices corresponding to the peak locations are indicated. Figure 6.7a) shows the pattern obtained for the film deposited without the use of the distilled water filter. This X-ray diffraction pattern indicates no preferred orientation of the grains. However, the X-ray pattern for the GaAs film obtained with the use of the filter, shown in Fig. 6.7b), indicates preferred orientation as the (220) peak is the only major peak observed along with a small (331) peak. These results, shown in Figs. 6.7a) and 6.7b), were reproduced in other films deposited with and without the use of the distilled water optical filter.

In addition, the optical transmittance through these films was investigated. The transmittance data clearly showed GaAs band-gap absorption for wavelengths less than approximately 900 nm. These results were obtained for films deposited with or without the distilled water filter.

Separate experiments were also carried out on the photochemical vapor deposition of arsenic from arsine and of gallium from triethylgallium using the Hg-Xe arc lamp. For both cases, some deposition did occur. However, for deposition conditions as reported for the film shown in Fig. 6.4, the deposition rates for gallium or arsenic were much lower than the deposition rate for GaAs. The GaAs deposition rate was more than two times higher than that for gallium and more than two orders of magnitude higher than that achieved for arsenic from arsine. Similar results were obtained for a variety of AsH_3 and triethylgallium flow rates. These observations along with the observation of excess arsenic along the edges of the deposition suggests that availability of gallium is the rate-limiting step. The reduction in the incident photon flux

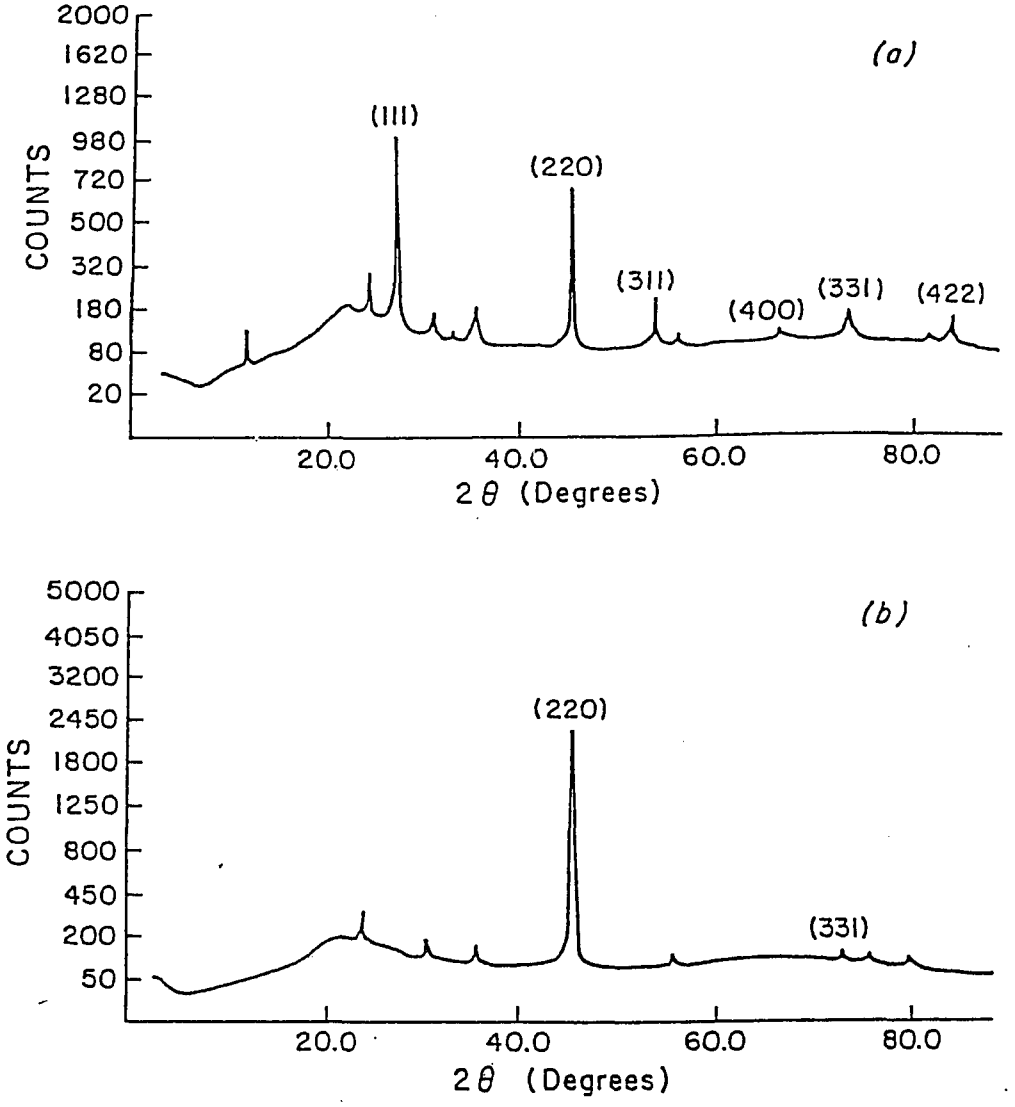

Figure 6.7 X-ray Diffraction Patterns of Films Obtained (a) Without the Use of and (b) With the Use of a Distilled Water Filter.

by approximately 43% for wavelengths below 225 nm with the use of the distilled water filter was found to reduce the film thickness by 64%. This reduction in film thickness is somewhat greater than anticipated by photolytic means alone. Hence, pyrolytic effects due to heating of the depositing film by incident light also plays a role in the film growth. Thermal decomposition of triethylgallium can occur at temperatures as low as 250°C.[12] However, it is clear for the work reported here that the film nucleation and initial growth proceeds by photolytic means only.

6.2 Photochemical Vapor Deposition of Gallium Arsenide on Gallium Arsenide Using a Hg-Xe Arc Lamp

In order to deposit GaAs on opaque substrates, window fogging must be eliminated. To accomplish this, the deposition chamber was modified to provide for a nitrogen purge of the window as shown in Fig. 6.8. Chamber pressure during deposition was maintained at 2 Torr. The substrate holder temperature was raised to 110°C prior to irradiation of the substrate by the 1000 watt Hg-Xe arc lamp. The arc lamp output was again focused to a 0.64 cm diameter spot size using two ultraviolet-grade plano-convex lenses. For this particular study, the nitrogen flow rate through the organometallic bubbler was maintained at 10 sccm utilizing a needle valve at the output of the bubbler to maintain a constant bubbler pressure. By controlling the bubbler temperature, a triethylgallium flow rate of 8×10^{-3} sccm, as determined using the vapor pressure data reported by Plass et al.,[15] was maintained. The arsine in H_2 flow rate was varied from about 40 sccm to about 150 sccm.

In discussing light-driven deposition in which the light beam is incident onto

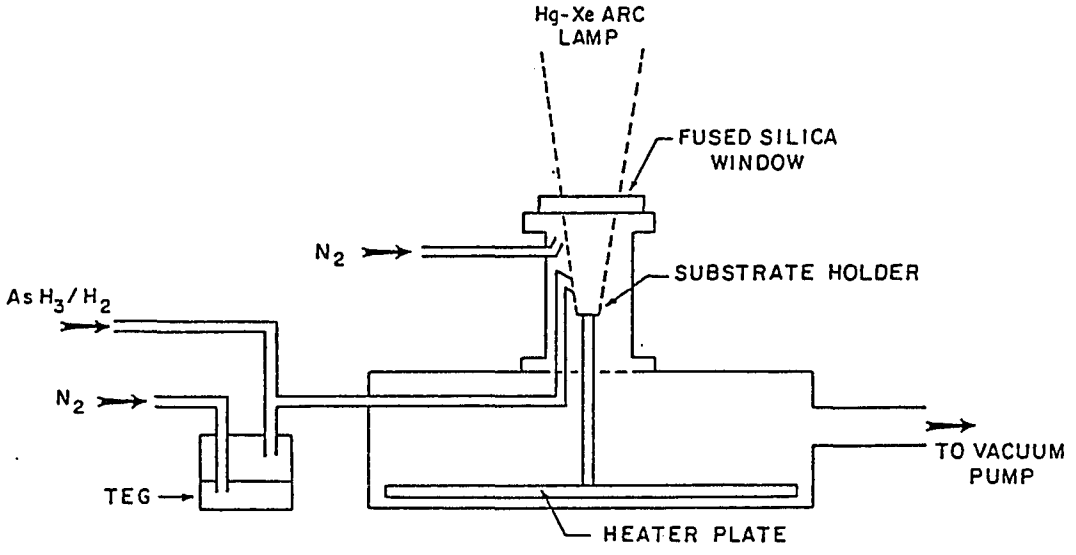

Figure 6.8 Chamber Utilized to Deposit GaAs on GaAs and Si Substrates Using the Hg-Xe Arc Lamp.

the substrate surface, the question of actual surface temperature is difficult to deal with. Treatment of this problem generally takes the form of either solving, with various approximations, the heat flow equation to get an estimate of the surface temperature or by experimentally measuring the temperature by some method. Theoretical solutions range from analytical,[91,92] which assume simplified geometries, to numerical analyses utilizing, for instance, finite difference techniques.[93–96] The most popular analytical solution, which gives a simple expression for the maximum temperature rise at the center of the beam spot, assumes that the sample consists of a semi-infinite slab which is a gross approximation for semiconductor wafers. Our measurements have indicated that for many cases this treatment gives results which are significantly smaller than the measured surface temperature rise. In addition, numerical treatments must make assumptions about the boundary conditions, specifically about the rear heat sink, making such treatments useful only for the selected conditions.

Results from Gluck et al.[28] suggest that the temperature rise at the back surface of a thin semiconductor sample whose lateral dimensions are comparable to that of the light beam spot size is well within 1°C of the temperature at the irradiated front surface. Based on this, we have made an attempt to experimentally determine the substrate surface temperature under irradiation. The temperature at the back of the sample was monitored with a 0.254 mm diameter chromel-alumel thermocouple. A drop of less than 1.0 mm diameter liquid gallium was used to help the thermocouple make good thermal contact to the sample. The difference in the measured temperature rise using the gallium as a thermal contact as opposed to measuring the temperature rise using a thermocouple only in physical contact with the sample was as much as 66%.

In order to avoid influencing the reactions in the chamber by the presence of liquid gallium, all temperature measurements were performed on a separate apparatus outside the deposition chamber using a sample mount similar to the one used in the deposition chamber.

Figure 6.9 shows the time dependence of the temperature rise for a Cr-doped GaAs sample 1 cm x 1 cm in size. The optical power was 9.4 watts with an initial temperature of 103°C. Within 30 seconds of exposing the sample to the arc lamp radiation, the temperature rose to 90% of its final value. Figure 6.10 shows the final substrate temperature versus input optical power. For the optical power considered, the relationship between temperature rise and incident power is approximately linear consistent with results reported by Gluck et al.[28]

Figure 6.11 shows a plot of the deposition rate as a function of optical power. These growth rates were for the region of the substrate exposed to the arc lamp beam. The figure shows a slight decrease in the deposition rate as the optical power is decreased. The temperature of the substrate induced by the arc lamp radiation is also shown in the figure. From the optical absorption data reported in the literature,[38,44] the photolytic processes are expected to play a major role in the decomposition of the reactants. However, the fact that the slope obtained from this curve is approximately what has been reported for kinetically-controlled pyrolytic growth in the low temperature regime[13] suggests that thermal processes also play a role in the decomposition of the reactants at the surface.

The film thickness in the region outside the arc lamp beam spot was also measured and found to be approximately the same as that obtained in the region inside the

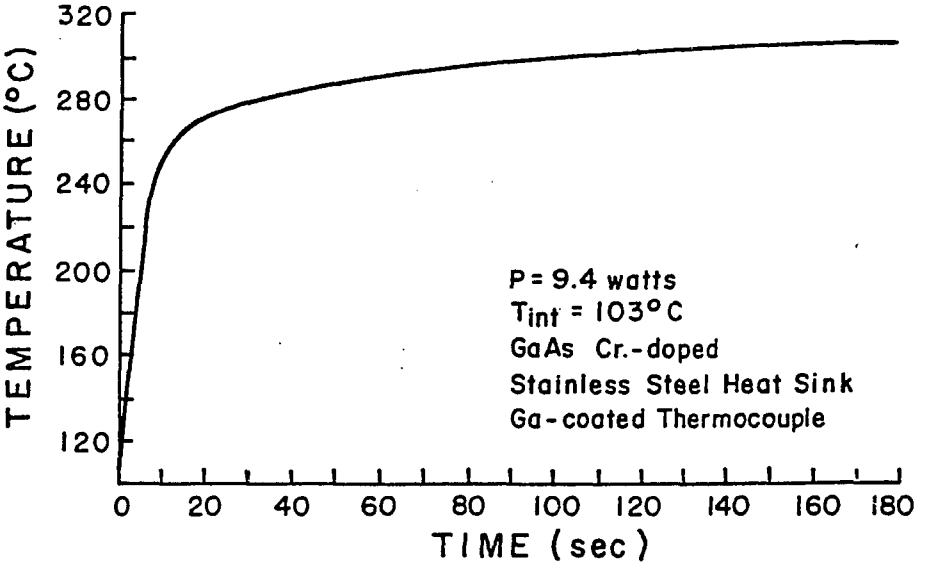

Figure 6.9 Temperature Rise Versus Time for a 1 cm^2 GaAs Substrate Irradiated with 9.4 Watts Optical Power from a Hg-Xe Arc Lamp.

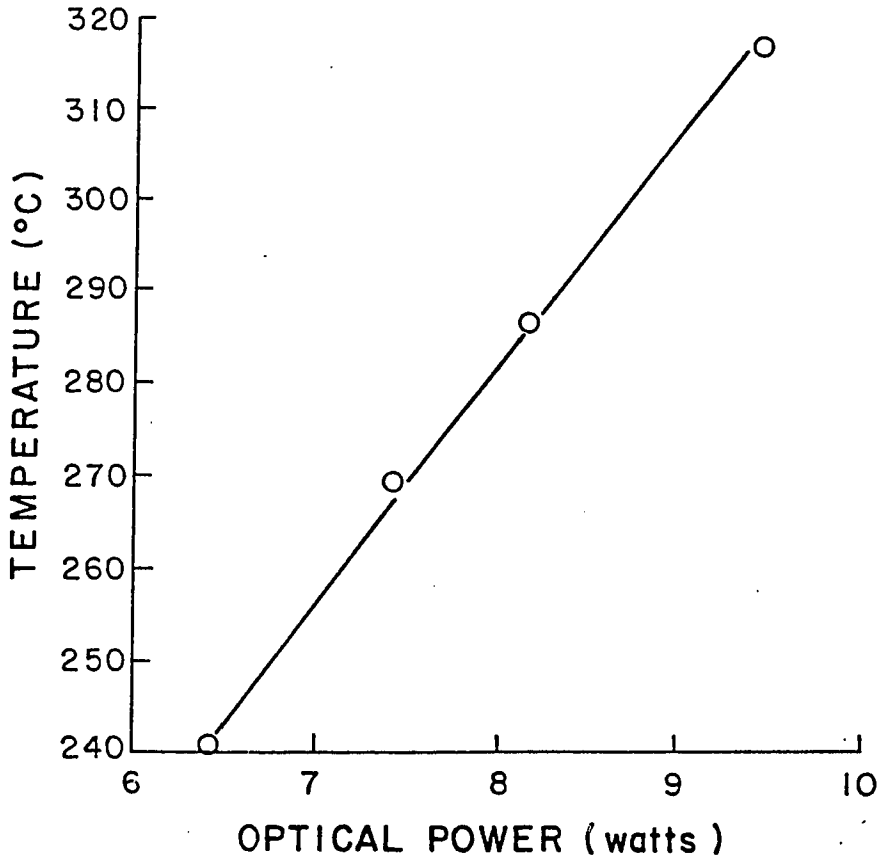

Figure 6.10 Final Temperature Versus Optical Power for a GaAs Substrate. Initial Temperature Was 100°C.

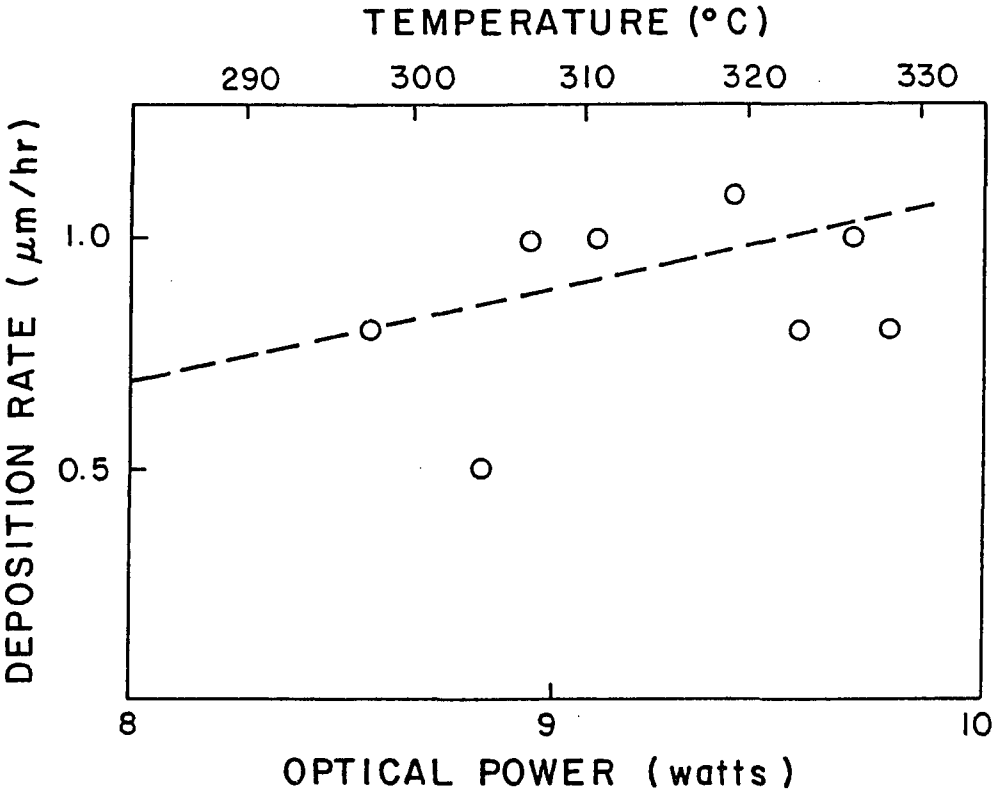

Figure 6.11 Growth Rate Versus Optical Power for GaAs Films Grown on Cr-Doped GaAs Substrates. AsH_3 in H_2 Flow Rate Was 62 sccm.

beam spot. When irradiated by the arc lamp beam, the entire GaAs substrate heats up sufficiently to allow pyrolytic mechanisms to participate in the deposition process. Diffusion of decomposition products of the gas-phase reactants also causes deposition outside the arc lamp beam spot in a photolytic deposition process. However, for the later case the deposition rate is expected to decrease as one moves away from the beam spot. The fact that, for the GaAs substrates, the deposition rate changed very little as a function of position on the substrates suggests that the surface diffusion rate of the adsorbed species is quite significant at these temperatures. The observation that the growth rate is not very high is reasonable as the total radiation which would be absorbed by the TEG and arsine molecules is only 40 mw based on optical absorption data reported in the literature.[38,44]

The effect of ultraviolet radiation on the gallium arsenide growth process is not limited to dissociation of the reactants. Recent studies have shown that irradiation of the semiconductor surface during conventional pyrolytic OMCVD provides for significant improvement in the surface morphology of films deposited in the presence of ultraviolet radiation.[47] This suggests that the ultraviolet radiation interacts with the depositing film and/or the adsorbed species in such a way as to enhance the surface kinetic processes necessary for crystalline formation. This effect is illustrated by the X- ray diffraction data for the photodeposited films obtained in this study. For all of the samples deposited at optical power greater than 9.0 watts, the region of the film where the arc lamp beam was incident onto the substrate produced only (200) and (400) diffraction peaks for (100) oriented substrates. Figure 6.12a) shows a typical diffraction pattern for films grown at arc lamp powers greater than 9.0 watts. This

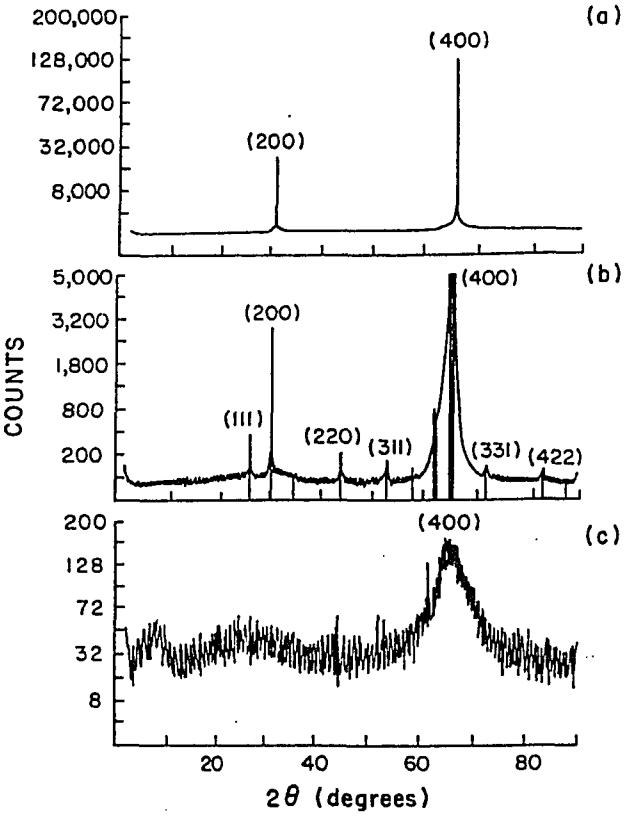

Figure 6.12 X-ray Diffraction Pattern for GaAs Films on GaAs Substrates. The Diffraction Patterns were Obtained from a Film Deposited at an Optical Power of 9.4 Watts (a) at the Center and (b) at the edge. The Diffraction Pattern in (c) Was Obtained from the Center of a Film Deposited at 8.8 Watts.

pattern indicates that the deposited films are single crystal with the same orientation as the substrate. However, X-ray diffraction patterns for the deposited film outside the arc lamp spot location produced peaks other than the (200) and (400) peaks as shown in Fig. 6.12b) indicating misoriented polycrystalline formation. This is in agreement with the SEM micrographs shown in Figs. 6.13 and 6.14 where the morphology is seen to be much different outside the beam spot location as opposed to within the beam spot. At arc lamp powers less than 9.0 watts, however, broad peaks were observed in the diffraction pattern as shown in Fig. 6.12c) for the region of the deposit directly exposed to the arc lamp beam. This indicates that the deposited film is polycrystalline although the orientation of the film remained that of the substrate. The preferred orientation of the film deposited at optical powers greater than 9.0 watts can be verified by observing Fig. 6.15. This SEM micrograph of a photodeposited film shows definite orientation of defects in the deposited film. This film was deposited with deposition conditions identical to that of the film shown in Fig. 6.13 except that the flow rate of 10% arsine in hydrogen was 100 sccm.

In addition to the crystallinity, the electrical properties of the photodeposited films were determined using room temperature van der Pauw measurements. Figure 6.16 shows the results obtained for the carrier concentration as a function of arc lamp incident power. Conditions for deposition were the same as those described for Fig. 6.12. The carrier type for the deposited films changes from n-type to p-type as the optical power is reduced below 9.0 watts. This corresponds with the observed change in the X-ray diffraction pattern noted earlier. The substrate temperature at which this transition occurs is approximately 310°C. The origin of this n-type to p-type

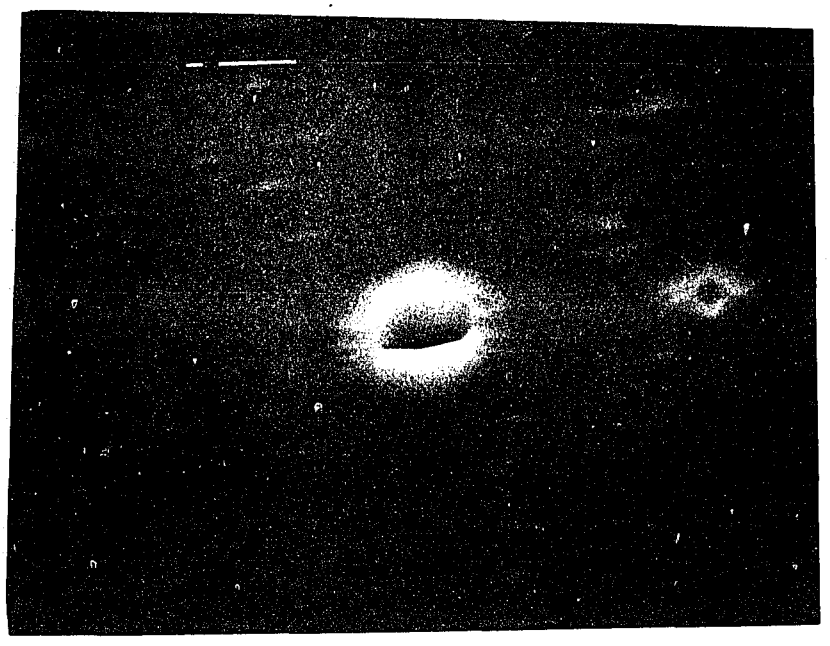

Figure 6.13 SEM Micrograph of the Surface of a Film Grown Inside the Beam Spot with an Optical Power of 9.4 Watts. Longest Line Equals 1.0 μm.

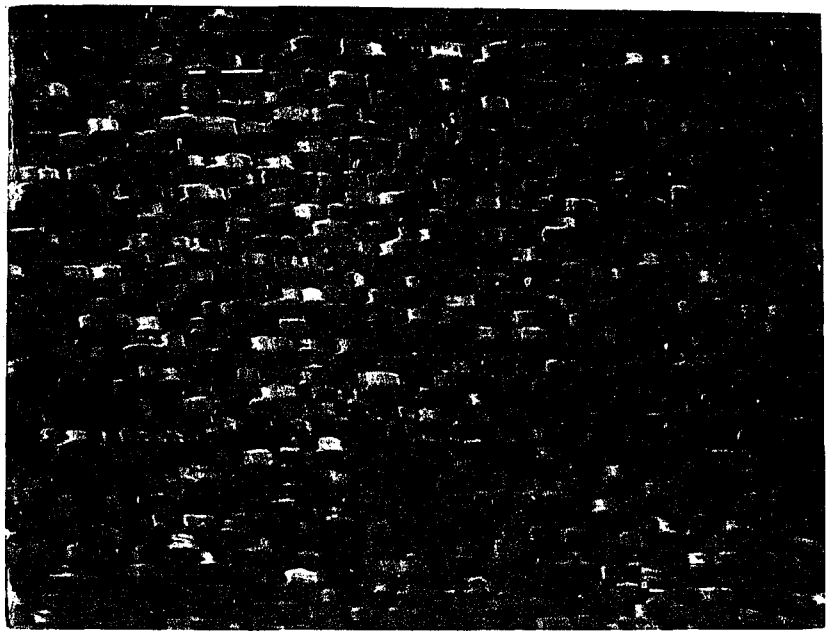

Figure 6.14 SEM Micrograph of the Surface of a Film Grown Outside the Beam Spot with an Optical Power of 9.4 Watts. Longest Line Equals 1.0 μm.

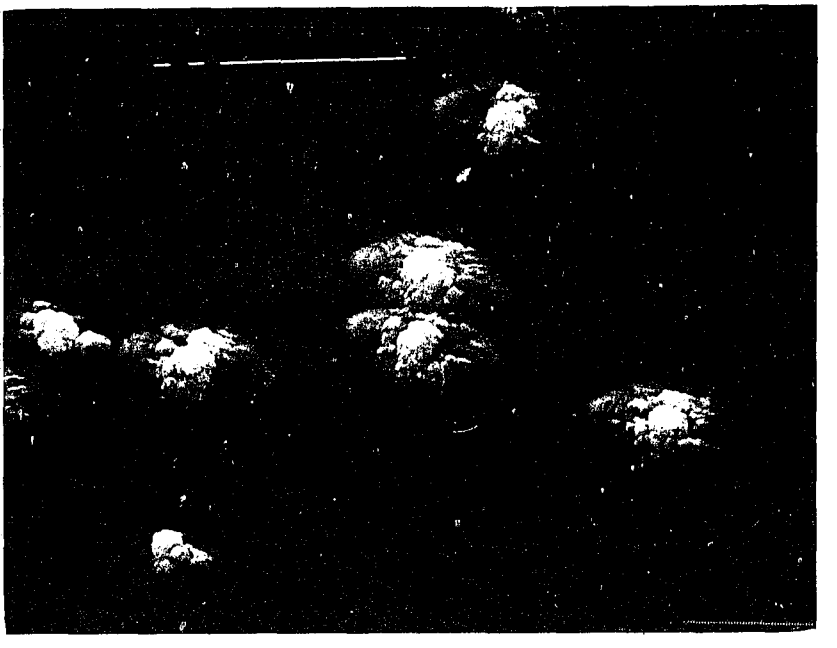

Figure 6.15 SEM Micrograph of GaAs on GaAs Showing Orientation of Surface Defects. Longest Line Equals 10 μm.

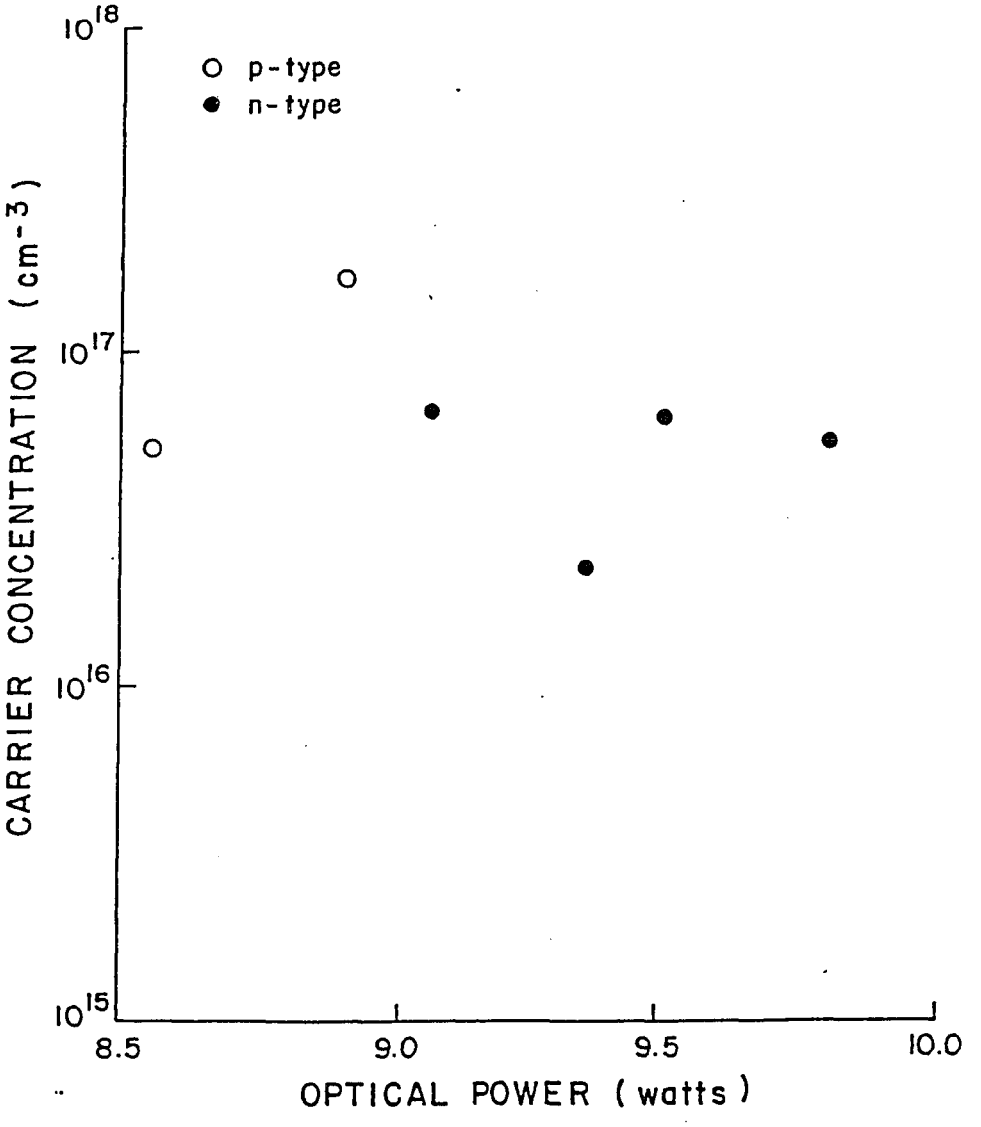

Figure 6.16 Carrier Concentration Versus Optical Power for GaAs Films Grown on GaAs Substrates.

conversion is not clear although a similar transition is reported for pyrolytic OMCVD of GaAs at approximately 420°C.[15] However, the high background carrier concentrations in the samples reported here along with the poor crystallinity of the p-type films make the results difficult to interpret. Figure 6.17 shows the room temperature Hall mobilities measured for these samples.

The influence of the arsine flow rate on the properties of these photodeposited films was also studied. Figure 6.18 shows the film thickness obtained as a function of AsH_3 flow rate. These films were deposited with an optical power of 9.4 watts. In conventional organometallic chemical vapor deposition of GaAs performed in the kinetically-controlled regime, the growth rate only weakly depends on the arsine flow for AsH_3/TEG ratios greater than 5.[10] In this study, growth rate was found to depend strongly on the AsH_3 flow rate even though the AsH_3-to-TEG ratios were well in excess of several hundred. This behavior can be understood by considering the reported growth of GaAs using vacuum OMCVD in which no growth occurs unless the arsine molecules are cracked prior to impingement onto the substrate.[97] This suggests that the deposition of GaAs by OMCVD proceeds via a gas-phase reaction between the metal alkyl and a product such as AsH_2 or AsH formed by the decomposition of arsine. For vacuum OMCVD, the collision rate between the arsenic-bearing species produced through decomposition of arsine by the heated substrate and the triethylgallium molecules is insufficient to obtain growth without pre-cracking the arsine. At a higher pressure of 2 Torr, one would expect an increase in this collision rate. However, at a lower substrate temperature of 317°C, the cracking efficiency of arsine is extremely low leading to a decrease in the collision rate of cracked arsine and

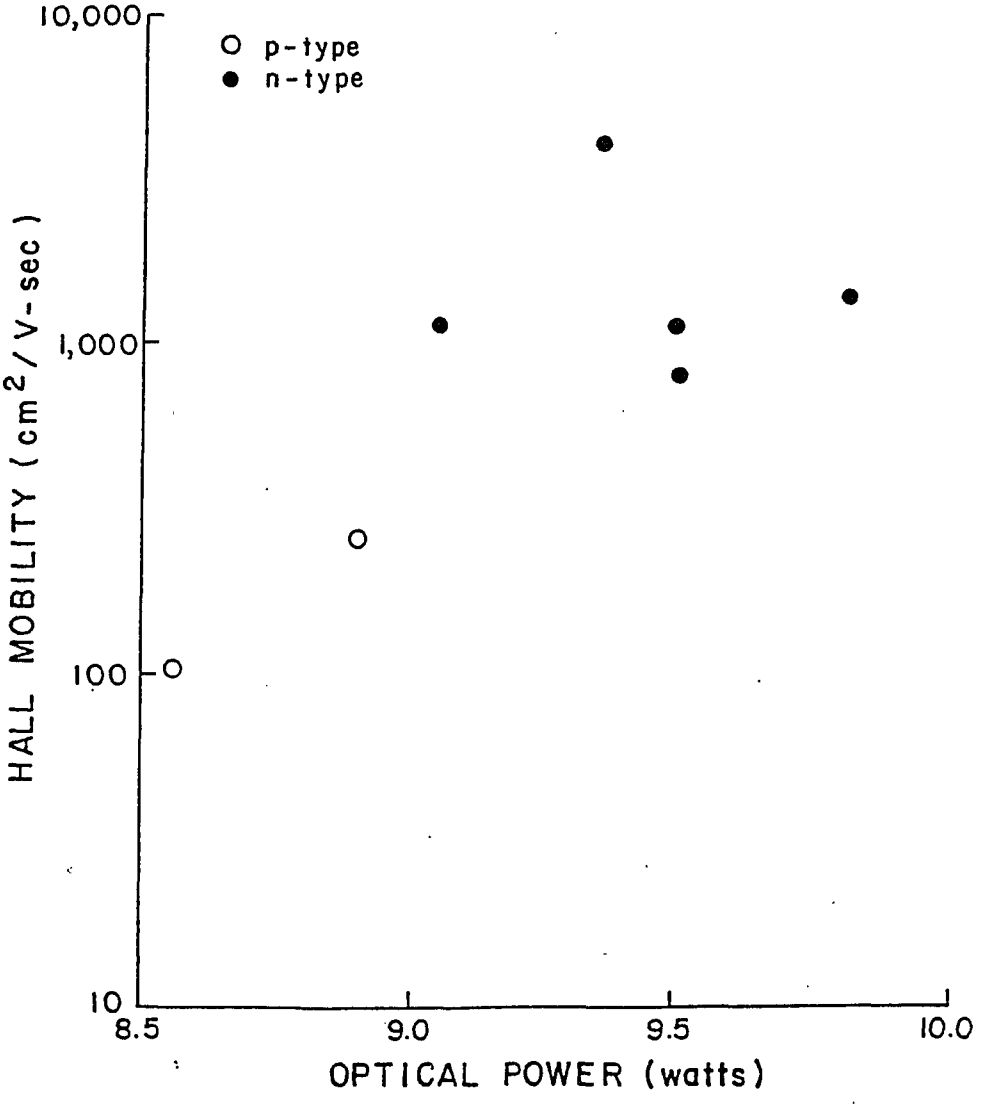

Figure 6.17 Room Temperature Hall Mobility Versus Optical Power for GaAs Thin Films.

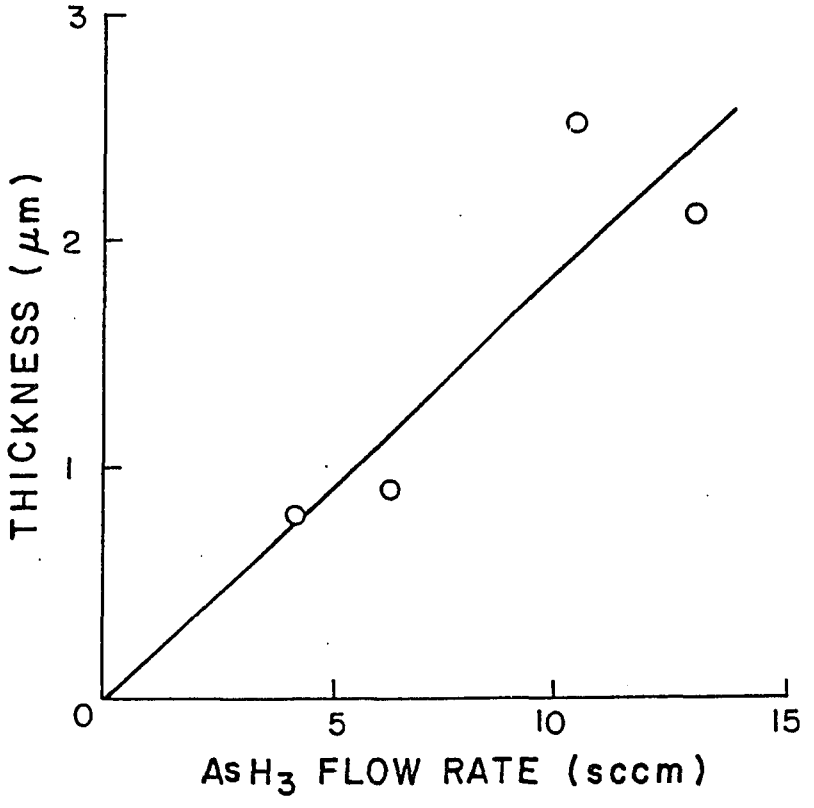

Figure 6.18 Film Thickness Versus Arsine Flow Rate for GaAs Films Obtained with an Optical Power of 9.4 Watts.

the organometallic.[9,98] At 317°C, one would expect the thermal decomposition rate of TEG to be low as well based on results reported by Putz,[22] Mashita[14] and Yoshida[12]. When arsine (and triethylgallium) are being decomposed by photochemical means, the rate of production of decomposed arsine depends directly on the concentration of arsine and hence the flow rate.

Figure 6.19 shows the room temperature Hall mobility on n-type films as a function of the arsine flow rate. In this figure, the flow rates shown are for the arsine and not for the arsine/hydrogen mixture. As seen in the figure, mobility increases with increasing AsH_3 flow. Figure 6.20 shows a SEM micrograph of the surface of a film deposited at a flow rate of 4.1 sccm. Comparing this to Fig. 6.13 where the AsH_3 flow rate was 6.17 sccm, it is clear that the morphology improves with increasing AsH_3 flow rate. This improvement in mobility with increasing arsine flow rate may be the result of decreased crystalline defects within the deposited film as evidenced by the change in surface morphology.

6.3 Photochemical Vapor Deposition of Gallium Arsenide on Silicon Using a Hg-Xe Arc Lamp

Silicon was chosen as an alternative substrate material for photodeposition of GaAs. Silicon differs in thermal conductivity but has a crystal lattice symmetry that is similar to that of GaAs. The difference in the thermal response of silicon versus GaAs substrates was evident as the temperature of the silicon substrate, irradiated with 9.4 watts of optical power from the arc lamp with a beam diameter of 6.4 mm, rose to only 210°C as opposed to 317°C for the GaAs substrate. Figure 6.21 shows the X-ray

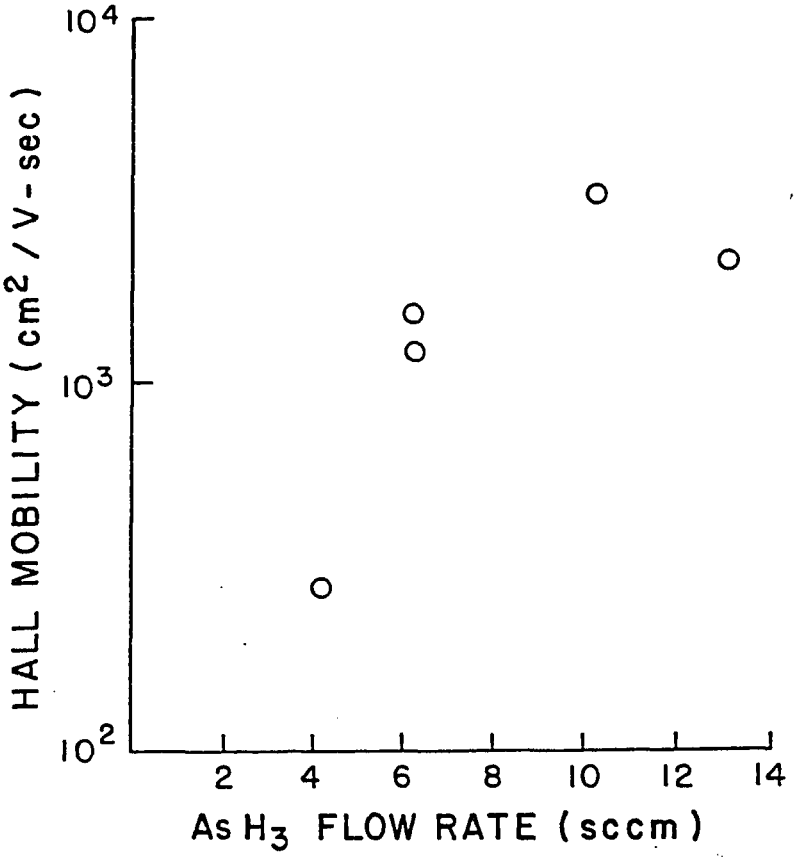

Figure 6.19 Room Temperature Hall Mobility Versus Arsine Flow Rate for GaAs Films Obtained with an Optical Power of 9.4 Watts.

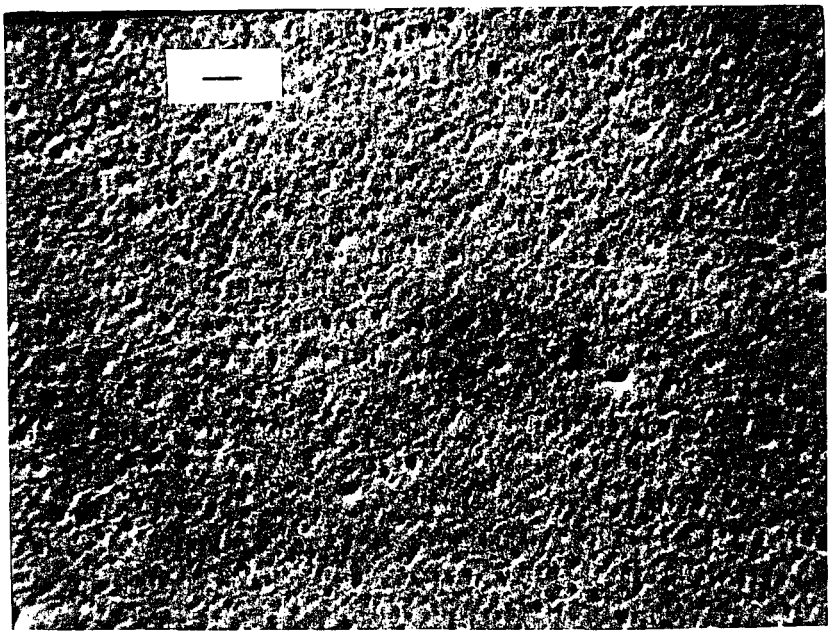

Figure 6.20 SEM Micrograph of a Film Photodeposited with an Arsine Flow Rate of 4.1 sccm. The Optical Power for this Film Was 9.4 Watts. Longest Line Equals 1 μm.

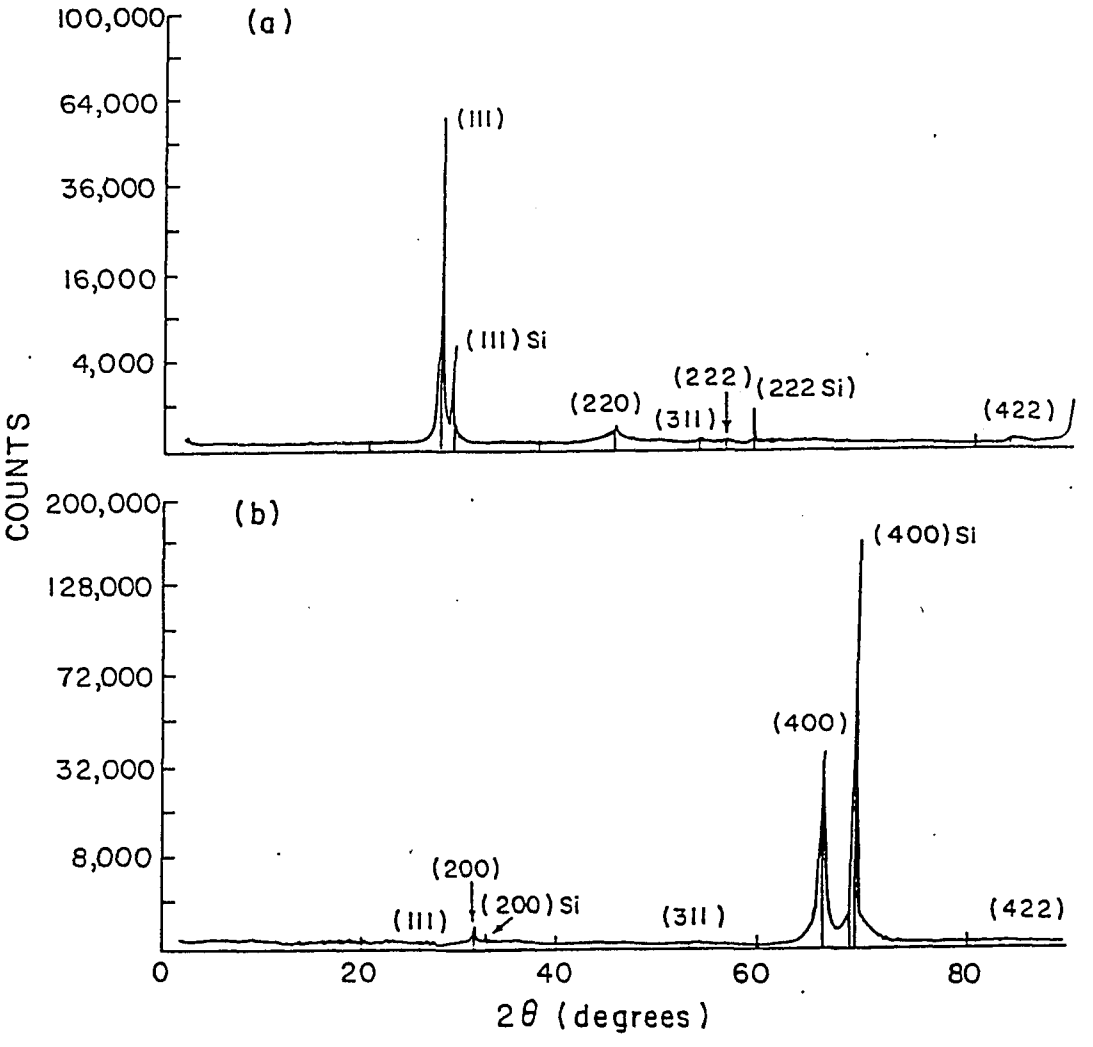

Figure 6.21 X-ray Diffraction Pattern for GaAs Films Photodeposited on (a) (111) Silicon and (b) (100) Silicon Substrates.

diffraction data for films deposited on (111) and (100) silicon substrates with an optical power of 9.4 watts. The silicon substrates were 1 cm square. Flow rates were the same as those described in Fig. 6.13. Unlike the photodeposited films on GaAs substrates, the GaAs on Si films did show diffraction peaks corresponding to orientations other than that of the substrate. However, the GaAs peaks coinciding with the silicon substrate orientation were more than 2 orders of magnitude larger than any other GaAs peak indicating that the majority of the GaAs film maintained the same orientation as the Si substrate. This is seen to be true for both (111) and (100) oriented substrates. The fact that oriented GaAs films can be deposited on substrates with significantly different thermal properties and hence substrate temperatures indicates the photolytic effect of ultraviolet radiation on the crystal growth kinetics at these low substrate temperatures.

Figures 6.22 through 6.25 shows SEM micrographs of the film cross-section as well as the surface morphology of a GaAs film grown on a (111) silicon substrate. From the cross-section, the grain boundaries are clearly evident verifying that these films are polycrystalline. The film thickness is seen to be 1.6 micrometers at the center of the beam spot location. Unlike the films photodeposited on GaAs substrates, the films deposited on the silicon substrates showed considerable variation in film thickness as a function of position on the substrate as shown by the surface profile in Fig. 6.26. The point of zero thickness shown in this figure was chosen arbitrarily and does not represent the film-substrate interface. The thickness of the GaAs film deposited on the (111) Si substrate dropped to 0.3 micrometers near the edge of the substrate as determined with an SEM cross-section of the film. Figure 6.27 shows the

Figure 6.22 SEM Micrograph of the Cross-Section of a GaAs Film Deposited on (111) Silicon. Longest Line Equals 1 μm.

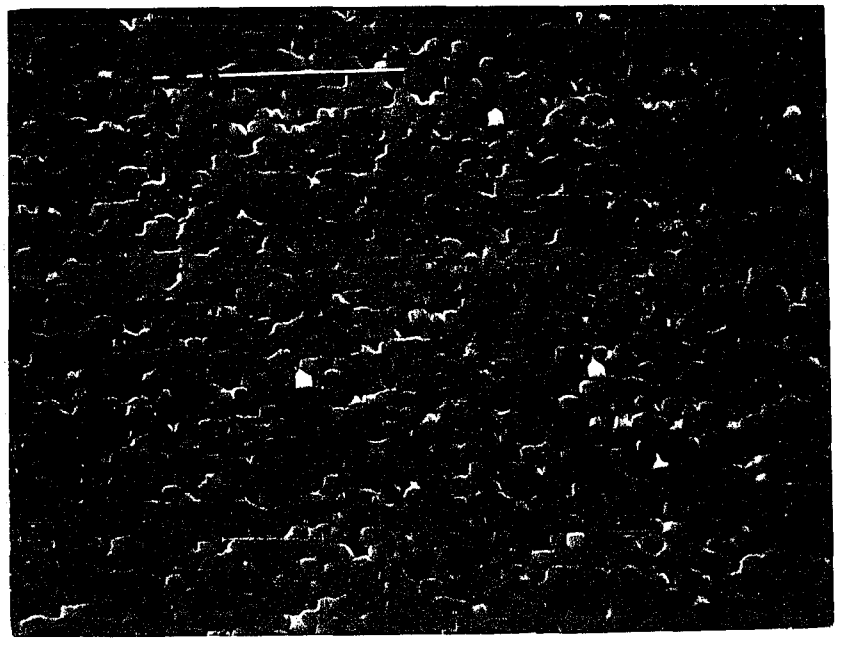

Figure 6.23 SEM Micrograph of the Surface Morphology of a GaAs Film Photodeposited on (111) Silicon at the Center of the Arc Lamp Beam Spot Location. Longest Line Equals 10 μm.

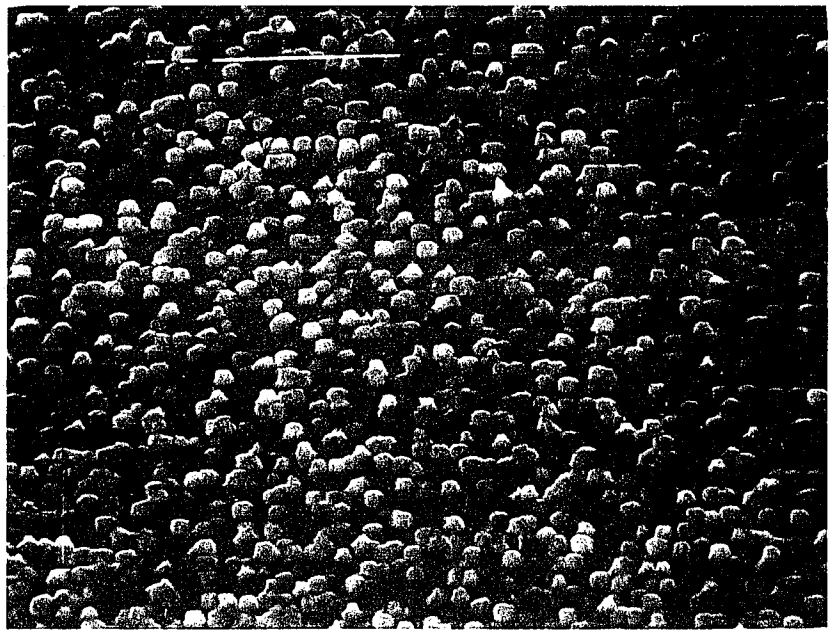

Figure 6.24 SEM Micrograph of the Surface Morphology of a GaAs Film Photodeposited on (111) Silicon Near the Edge of the Arc Lamp Beam Spot. Longest Line Equals 10 μm.

Figure 6.25 SEM Micrograph of the Surface Morphology of a GaAs Film Photodeposited on (111) Silicon Outside of the Arc Lamp Beam Spot Location. Longest Line Equals 10 μm.

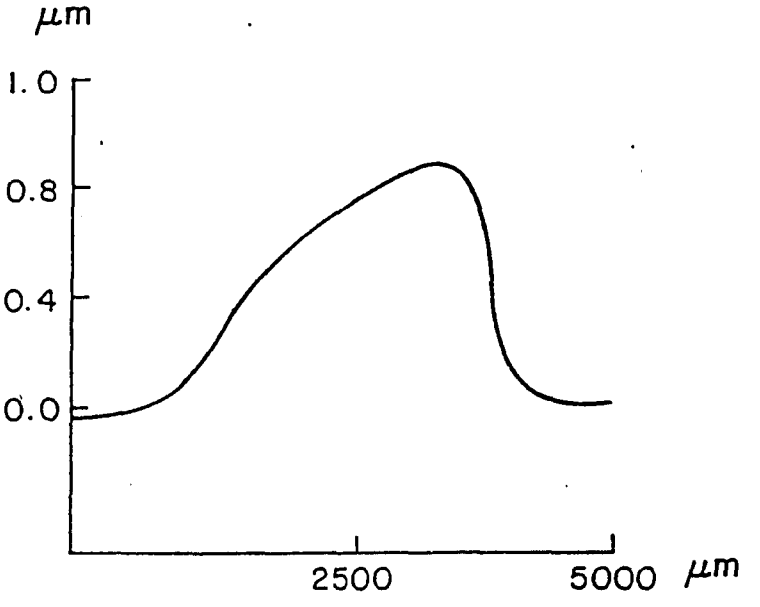

Figure 6.26 Surface Profile of GaAs Film Photodeposited on Silicon.

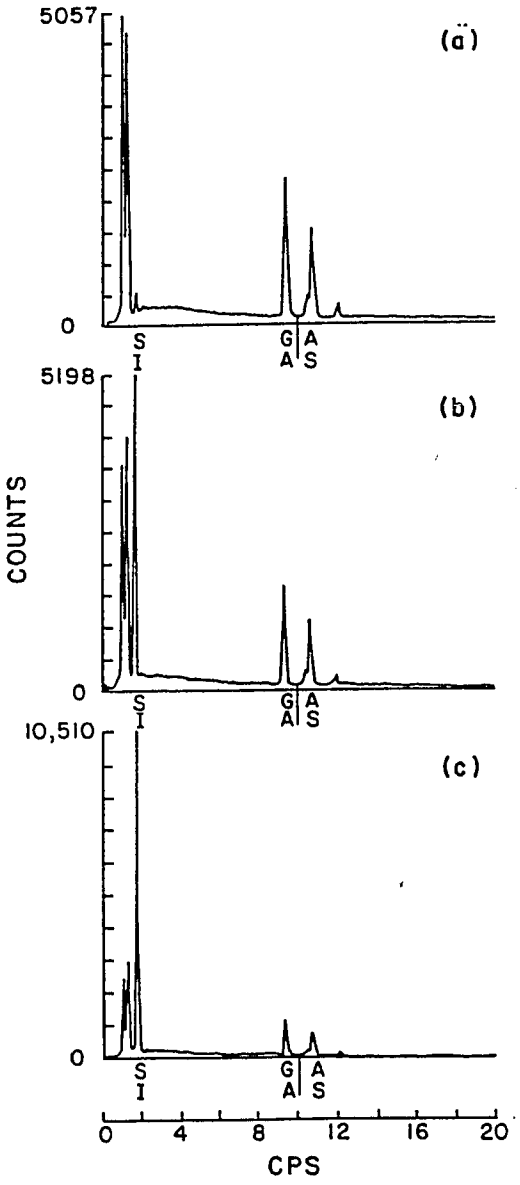

Figure 6.27 Energy-Dispersive Spectrometry Measurements for a GaAs Film on a Silicon Substrate. The Spectra Were Taken (a) at the Center, (b) at the Edge and (c) Outside of the Arc Lamp Beam Spot Location.

results of energy-dispersive spectrometry measurements for one of the films deposited on (100) silicon. By following the increase in the silicon peak, it is clear that most of the growth was limited to the beam spot location. This result suggests that the mechanism responsible for the apparent lack of position dependence of the deposition rate observed on GaAs substrates is thermal is nature. The deposition that occurs for the case of silicon substrates is dominated by the photo-induced decomposition of the reactants as thermal decomposition will be insignificant at 210°C. The deposition extends beyond the confines of the beam spot location due to diffusion of the products of the photodecomposition as mentioned earlier. The deposition rate at the center of the beam spot location for the GaAs photodeposited on Si is slightly higher than that obtained for the GaAs deposited on GaAs substrates. This result indicates that photo-initiated decomposition of the reactants is significant. In the case of GaAs films grown on GaAs substrates, thermal and photolytic mechanisms combine to give the observed film growth with surface diffusion effectively eliminating any localization in the deposition rate. However, the quality of the deposited film experiences localization for both the GaAs and Si substrates.

From the energy-dispersive spectrometry measurements, it was found that the GaAs on Si films were not stoichiometric. These measurements revealed that the GaAs films were consistently arsenic rich consisting of approximately 55% As and 45% Ga. The only exception to this was observed on one film which at the center of the beam spot location was near stoichiometric GaAs with the rest of the film away from the center and outside of the arc lamp beam spot being arsenic rich. As mentioned earlier, the temperature of the substrate was determined to be approximately 210°C. At this

temperature, the vapor pressure of arsenic is not high enough to insure the evaporation of excess arsenic from the growing film surface resulting in As rich films. This is consistent with results we have reported earlier on the photodeposition of GaAs on fused silica.

Auger electron spectroscopy measurements of the deposited film, shown in Fig. 6.28, were basically the same at all points on the substrate. The spectra shown in Fig. 6.28 was taken outside the beam spot location after removing approximately 40 nm from the surface by sputtering. Note that the carbon peaks indicates less than 0.2% carbon incorporation which is much less than that reported elsewhere for photodeposited GaAs using organometallics.

The results of this study suggest that photolytically-driven chemical vapor deposition of Ga_xAs_{1-x} at greatly reduced temperatures (200°C) is possible. Although the mechanisms are not understood at this time, it also appears that the light-induced processes leading to enhancement of surface kinetics to promote improved crystalline quality occur at these low temperatures. However, the fact that non-stoichiometric Ga_xAs_{1-x} films were consistently obtained on the silicon substrate at 210°C may impose a restriction on the minimum substrate temperature as the evaporation of excess As is necessary in obtaining electronically useful thin films.

6.4 Photochemical Vapor Deposition of GaAs Using an ArF Excimer Laser

In this Section, deposition of GaAs on a variety of substrate materials is described using an ArF excimer laser. This light source emits at 193 nm with 35 mJ energy per pulse and a repetition rate of 20 Hz. In order to separate the effects of

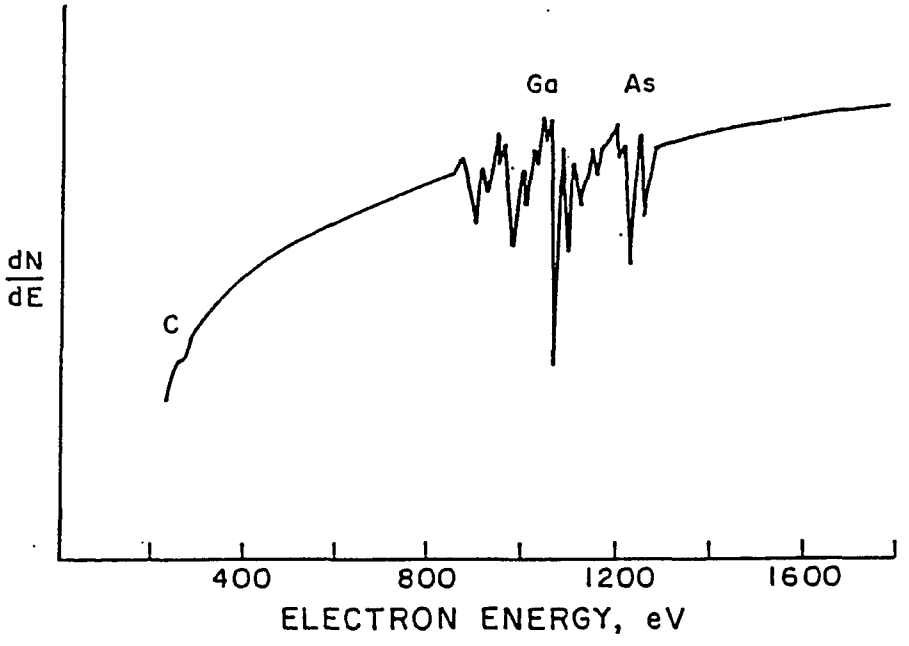

Figure 6.28 Auger Electron Spectroscopy of GaAs Film Photodeposited on Silicon.

absorption of light by surface-adsorbed species versus gas-phase species, the laser beam was introduced parallel to the substrate. The beam was focused with a fused silica lens. The deposition chamber, shown in Fig. 6.29, was redesigned to accommodate the parallel beam geometry. Modification of the chamber also included the substrate holder allowing for a maximum substrate temperature of approximately 600°C.

Figure 6.30 shows the experimental set-up used for these experiments. A Hg-Xe arc lamp was used in conjunction with the laser with the arc lamp radiation incident perpendicular to the substrate. The optical output of the arc lamp was much less than that used in the experiments reported in Section 6.2 or 6.3 with the principal effect of the arc lamp radiation being to heat the substrates. The arc lamp radiation power density was 0.85 watts/cm^2. The final temperature of the substrates was determined taking into account the effect of the arc lamp radiation.

Deposition was carried out on fused silica, silicon and gallium arsenide substrates. The deposited films were smooth and featureless. Both the film deposition rate and the composition of the film was found to depend on the substrate temperature with the films deposited at low temperatures being arsenic-rich. The films became gallium-rich at higher substrate temperatures as shown in Fig. 6.31. In this figure, GaAs was used as the substrate material and the deposition conditions included a 10% AsH_3 in H_2 flow rate of 82 sccm, a N_2 flow rate through the TEG bubbler of 9.8 sccm, a bubbler temperature of 30°C, and a deposition time of 60 min. A 250 sccm N_2 purge of each window was provided with a chamber pressure of 1500 mTorr. The deposition rate on fused silica at 200°C was 0.15 μm/hr with the film containing less than 1% Ga. As seen in Fig. 6.31, the incorporation of gallium increases dramatically between 320

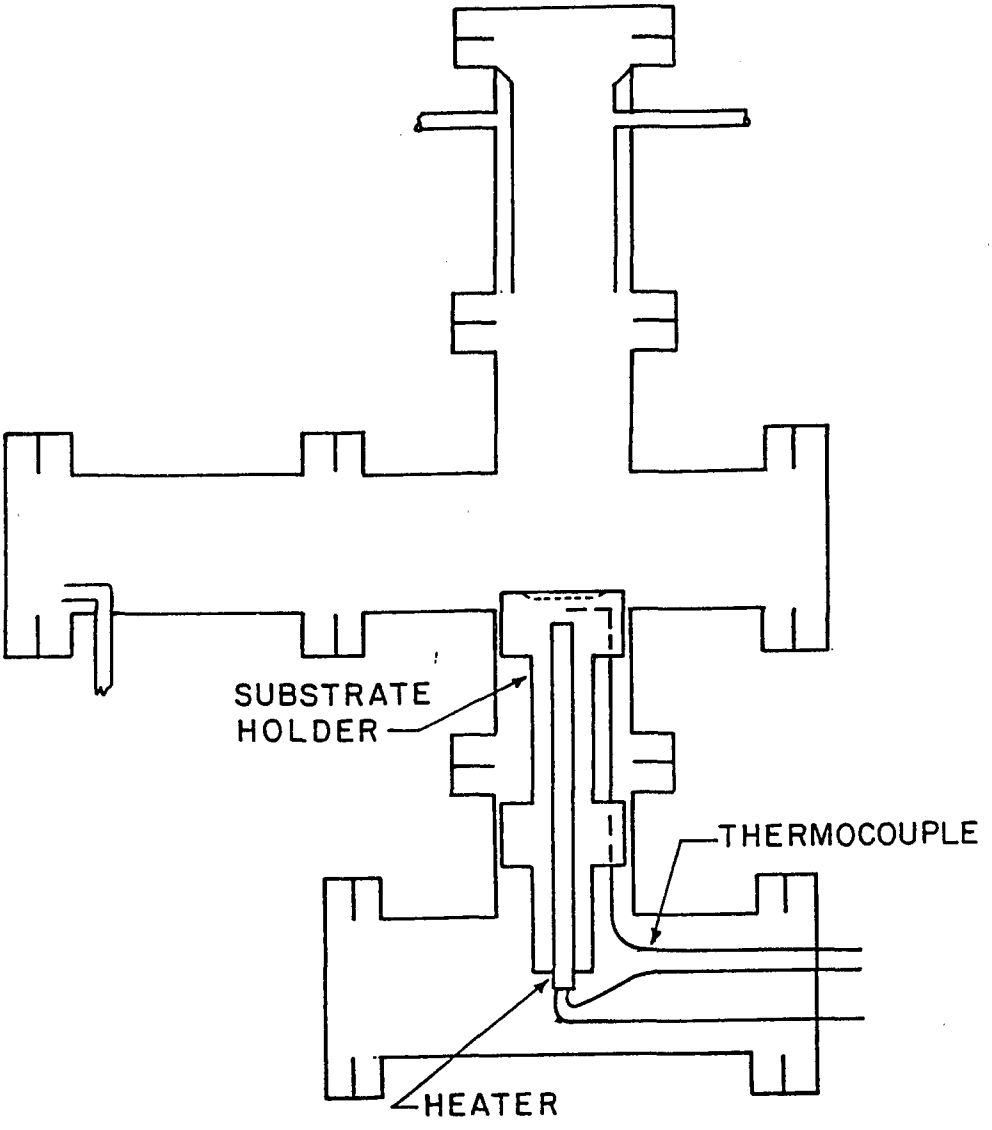

Figure 6.29 Chamber Utilized for Laser Deposition of GaAs.

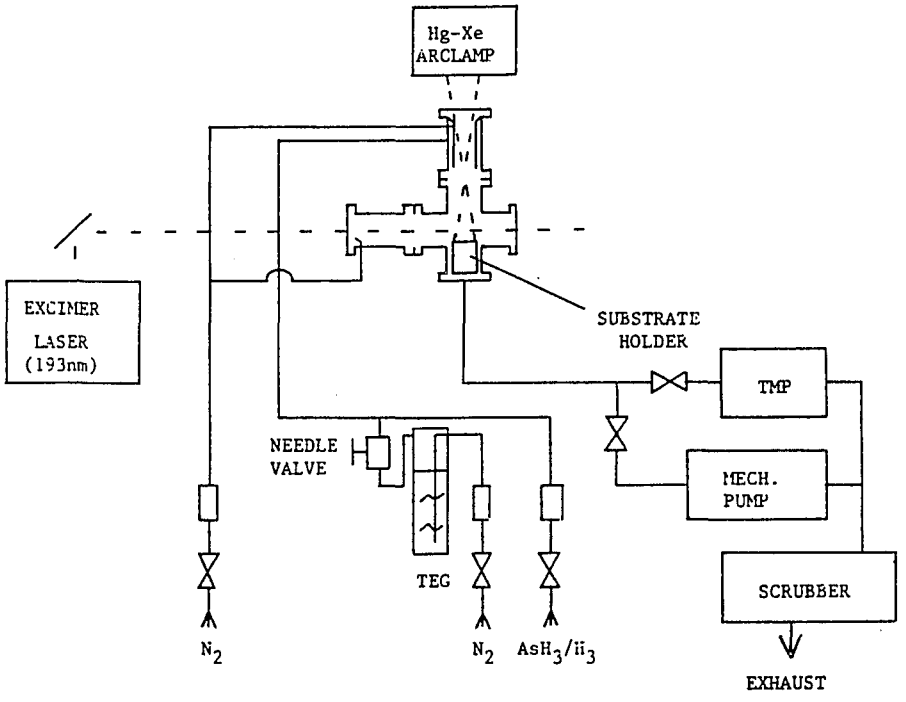

Figure 6.30 Experimental Set-Up for Deposition with a Parallel Beam Utilizing Laser Radiation.

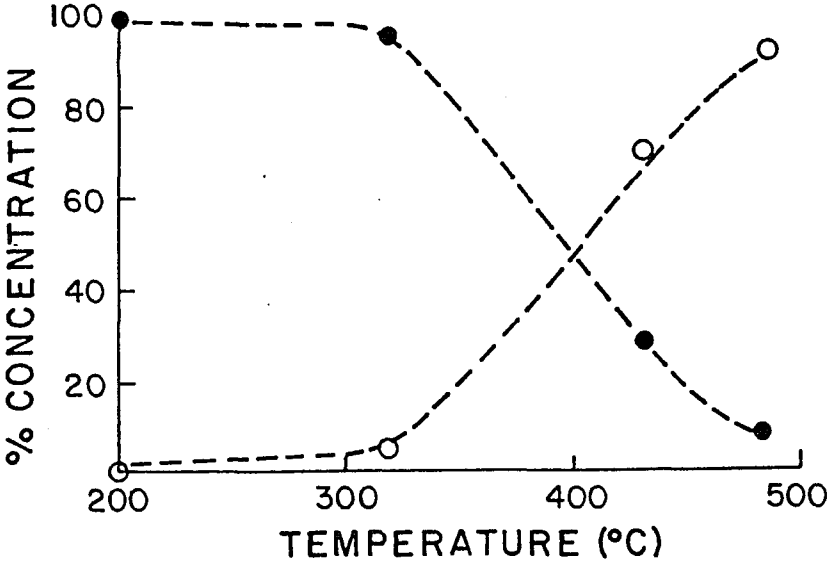

Figure 6.31 Film Concentration as a Function of Substrate Temperature. The Solid Circles Represent Arsenic Concentration with the Open Circles Representing Gallium Concentration.

and 485°C. This appears to be due to the thermal decomposition of TEG at the substrate surface coupled with the increased vapor pressure of arsenic.

Figure 6.32 illustrates the dependence of the composition of the depositing thin film on the distance of the laser beam above the substrate surface. For this experiment, the angle of incidence was approximately 4° with the minimum distance of the laser beam above the substrate approximately 1 mm resulting in a variation in the distance of the laser beam above the substrate of less than 0.5 mm. The substrate temperature was approximately 435°C with the substrate being GaAs. As seen in the figure, the amount of arsenic incorporated into the film increased as the distance from the laser beam to the substrate decreased. The gallium deposition rate is limited by the pyrolytic decomposition of TEG at the substrate surface which is independent of the presence of the laser. The arsenic deposition rate is limited by diffusion of photolytically decomposed molecules from the laser beam to the substrate surface. In Chapter 7, these results will be utilized qualitatively in developing a first order model for the light-driven deposition of GaAs.

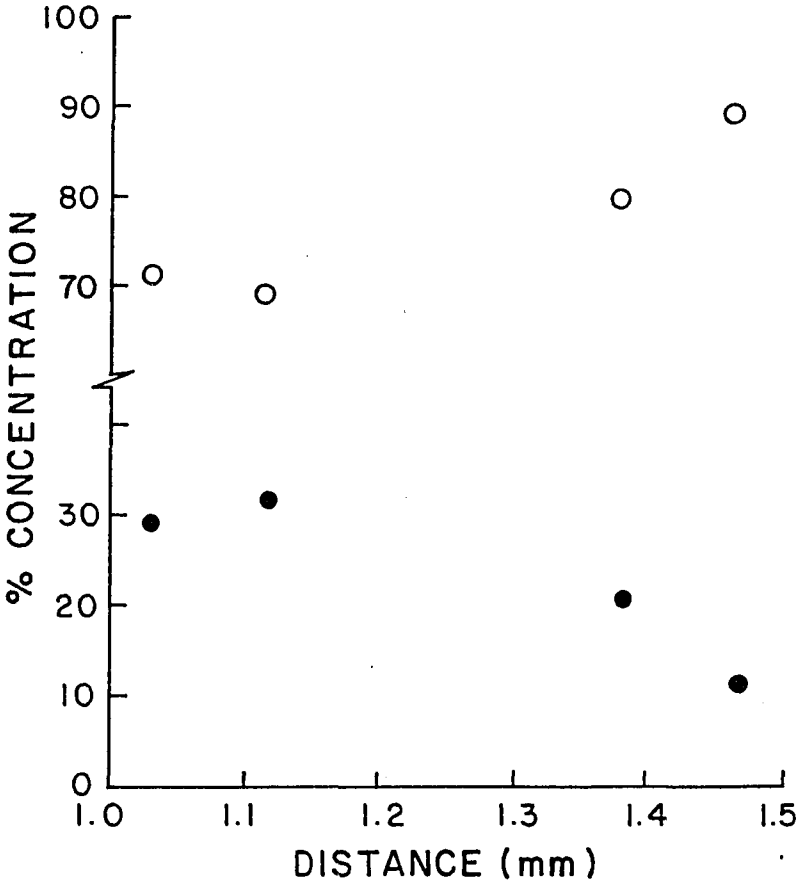

Figure 6.32 Film Concentration as a Function of the Distance Between the Laser Beam and the Substrate Surface. The Solid Circles Represent Arsenic Concentration with the Open Circles Representing Gallium Concentration.

CHAPTER 7

MECHANISMS INVOLVED IN LIGHT-DRIVEN CHEMICAL VAPOR DEPOSITION OF GaAs

7.1 Mass Spectroscopic Study of Photolytic Decomposition of Triethylgallium and Arsine

In attempting to understand the photochemical vapor deposition of GaAs, it is of use to know the products of photodissociation of the reactants. Mass spectrometry was used to help identify these photoproducts for triethylgallium, arsine and the combination of the two reactants in the presence of ultraviolet radiation. Figure 7.1 shows the experimental set-up used to perform this study. A Dycor M200M quadrupole gas analyzer with a pressure reduction arrangement was used. The chamber was initially pumped down to 10^{-6} Torr with a turbomolecular pump. For recording of the mass spectrum, the evacuated chamber was sealed. A small amount of reactant was then leaked into the chamber until the pressure reached a pre-determined value (typically 2 Torr). The gas analysis data was taken in stagnant conditions with no gas flowing. In addition, a Hg-Xe arc lamp was made to pass parallel to the susceptor for this spectroscopic study.

The photolytic decomposition of triethylgallium was studied using this apparatus. As the carrier gas was N_2, the peak at mass-to-charge ratio of 28 was used to normalize all other peaks. The cracking pattern for triethylgallium in nitrogen at room temperature was recorded and shown to be essentially the same as that reported elsewhere.[12,14] In order to observe the change in the mass spectrum in the presence of

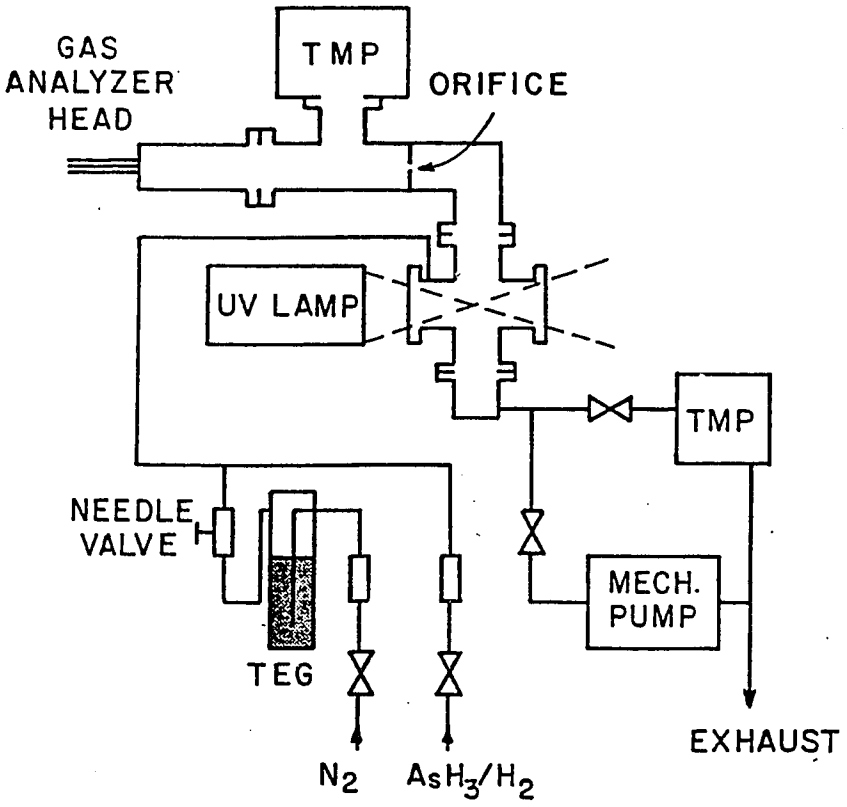

Figure 7.1 Experimental Set-Up Utilized for the Mass Spectrometry Study.

the Hg-Xe arc lamp radiation, the normalized spectrum obtained at room temperature was subtracted from the normalized spectrum obtained at room temperature in the presence of the ultraviolet radiation. The results are shown in Fig. 7.2. It appears that the fragmentation of triethylgallium due to photolysis is quite similar to that reported for the thermal decomposition of this organometallic with ethylene (C_2H_4) and butane (C_4H_{10}) produced with no indication of ethane (C_2H_6). This suggests that photodissociation of triethylgallium is similar to the β-elimination reaction observed for pyrolytic decomposition as discussed in Chapter 2. Peaks at a mass-to-charge ratio of 15 and 16, indicative of methane, were observed as well. However, the occurrence of these peaks was too inconsistent to be conclusive.

Additional information was obtained on the cracking pattern of TEG from analysis of films deposited on fused silica with the substrate temperature less than 240°C from the photodissociation of TEG using a Hg-Xe arc lamp. Films were found, using AES, to consist of approximately 65% carbon. This suggests that the film which is deposited consists of a gallium atom with one ethyl radical attached.

Although it is not possible, based upon available data, to specify the precise path of photodecomposition of TEG, some preliminary conclusions can be drawn. The results of this work can be explained by the following reaction pathway:

$$(C_2H_5)_3Ga + h\nu \rightarrow (C_2H_5)_2GaH + C_2H_4 \quad (7.1)$$

$$(C_2H_5)_3Ga + h\nu \rightarrow (C_2H_5)_2Ga + C_2H_5 \quad (7.2)$$

$$C_2H_5 + C_2H_5 \rightarrow C_4H_{10} \quad (7.3)$$

$$C_2H_5 \rightarrow C_2H_4 + H \quad (7.4)$$

$$(C_2H_5)_2GaH(ad) \rightarrow C_2H_4 + H_2 + C_2H_5Ga(ad) \quad (7.5)$$

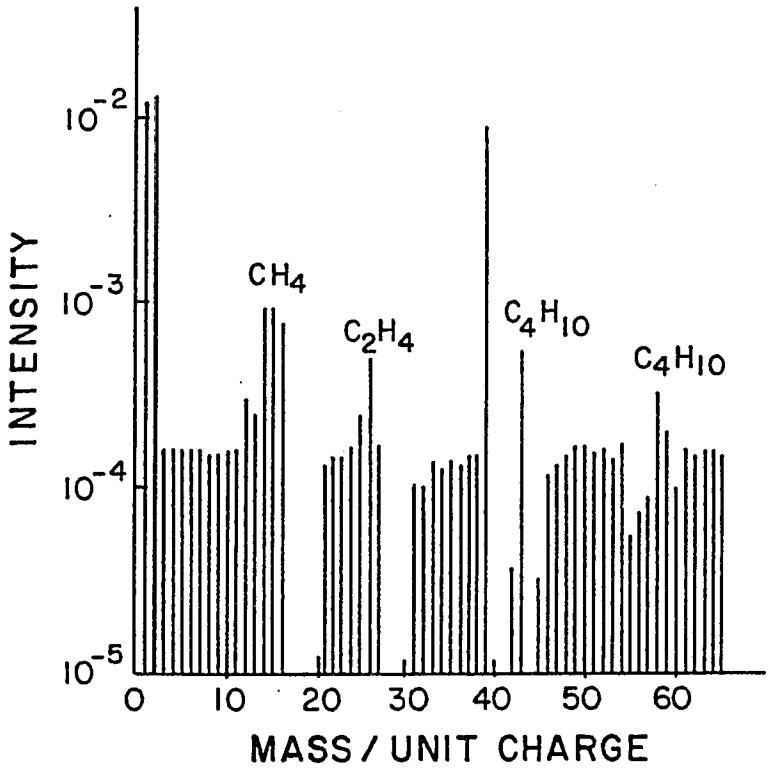

Figure 7.2 Normalized Mass Spectrometer Data for TEG in N_2 Exposed to Ultraviolet Radiation. Cracking Pattern of TEG in N_2 at Room Temperature with No UV Light Present has been Subtracted from the Spectrum.

where (ad) indicates a surface-adsorbed species. Although this set of reactions is incomplete, it does not allow for the production of ethane (C_2H_6) which is in agreement with the data.

The effect of the UV radiation from the Hg-Xe arc lamp was investigated for AsH_3 as well. Figure 7.3 shows the net change in the mass spectrum after exposure of the reactant to UV radiation for 60 min. In this bar graph, dashed lines represent a negative change in the spectrum. The initial partial pressures of AsH_3 and H_2 were 140 and 1260 mTorr, respectively. Total optical output was approximately 12 watts. A significant decrease in the peaks corresponding to arsine was observed indicating that photolysis of AsH_3 has occurred with the arc lamp radiation. The additional peaks observed may be attributed to the release of hydrocarbons adsorbed on the apparatus walls from previous experiments.

Figure 7.4 shows the net change in the mass spectrum with ultraviolet radiation exposure for an AsH_3–TEG–H_2–N_2 mixture. The spectrum was normalized using the mass-to-charge ratio of 28 as the reference. The peaks found for UV exposure of TEG-N_2 and AsH_3–H_2, shown in Figs. 7.2 and 7.3, were also found present in the spectrum for the combined system. There are also some peaks which were not present in the previous spectra. Of particular interest is the peak at a mass-to-charge ratio of 30 which corresponds to the formation of ethane. A reaction appears to occur between the ethyl radical and a hydrogen-bearing species producing ethane. It has not been determined, however, whether this involves the molecular hydrogen or the hydrogen from the arsine molecules or photofragments. Mashita et al. have proposed that ethyl radicals interact with arsine molecules resulting in the reaction[14]

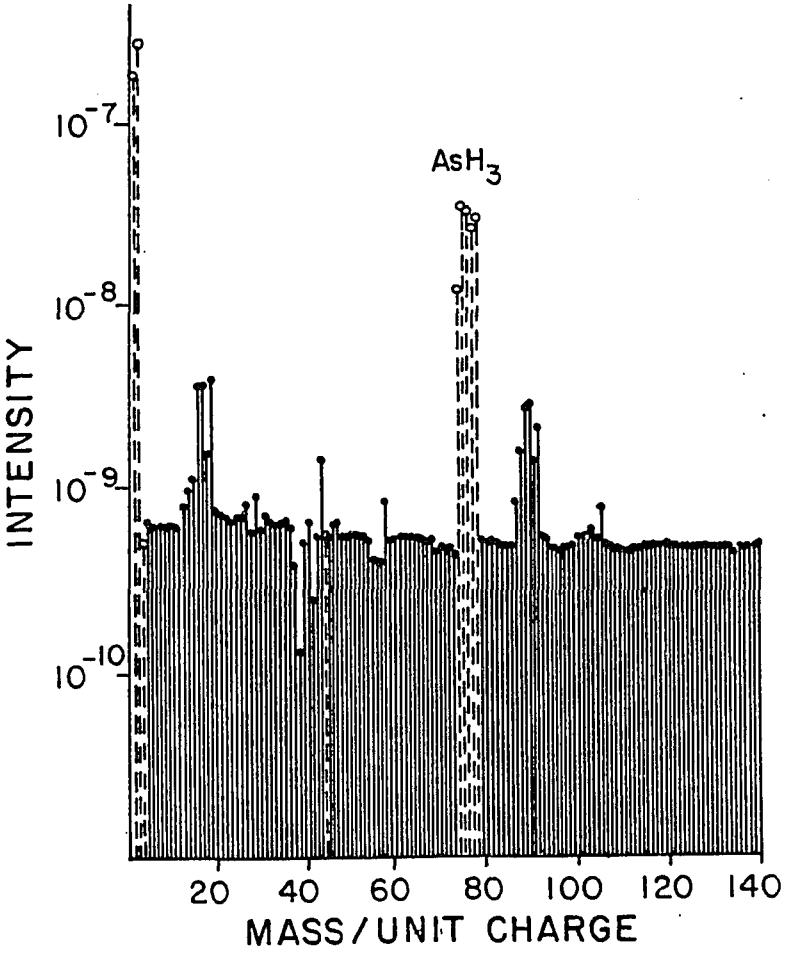

Figure 7.3 Net Change in Mass Spectrum for AsH_3 in Hydrogen Exposed to Ultraviolet Radiation. No Normalization was Performed.

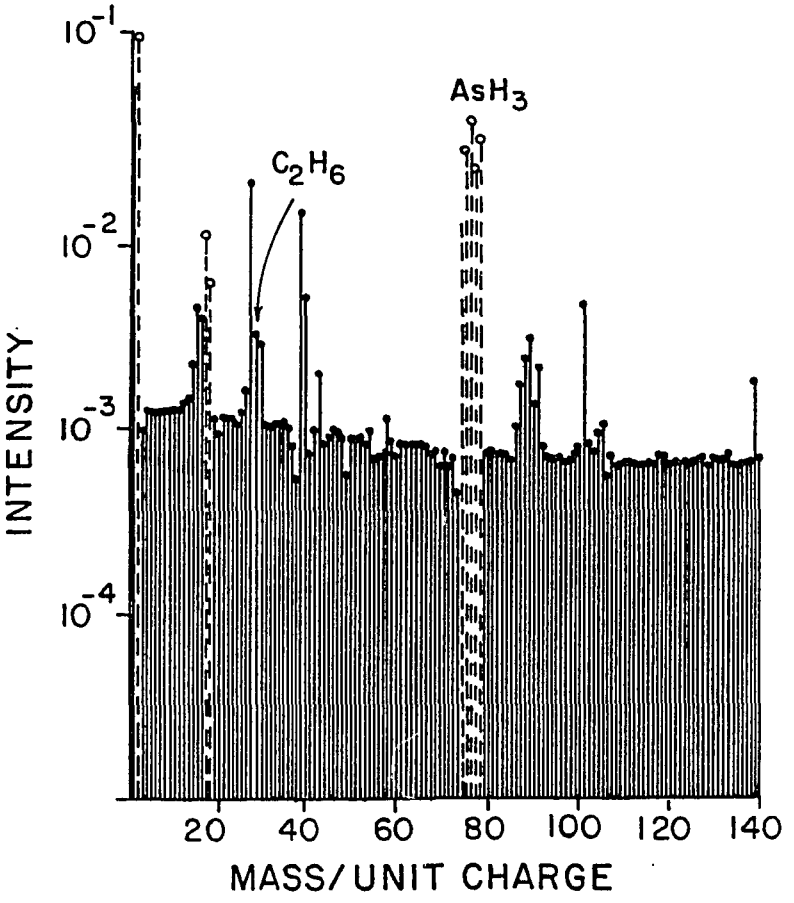

Figure 7.4 Normalized Mass Spectrometer Data for an AsH_3-TEG-H_2–N_2 Mixture Exposed to UV Radiation. The Cracking Pattern for the Mixture with No UV Radiation Present has been Subtracted from the Spectrum.

$$C_2H_5 + AsH_3 \rightarrow C_2H_6 + AsH_2 \qquad (7.6)$$

In addition, a peak corresponding to $(C_2H_5)GaH$ is also present in the spectrum.

The Auger electron spectra taken for the GaAs films deposited on fused silica reported in Section 6.1 contained no detectable carbon. This was true for the film deposited at the center of the beam spot location as well as for the As rich film deposited towards the edge of the beam spot where heating of the depositing film is less. This is in contrast to what was observed for the photolysis of TEG in N_2 where the deposited film was found to contain 65% carbon. It appears that the ethyl radicals are satisfied by the hydrogen available from either the molecular hydrogen or the arsine.

From the mass spectroscopic study, it is clear that photolytic decomposition occurs in the gas phase with the Hg- Xe arc lamp radiation. In obtaining growth with incident ultraviolet radiation, the additional possibility exists that photodecomposition is dominated by absorption from the surface-adsorbed molecules. In fact, depending on how the surface-adsorbate interaction affects the optical absorption of the molecules, the absorption cross-section may be increased at the wavelengths available from the light source. The results presented in Section 6.3 for photodeposition of GaAs using incident Hg-Xe arclamp radiation lend support to optical absorption by the adsorbate as being dominant in photolytic decomposition leading to deposition. A significant deposition rate on Si substrates at approximately 210° of 1.6 μm/hr was obtained at the beam spot location with the deposition localized. Outside the beam spot location, a deposition rate of only 0.3 μm/hr was realized with this deposition occurring due to diffusion of photofragments in the gas-phase formed within the arc lamp beam spot.

7.2 Model for Light-Driven Chemical Vapor Deposition of Gallium Arsenide

In the preceding Chapters, three mechanisms for dissociation of the reactant have been utilized, namely photolysis, Hg-photosensitization and pyrolysis. Each mechanism leads to a somewhat different behavior when utilized for deposition. As stated in Chapter 2, certain aspects of the mechanisms involved in conventional OMCVD of GaAs are not yet well understood. The use of light to achieve deposition complicates the matter further. However, based on the work reported here and elsewhere in the literature, it is possible to develop a first order model to explain several aspects of the observed behavior. In the remainder of this Chapter, such a model is developed for light-driven deposition of GaAs. Whenever possible, experimental observations will be used to support the validity of this model.

For pyrolytically-driven photochemical vapor deposition in which the effect of the light source is simply to heat the substrate, the growth behavior should be quite similar to conventional OMCVD. The Langmuir-Hinshelwood mechanism discussed in Chapter 2 should explain the kinetics of growth with a localized growth rate, R_g, determined by[10]

$$R_g(r,T) = \frac{K_1 \beta_{AsH_3}\beta_{TEG} P_{AsH_3} P_{TEG} \exp(-\Delta E/RT)}{(1 + \beta_{AsH_3} P_{AsH_3})(1 + \beta_{TEG} P_{TEG})} \qquad (7.7)$$

where ΔE is the apparent activation energy for pyrolytic decomposition of the reactants. Although β_{AsH_3}, β_{TEG} and K_1 will depend on temperature, the dominant temperature dependence will be contained within the exponential term. The temperature distribution is given by the heat equation which can be written in cylindrical coordinates as

$$\frac{\partial T}{\partial t} = D(T)\left[\frac{1}{r}\frac{\partial T}{\partial r} + \frac{\partial^2 T}{\partial r^2} + \frac{\partial^2 T}{\partial z^2} + \frac{\partial \ln \kappa}{\partial T}\left[\left(\frac{\partial T}{\partial r}\right)^2 + \left(\frac{\partial T}{\partial z}\right)^2\right] + \frac{(1-R)\, I'_o \alpha}{\kappa}\exp(-r^2/r_o^2)\exp(-\alpha z)\right] \tag{7.8}$$

where r_o is the radius of the light beam, $\kappa(T)$ is the thermal conductivity, $D(T)$ is the thermal diffusivity, α is the optical absorption coefficient, I'_o is the light intensity and R is the reflectivity. This equation takes advantage of the symmetry of the beam and assumes that the light beam has an intensity distribution which is Gaussian.

Equation (7.7) explains the observed deposition rate only in the low temperature kinetically-controlled regime where the thermal decomposition of the surface-adsorbed reactants is rate-limiting. At higher temperatures, mass transport will become the rate-limiting process. As the temperature of the depositing film irradiated with an inhomogeneous light beam may vary as a function of position on the film surface, the deposition rate and possibly the rate-limiting step may differ at differing positions on the film. In this case, the properties of the depositing film should depend strongly on position. This is indeed observed in Sections 5.3 and 6.1 for the films deposited on quartz and fused silica substrates. At the edge of the depositing film, the evaporation of excess arsenic is the dominant event which determines the film properties. The temperature of this portion of the film, as mentioned earlier, is too low to ensure evaporation of excess arsenic resulting in As rich films. At the center of the depositing film where the temperature is maximum, mass transport can become the rate-limiting step for high enough optical densities. It appears that reactant depletion is responsible for the "crater" effect observed at the center of some of the films deposited on fused silica and quartz.

For photolytically-driven chemical vapor deposition of GaAs, the mechanisms of growth are much less certain. The possibility exists that photodissociation occurs for gas-phase and/or surface-adsorbed species. Incomplete photodissociation of the reactants with complete dissociation of the photofragments occurring by pyrolytic mechanisms is the most favorable when the optical density is insufficient for multi-photon processes. In this case, the kinetics of growth can be quite complex. Consider the case where incomplete photodissociation of the reactants occurs with subsequent pyrolytic dissociation occurring without the need for interaction between the two reactants. In this case, the deposition of each component can be treated independently. For optical absorption by surface-adsorbed species, the deposition rate, R_g, can be written as

$$R_g(r) = \left[K_1 N_{ad,AsH_3}\sigma_{AsH_3} + K_2 N_{ad,TEG}\sigma_{TEG}\right]\frac{P\exp(-r^2/r_o^2)}{h\nu r_o^2} \tag{7.9}$$

where N_{ad,AsH_3} and $N_{ad,TEG}$ are the density of adsorbed arsine and TEG molecules on the surface, σ_{AsH_3} and σ_{TEG} are the dissociation cross-section for arsine and TEG, and P is the optical power.[99,100] The density of the adsorbed molecules will depend on the adsorption isotherm which is valid. A similar expression holds for optical absorption by the gas-phase species and is given by

$$R_g(r) = \frac{P}{h\nu r_o^2}\left[K_3 s_{AsH_3}\sigma_{AsH_3}\int d\phi\int dz\int r'dr'\frac{P_{AsH_3}}{T}\left(\frac{z^{2/3}}{r'^2+z^2-2rr'\cos\phi\ r^2}\right)^{3/2}\exp(-r'^2/r^2)\right.$$

$$\exp\left(\frac{(r'^2+z^2-2rr'\cos\phi+r^2)^{1/2}}{\lambda_{AsH_3'}}\right) + K_4 s_{TEG'}\sigma_{TEG}\int d\phi\int dz\int r'dr'\frac{P_{TEG}}{T}$$

$$\left.\left(\frac{z^{2/3}}{r'^2+z^2-2rr'\cos\phi+r^2}\right)^{3/2}\exp(-r'^2/r_o^2)\exp\left(\frac{(r'^2+z^2-2rr'\cos\phi+r^2)^{1/2}}{\lambda_{TEG'}}\right)\right] \tag{7.10}$$

where s_{AsH_3}, and s_{TEG}, are the sticking coefficients, T is the local temperature of the gas, and λ_{AsH_3}, and λ_{TEG}, are the average distances traveled by the photofragments before reaction with other reactants occurs. The deposition rate of each component is proportional to the partial pressure of the corresponding reactant.

Another possibility occurs when, along with photodissociation, interaction between the reactants takes place. This interaction may be between photofragments and reactant molecules, or it may involve the surface adsorption of the reactant species on particular surface sites. In this case, growth can be described by an expression similar to Eqn. (7.7) with a reduced activation energy as the initial decomposition of the reactants occurs by means of photolysis instead of pyrolysis. If partial photodissociation of the reactants occurs in the gas-phase, Eqn. (7.7) will be valid with the modification that the partial pressure of arsine and triethylgallium will be replaced by an expression for the partial pressure of the photofragment at the surface with the pressure proportional to the term in Eqn. (7.10) pertaining to that particular reactant. As these photofragments are radicals, some will react with other components in the gas-phase prior to arriving at the surface. This has already been alluded to in the work reported in Chapter 4 on Hg-photosensitized decomposition of arsine in the presence of TEG. As such, the actual chemical processes leading to deposition may be quite complex and difficult to track. If, however, the partial photodissociation occurs for surface-adsorbed molecules leading to thin film deposition, the mechanism of growth is given by Eqn (7.7) with a reduction in the apparent activation energy as the initial decomposition is driven photolytically instead of thermally. In this case, interaction of the products of photodissociation with other molecules is dominated by those at or

near the surface. This interaction may be related to the initial surface adsorption of undecomposed molecules.

In reality, some or all of these mechanisms may occur simultaneously with the dominant one determined by the processing parameters. In the case where the light is incident perpendicular to the substrate surface, all of these mechanisms may be involved in the deposition process. For the work reported in Chapter 6 on the photochemical vapor deposition of GaAs utilizing TEG and AsH_3, deposition can best be modeled by four terms which are qualitatively described as:

(1) Partial photolytic decomposition of the gas-phase or surface-adsorbed molecules leading to independent deposition of each individual component of the compound.

(2) Partial photolytic decomposition of gas-phase or surface-adsorbed molecules with interaction between the adsorbed species leading to deposition.

(3) Partial photolytic decomposition of gas-phase or surface-adsorbed species with pyrolytic decomposition occurring for only one of the reactants leading to deposition.

(4) Pyrolytic decomposition of both of the reactants leading to deposition.

Pyrolytic decomposition will not occur for very low substrate temperatures. In this case, deposition occurs by photolysis of either the surface-adsorbed or gas-phase molecules Deposition will be described by Eqn. (7.9) for surface-adsorbed and Eqn. (7.10) for gas-phase species if adsorption and deposition of each component is independent of the other with the deposition rate of each dependent on the partial pressure of the corresponding reactant. This is evident from the results reported in

Sections 5.3 and 6.1 for the films deposited with the arc lamp on quartz and fused silica substrates. For the film deposited near the edge of the arc lamp beam spot location, the temperature of the film will be less than that necessary for pyrolysis to occur. Eqns. (7.9) and (7.10) predict that, for the AsH_3 rich atmosphere used in the experiment reported in Chapter 6, photolysis will result in As rich films. This is, in fact, observed from the compositional studies of the edges of these films. This model also explains the results reported in Section 6.4 on deposition using an ArF laser beam parallel to the quartz substrate with a substrate temperature of 200°C. Again, the deposition of As is seen to be dominant with Eqn (7.10) qualitatively explaining the observed behavior with the deposition rate of each component determined by the relative concentration of the reactants.

The behavior of deposition when the light is perpendicular to the substrate gives very different results from those observed with the light beam parallel to the substrate. Photolysis of surface-adsorbed species results in a greater probability that photofragmentation will result in film deposition as the photofragment already resides on the surface. In addition, the adsorption isotherms which determine surface coverage may lead to certain species adsorbing preferentially on certain surface sites. The results from the photodeposition of GaAs on Si using a perpendicular arc lamp beam suggest this to be so. In this case, significant film deposition by photolysis is seen to occur at 210°C with the film being near stoichiometric. This is in contrast to the results for the parallel laser beam deposition discussed earlier in this Section where the film contained less than 1% Ga.

To understand this behavior, consider the process of TEG and AsH_3 adsorption

on a GaAs surface. This will be the case for the silicon substrates after a few monolayers of GaAs have formed. At 200°C, the adsorption of AsH_3 and TEG will not be indiscriminate but will depend on the presence of As and Ga vacancies at the surface. As such, the ratio of the density of adsorbed AsH_3 to adsorbed TEG may be much different from the ratios of the partial pressures of the reactants. Photolysis of surface-adsorbed species will favor stoichiometric GaAs film deposition more so than gas-phase photolysis. For this reason, the films deposited at 200°C for a perpendicular beam geometry contained much more gallium than the films deposited with parallel beam configuration at this substrate temperature. For the perpendicular incidence case, the deposition rate is more accurately described by Eqn. (7.7) with the apparent activation energy reduced due to the fact that initial bond breaking occurs by photolytic means. Indirect interaction between the reactants is present in this case as the availability of an As vacancy on the surface depends on the incorporation of a Ga atom as this is how such vacancies are created.

As the temperature of the substrate increases, N_{ad,AsH_3} in Eqn. (7.9) and s_{AsH_3}' in Eqn. 7.10 decreases rapidly. This is apparent from the behavior shown in Fig. 4.4 where As deposition on quartz decreased rapidly with increased As evaporation. In addition, pyrolytic decomposition of TEG becomes significant allowing for both photolytic and pyrolytic mechanisms to contribute. From Fig. 6.31, it is seen than as the substrate temperature increases, the increase in the evaporation rate of arsenic combines with the increased pyrolytic decomposition rate of TEG resulting in a transition from arsenic-rich to gallium-rich thin film deposition. Pyrolytic decomposition of TEG occurs at a lower substrate temperature than that for arsine. For photolytic

decomposition of surface-adsorbed molecules, photolysis is efficient enough to provide a sufficient number of arsenic atom for stoichiometric or near-stoichiometric thin film formation to result. This is true because photodissociation of the reactant species occurs at the surface where thin film growth is occurring. This is seen to be the case from the results reported in Section 6.2 where stoichiometric GaAs thin films were deposited at 320°C.

Eventually, the temperature of the irradiated film becomes sufficient for pyrolysis of both reactants to take place. This is clearly the case for the center of the deposits obtained on fused silica using the arc lamp. In this case, deposition may simply given by Eqn. (7.7).

To summarize, gas-phase photolysis appears to be inefficient in leading to deposition due to photofragments being lost to diffusion away from the substrate as well as reactions which occur between the photofragments and other gas-phase species. Significant deposition by this mechanism is possible only for high reactant densities along with high optical densities at the wavelengths absorbed by the molecules. For the AsH_3-TEG system, this leads to inefficient use of the reactants which, from a practical point of view, is especially severe for the expensive organometallic. At substrate temperatures low enough such that the sticking coefficients for the arsenic and gallium bearing species are comparable, the stoichiometry of the film will be determined by the partial pressure ratios of the two reactants. This is especially true for deposition due to gas-phase photolysis. It appears that this mechanism is dominant only for parallel beam configurations.

For a perpendicular beam configuration, optical absorption by both the surface-

adsorbed species and the substrate is possible. Photolysis of the surface-adsorbed species will generally be more efficient in deposition than photolysis in the gas-phase. For the photolysis of surface-adsorbed species, the stoichiometry of the film will depend on the adsorption isotherms of the reactants involved.

As the substrate temperature is increased, the sticking coefficient for arsenic decreases with the only arsenic remaining on the surface being bound to an arsenic vacancy. In addition, at a sufficiently high temperature, pyrolytic decomposition of TEG begins to contribute to the deposition rate. In this case, it is possible for deposition to proceed through the pyrolysis of TEG and the photolysis of AsH_3. At still higher temperatures, pyrolysis of both reactants becomes significant with contributions from photolysis to the deposition rate becoming less significant.

CHAPTER 8

CONCLUSIONS

The objectives of this study have been to investigate the use of photochemical means to achieve thin film deposition of gallium arsenide at low substrate temperatures. This effort included determination of the pertinent growth parameters necessary in obtaining stoichiometric thin films, characterization of these films, and to a limited extent understanding the mechanisms involved in the deposition process. It was found that by direct ultraviolet irradiation of the growing gallium arsenide surface, single crystal growth could be achieved at substrate temperatures as low as 320°C as opposed to temperatures greater than 400°C normally used in conventional organometallic chemical vapor deposition. This represents a contribution towards achieving low temperature single crystal thin film growth of gallium arsenide.

The major contributions of this research can be summarized as follows:

1. The deposition of arsenic thin films by means of Hg-photosensitization of AsH_3 was achieved. The deposition process was seen to be controlled by the formation of AsH_2. For thin films deposited on quartz, rhombohedral-phase structures formed for substrate temperatures above 200°C. In addition, the Hg content in the films was shown to decrease significantly with a moderate increase in the substrate temperature.

2. Hg-photosensitization of AsH_3 was incorporated into the deposition of GaAs with triethylgallium serving as the gallium reactant. Although parasitic reactions prevent the deposition of thin films utilizing Hg-photosensitization alone, deposition of

GaAs was achieved with the addition of a second broadband UV light source. The composition of the photodeposited films was shown to be dependent on the local optical density as stoichiometric GaAs films were obtained for those regions of the deposit where the film temperature was sufficiently high to ensure evaporation of excess arsenic.

3. Direct photochemical vapor deposition of GaAs thin films on fused silica substrates utilizing photolysis to decompose the reactant molecules was successfully achieved. Again, the composition of the deposited film was found to be dependent on the substrate film surface temperature with arsenic-rich films resulting for insufficient film heating.

4. Stoichiometric single crystal epitaxial GaAs thin film growth was achieved at a substrate temperature of approximately 320°C by direct irradiation of a GaAs substrate with ultraviolet radiation from a Hg-Xe arc lamp. It was found that the presence of the ultraviolet radiation at the growing film surface enhances the kinetics leading to single crystal growth. Near-stoichiometric GaAs thin film deposition was achieved at 210°C by direct irradiation of a silicon substrate.

5. Utilizing an ArF excimer laser with the laser beam parallel to the substrate, it was shown that the kinetics of growth with gas-phase photolysis are much different from the case where photodissociation occurs for surface-adsorbed species. Stoichiometric thin film formation was shown to be difficult at low substrate temperatures as the photolytically-driven deposition rates of the individual components depends strongly on the partial pressure ratios of the reactants.

6. Using mass spectrometry, it was shown that photolytic decomposition of

AsH_3 and TEG yields similar products as that produced by pyrolysis of these reactants.

7. A first-order model for light-driven chemical vapor deposition has been developed. It shows that, for direct irradiation of the semiconductor surface, the kinetics of growth are determined by the adsorption isotherms with the adsorption process favoring stoichiometric GaAs thin film deposition. For the case where photodissociation occurs in the gas-phase, the deposition of the components of the compound occur independently with film composition determined by the partial pressures of the reactants.

A portion of this work has been accepted for publication. This includes the work reported on Hg-photosensitized chemical vapor deposition of GaAs in Chapter 5[101] as well as the work reported in Chapter 6 on photolytically-driven chemical vapor deposition of GaAs on quartz[102] and GaAs[103] substrates utilizing the Hg-Xe arc lamp output.

Recommendations for continuing research are:

1. Gallium arsenide thin film deposition by direct irradiation of the substrate surface with the 193 nm excimer laser radiation. Particular attention should be given to the use of low pulse energies with high repetition rates to maximize photolytically-driven deposition while minimizing the effect of surface heating.

2. Laser-induced fluorescence measurements to help identify the photoproducts.

3. Investigate further the incorporation of carbon into the GaAs films from the organometallic using secondary ion mass spectrometry.

4. Incorporate a second group III reactant into the deposition system for the photochemical growth of a ternary compound.

5. Investigate the use of a less toxic arsenic-bearing reactant to replace the use of arsine.

REFERENCES

1. H. M. Manasevit, Appl. Phys Lett. **11** , 156 (1968).
2. H. M. Manasevit and W. I. Simpson, J. Electrochem. Soc. **116** , 1725 (1969).
3. M. R. Leys and H. Veenvliet, J. Crystal Growth **55** , 145 (1981).
4. V. S. Ban, J. Electrochem. Soc. **125** , 317 (1978).
5. S. Berkman, V. S. Ban and N. Goldsmith, in "Heterojunction Semiconductors for Electronic Devices," edited by G. W. Cullen and C. C. Wang (Springer, New York, 1977) p. 264.
6. Y. Monteil, M. P. Berthet, R. Favre, A. Hariss and J. Bouix, J. Crystal Growth **77** , 172 (1986).
7. M. Koppitz, W. Richter, R. Bahnen and M. Heyen, in "Laser Processing and Diagnostics," edited by D. Bauerle (Springer-Verlag, Berlin, 1984) p.530.
8. G. B. Stringfellow, J. Crystal Growth **68** , 111 (1984).
9. K. Tamaru, J. Phys. Chem. **59** , 777 (1955).
10. D. H. Reep and S. K. Ghandi, J. Electrochem. Soc. **130** , 675 (1983).
11. M. G. Jacko and S. J. W. Price, Canadian J. Chem. **41** , 1560 (1963).
12. M. Yoshida, H. Watanabe and F. Uesugi, J. Electrochem. Soc. **132** , 677 (1985).
13. M. Susuki and M. Sato, J. Electrochem. Soc. **132** , 1684 (1985).
14. M. Mashita, S. Horiguchi, M. Shimazu, K. Kamon, M. Mihara and M. Ishii, J. Crystal Growth **77** , 194 (1986).
15. C. Plass, H. Heinecke, O. Kayser, H. Luth and P. Balk, J. Crystal Growth **88** , 455 (1988).

16. W. Tsang, Appl. Phys. Lett. **45** , 1234 (1985).

17. R. Bhat, Paper J-1 presented at the 23rd Annual Electronic Materials Conference, Santa Barbara, CA, 20- 22 June, 1984.

18. D. J. Schlyer and M. A. Ring, J. Organometal. Chem. **114** , 9 (1976).

19. J. Nishizawa and T. Kurabayashi, J. Electrochem. Soc. **130** , 413 (1983).

20. J. E. Butler, N. Bottka, R. S. Sillmon and D. K. Gaskill, J. Crystal Growth **77** , 163 (1986).

21. S. P. DenBaars, B. Y. Maa, P. D. Dapkus, A. D. Danner and H. C. Lee, J. Crystal Growth **77** , 188 (1986).

22. N. Putz, H. Heinecke, M. Heyen, P. Balk, M. Weyers and H. Luth, J. Crystal Growth **74** , 292 (1986).

23. J. P. Simons,"Photochemistry and Spectroscopy," (Wiley, London 1971).

24. W. A. Noyes and P. A. Leighton,"The Photochemistry of Gases," (Reinhold, New York, 1941).

25. G. K. Rollefson and M. Burton,"Photochemistry and the Chemical Reactions, " (Prentice-Hall, New York, 1939).

26. W. Ho, Comments Cond. Mat. Phys. **13** , 293 (1988).

27. H. Gerischer, Faraday Discussions of the Chem. Soc. **58** , 219 (1974).

28. N. S. Gluck, Z. Ying, C. E. Bartosch and W. Ho, J. Chem. Phys. **86** , 4957 (1987).

29. D. Bauerle,"Chemical Processing with Lasers," (Springer-Verlag, Berlin, 1986).

30. D. J. Ehrlich and J. Y. Tsao, J. Vac. Sci. Technol. **B1** , 969 (1983).

31. J. G. Black, S. P. Doran, M. Rothschild and D. J. Ehrlich, Appl. Phys. Lett. **50** ,

1016 (1987).

32. Y. Ritz-Froidevaux, R. P. Salathe and H. H Gilgen, Appl. Phys. A **37** , 121 (1985).

33. J. Haigh and M. R. Aylett, Prog. Quant. Electr. **12** , 1 (1988).

34. D. Bauerle, in "Laser Processing and Diagnostics," ed. by D. Bauerle (Springer-Verlag, Berlin, 1984) p. 166.

35. I. P. Herman,"Laser Processing and Diagnostics," ed. by D. Bauerle (Springer -Verlag, Berlin, 1984) p. 396.

36. J. Y. Tsao and D. J. Ehrlich, J. Crystal Growth **68** , 176 (1984).

37. S. J. C. Irvine, CRC Critical Reviews in Solid State and Materials Sciences **13** , 279 (1987).

38. G. H. Cheesman and H. J. Emeleus, J. Chem. Soc., 2847 (1932).

39. C. M. Humphries, A. D. Walsh and P. A. Warsop, Discussions Faraday Soc. **35** , 148 (1963).

40. R. F. Karlicek, B. Hammarlund and J. Ginocchio, J. Appl. Phys. **60** , 794 (1986).

41. T. Ni, Q. Lu, X. Ma, S. Yu and F. Kong, Chem. Phys. Lett. **126** , 417 (1986).

42. R. N. Dixon, G. Duxbury and H. M. Lamberton, Proc. Roy. Soc. A **305** , 271 (1968).

43. V. R. McCrary and V. M. Donnelly, J. Crystal Growth **84** , 253 (1987).

44. J. Haigh, J. Mat. Sci. **18** , 1072 (1983).

45. I. A. Frolov, B. L. Druz', P. B. Boldyrevskii and E. B. Sokolov, Izv. Akad. Nauk SSSR, Neorg. Mater. **13** , 906 (1977).

46. N. Putz, H. Heinecke, E. Veuhott, G. Arens, M. Heyen, H. Luth and P. Balk,

J. Crystal Growth **68** , 194 (1984).

47. P. Balk, H. Heinecke, N. Putz, C. Plass and H. Luth, J. Vac. Sci. Technol. A **4** , 711 (1986).

48. J. Haigh, J. Vac. Sci. Technol. B **3** , 1456 (1985).

49. M. R. Aylett and J. Haigh, Mat. Res. Soc. Symp. Proc. **17** , 177 (1983).

50. A. R. Calloway, T. A. Galantowicz and W. R. Fenner, J. Vac. Sci. Technol. A **1** , 534 (1983).

51. V. M. Donnelly, M. Geva, J. Long and R. F. Karlicek, Appl. Phys. Lett. **44** , 951 (1984).

52. V. M. Donnelly, D. Brasen, A. Appelbaum and M. Geva, J. Appl. Phys. **58** , 2022 (1985).

53. V. M. Donnelly, V. R. McCrary, A. Appelbaum, D. Brasen and W. P. Lowe, J. Appl. Phys. **61** , 1410 (1987).

54. J. Nishizawa, T. Kurabayashi and J. Hoshina, J. Electrochem. Soc. **134** , 502 (1987).

55. J. J. Zinck, P. D. Brewer, J. E. Jensen, G. L. Olsen and L. W. Tutt, Mat. Res. Soc. Symp. Proc. **75** , 233 (1987).

56. J. Nishizawa, H. Abe, T. Kurabayashi and N. Sakurai, J. Vac. Sci. Technol. A **4** , 706 (1986).

57. E. Tokumitsu, T. Yamada, M. Konagai and K. Takahashi, Mat. Res. Soc. Symp. Proc. (MRS Fall Meeting, 1987).

58. N. Suzuki, C. Anayama, K. Masu, K. Tsubouchi and N. Mikoshiba, Jpn. J. Appl. Phys. **25** , 1236 (1986).

59. T. Motooka, S. Gorbatkin, D. Lubben and J. E. Greene, J. Appl. Phys. **58** , 4397 (1985).

60. T. Motooka, S. Gorbatkin, D. Lubben, D. Eres and J. E. Greene, J. Vac. Sci. Technol. A **4** , 3146 (1986).

61. G. E. Blonder, G. S. Higashi and C. G. Fleming, Appl. Phys. Lett. **50** , 766 (1987).

62. H. Suzuki, K. Mori, M. Kawasaki and H. Sato, J. Appl. Phys. **64** , 371 (1988).

63. J. Nishizawa, Y. Kokubun, H. Shimawaki and M. Koike, J. Electrochem. Soc. **132** , 1939 (1985).

64. S. M. Bedair, J. K. Whisnant, N. H. Karam, M. A. Tischler and T. Katsuyama, Appl. Phys. Lett. **48** , 174 (1986).

65. S. M. Bedair, J. K. Whisnant, N. H. Karam, D. Griffis, N. A. El-Masry and H. H. Stadelmaier, J. Crystal Growth **77** , 229 (1986).

66. Y. Aoyagi, S. Masuda, S. Namba and A. Doi, Appl. Phys. Lett. **47** , 95 (1985).

67. Y. Aoyagi, M. Karazawa, A. Doi, S. Iwai and S. Namba, J. Appl. Phys. **60** , 3131 (1986).

68. A. Doi, Y. Aoyagi and S. Namba, Appl. Phys. Lett. **48** , 1787 (1986).

69. J. E. Epler, H. F. Chung, D. W. Treat and T. L. Paoli, Appl. Phys. Lett. **52** , 1499 (1988).

70. J. Y. Tsao and D. J. Ehrlich, Appl. Phys. Lett. **45** , 617 (1984).

71. Y. Rytz-Froidevaux, R. P. Salathe and H. H. Gilgen, Mat. Res. Soc. Symp. Proc. **17** , 29 (1983).

72. W. Roth, H. Krautle, A. Krings and H. Beneking, Mat. Res. Soc. Symp. Proc.

17 , 193 (1983).

73. H. Beneking, in "Laser Processing and Diagnostics," ed. by D. Bauerle (Springer-Verlag, Berlin, 1984) p.188.

74. K. A. Jones, Solid State Technology **28** (10), 151 (1985).

75. N. L. Simmons and A. O. Beckman, J. Am. Chem. Soc. **58** , 454 (1936).

76. J. C. Knight and J. E. Mahan, Solid St. Commun. **21** , 983 (1977).

77. G. N. Greaves, E. A. Davis and J. Bordas, Phil. Mag. **34** , 265 (1976).

78. W. A. Noyes and P. A. Leighton,"The Photochemistry of Gases," vol. 1, 1st edn. (Reinhold, New York 1941) p. 221.

79. P. W. Atkins,"Physical Chemistry," vol. 1, 2nd edn. (Freeman, San Francisco 1982) p. 870.

80. Compton and Turner, Phil. Mag. **48** , 360 (1924).

81. D. M. Smith, A. J. Leadbetter and A. J. Apling, Phil. Mag. **31** , 57 (1974).

82. G. Breitling and H. Richter, Mater. Res. Bull. **4** , 19 (1969).

83. W. M. Lau, T. C. Chan and R. P. Bult, Mater. Lett **5** , 88 (1987).

84. G. Leonhardt, A. Berndtsson, J. Hedman, M. Klasson, R. Nilsson and C. Nordling, Phys. Stat. Sol. (b) **60** , 241 (1973).

85. M. K. Bahl, R. O. Woodall, R. L. Watson and K. J. Irgolic, J. Chem. Phys. **64** , 1210 (1976).

86. L. Ley, R. A. Pollak, S. P. Kowalczyk, R. McFeely and D. A. Shirley, Phys. Rev. B **8** , 641 (1973).

87. D. P. Norton and P. K. Ajmera, in Proceedings of the 3rd International Photovoltaic Science and Engineering Conference, Tokyo, Japan (Intl.

PVSEC-3, Tokyo, 1987) p. 537.

88. S. Nishida, H. Tasaki, M. Konagai and K. Takahashi, J. Appl. Phys. **58** , 1427 (1985).

89. T. Saitoh, S. Muramatsu, T. Shimada and M. Migitaka, Appl. Phys. Lett. **42** , 678 (1983).

90. B. D. Cullity, "Elements of X-Ray Diffraction," p. 284, Addison-Wesley, Reading (1978).

91. M. Lax, J. Appl. Phys. **48** , 3919 (1977).

92. M. Lax, Appl. Phys. Lett. **33** , 786 (1978).

93. A. Kinrot, J. Bloch and Y. Zeiri, J. Phys. D: Appl. Phys. **21** , 975 (1988).

94. M. K. El-Adawi and S. A. Shalaby, J. Appl. Phys. **63** , 2212 (1988).

95. T. T. Kodas, T. H. Baum and P. B. Comita, J. Appl. Phys. **61** , 2749 (1987).

96. S. D. Allen, J. A. Goldstone, J. P. Stone and R. Y. Jan, J. Appl. Phys. **59** , 1653 (1986).

97. N. Putz, E. Veuhoff, H. Heinecke, M. Heyen, H. Luth and P. Balk, J. Vac. Sci. Technol. B **3** , 671 (1985).

98. S. Horiguchi, K. Kimura, K. Kamon, M. Mashita, M. Shimazu, M. Mihara and M. Ishii, Jpn. J. Appl. Phys. **25** , L979 (1986).

99. T. H. Wood, J. C. White and B. A. Thacker, Appl. Phys. Lett. **42** , 408 (1983).

100. T. H. Wood, J. C. White and B. A. Thacker,"Laser Diagnostics and Photochemical Processing for Semiconductor Devices," ed. by R. M. Osgood, S. R. J. Brueck and H. R. Schlossberg (North-Holland, New York 1983) p.35.

101. D. P. Norton and P. K. Ajmera, "Mercury-Sensitized Photochemical

Vapor Deposition of Gallium Arsenide on Quartz," J. Electrochem. Soc., to be published.

102. D. P. Norton and P. K. Ajmera, Appl. Phys. Lett. **53** , 595 (1988).

103. D. P. Norton and P. K. Ajmera,"Advanced Processing of Semiconductor Devices II" ed. by H. G. Craighead and J. Narayan, Proc. SPIE **945** , 55-61 (1988).

APPENDIX

A.1 Safety Precautions

The experiments performed in this work presented five safety hazards which required special attention. They were:

(1) Toxic Gas (AsH_3)

(2) Toxic Element (Hg)

(3) Flammable Gas (H_2)

(4) Pyrophoric Liquid (TEG)

(5) Ultraviolet Radiation

The use of AsH_3 presented the most serious health hazard. It is one of the most toxic gases known with a single inhalation of an atmosphere with 250 ppm arsine instantly fatal. Exposure to 25 ppm for 30 minutes is lethal with 6 ppm considered immediately dangerous to life and health. The limit for prolonged exposure is 0.05 ppm (TLV). The clinical effect of arsine involves mostly its attack of the red blood cells. Symptoms of exposure to arsine can become evident anywhere from 20 minutes to 36 hours after exposure. Symptoms initially are manifest in difficulties relating to the central nervous system. Giddiness, headache or light-headedness often are observed. Abdominal pains may also occur. The color of the sclera or the skin may appear coppery. Rapid respiration and pulse rates will likely occur. Obviously, arsine exposure requires immediate attention from a physician.

The safety system utilized in this work to minimize the risk of exposure of personnel to arsine is shown in Fig. A.1. The arsine bottle was kept in a gas cabinet in

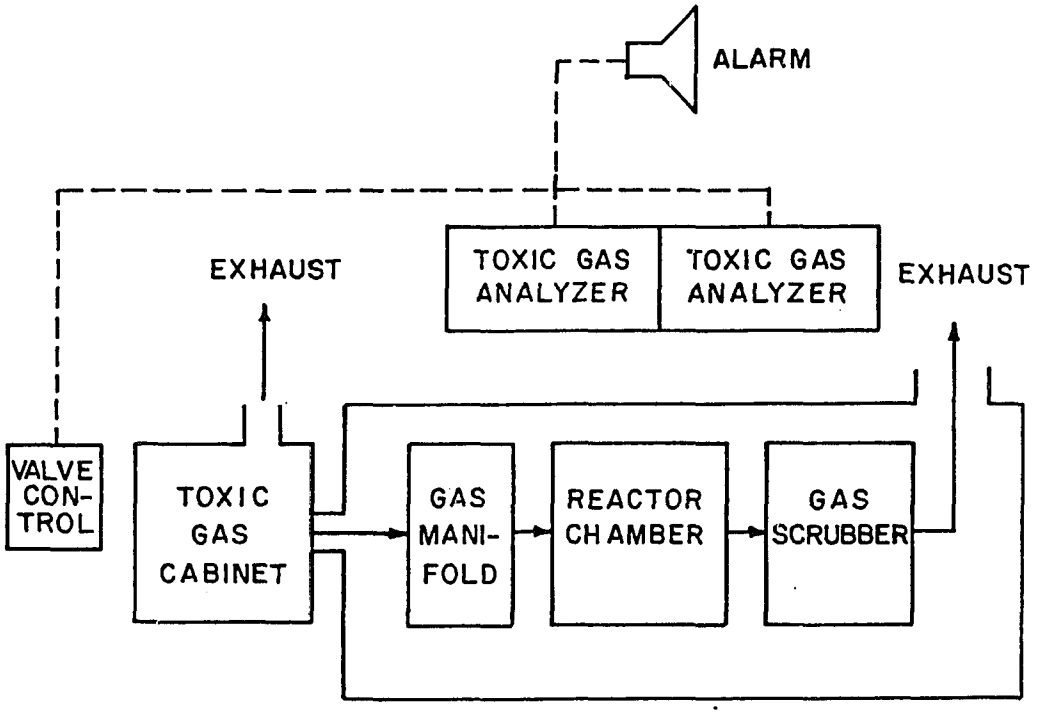

Figure A.1 Safety System for the Experiments Performed with Arsine .

which the exhaust fan was operated continuously. The experimental apparatus was enclosed in an enclosure constructed of acrylic and aluminum sheets. This enclosure was evacuated continuously with a dedicated exhaust fan in order to maintain a negative pressure inside the enclosure with respect to the room ambient pressure. The exhaust of both the gas cabinet and the enclosure were monitored with an arsine monitor with a minimum detectable limit of 5 ppb. These monitors were used to control an audible alarm system as well as an automatic shutoff valve located at the arsine bottle output. In addition to the above mentioned monitors, a portable AsH_3 monitor with a detectable limit of 50 ppb was also utilized. In order to eliminate the arsine from the reactor exhaust, a wet scrubber utilizing potassium permanganate was used. Two self-contained breathing apparatus were also available in case of emergency.

In order to utilize arsine in these experiments, a procedure had to be followed for every experiment without compromise to insure safe handling of this material. During periods of time when no experiment was in progress, the arsine bottle valve remained shut off with no arsine present in the gas lines. Experiments involving the use of arsine required the presence of two persons. Before introducing arsine into the reactant lines at the beginning of an experiment, the reactant lines were checked for leaks by vacuuming. Before opening the arsine bottle valve, all of the panels of the enclosure were put into place. The person opening the arsine bottle valve was required to wear the self-contained breathing apparatus while opening. A flow of approximately 1 slm of N_2 was provided in the exhaust line at the outlet of the vacuum pump to insure prompt delivery of the arsine to the scrubber. Upon completion of an experiment, the arsine bottle valve was closed and the reactant line were

vacuumed to 2 mTorr. This was followed by a nitrogen purge of the arsine line through the cross-purge assembly located at the bottle connection at a flow rate of 50 sccm for 30 minutes. This was followed by vacuuming the arsine line for 60 minutes.

In order to control the hazards introduced by Hg and H_2, the exhaust of the reactor was diluted with nitrogen. A copper trap was also used to trap the Hg. The pyrophoric liquid requires no exposure to air. A special fire extinguisher was also provided as a precaution. The ultraviolet radiation hazard was effectively controlled with the use of appropriate metal enclosures and specifically designed eye goggles.

VITA

David Paul Norton was born in Baton Rouge, Louisiana on May 17, 1962. He received his Bachelor's degree with honors in Electrical Engineering from Louisiana State University in 1984. Since June of 1984, he has been pursuing his graduate degree at Louisiana State University where he has served as an Alumni Federation Fellow, a research assistant and a teaching assistant in the Department of Electrical and Computer Engineering. He is a member of the Institute of Electrical and Electronic Engineers and the American Physical Society.

He is presently a candidate for the degree of Doctor of Philosophy in Electrical Engineering.

DOCTORAL EXAMINATION AND DISSERTATION REPORT

Candidate: David Paul Norton

Major Field: Electrical Engineering

Title of Dissertation: Photochemical Vapor Deposition of Gallium Arsenide Utilizing Ultraviolet Radiation

Approved:

P. K. Ajmera
Major Professor and Chairman

F. Glen Hembree
Dean of the Graduate School

EXAMINING COMMITTEE:

R C Goodlett

Agnyaschak

Subhash Kak

C I Sik Lee

M L Williams

Date of Examination:

April 14, 1989